WEATHERING AND GEOCHEMICAL FLUXES IN THE CANADIAN CORDILLERA: EVIDENCE FROM MAJOR ELEMENTS, RARE EARTH ELEMENTS, MERCURY, AND CARBON AND SULPHUR ISOTOPES IN THE FRASER, SKEENA AND NASS RIVERS

by
Jody Spence
B.Sc., University of Victoria, 1998

A thesis submitted in partial fulfillment of the
requirements for the degree of
DOCTOR OF PHILOSOPHY
in the School of Earth and Ocean Sciences

We accept this thesis as conforming
to the required standard

Supervisor: Dr. Kevin H. Telmer

ABSTRACT

Water and suspended particulate samples from the Fraser, Skeena and Nass River systems of the western Canadian Cordillera were analysed for dissolved major element concentrations (HCO_3^-, SO_4^{2-}, Cl^-, Ca^{2+}, Mg^{2+}, K^+, Na^+); $\delta^{13}C$ of dissolved inorganic carbon (DIC); and $\delta^{34}S$ of dissolved sulphate (SO_4^{2-}); rare earth elements (REE) – dissolved and adsorbed to the suspended particulate matter; and mercury (Hg) – dissolved, and associated with suspended particulate (adsorbed, organic bound, mineral bound). This data is used to quantify chemical weathering rates and exchanges of CO_2 between the atmosphere, hydrosphere, and lithosphere; to assess weathering and erosion processes in alpine versus valley regions of the watersheds; and to quantify the transfer of Hg from rocks to the surface environment. The main results of this work are:

(1) Important weathering processes in the Canadian Cordillera are: (i) carbonate dissolution by carbonic acid > (ii) silicate dissolution by carbonic acid ≈ (iii) carbonate dissolution by sulphuric acid derived from the oxidation of sulphides (coupled *sulphide-carbonate weathering*). DIC fluxes due to (ii) and (iii) are equivalent (~60×10^3 mol $C \cdot km^{-2} \cdot yr^{-1}$). *Sulphide-carbonate weathering* may therefore be a long-term source of atmospheric CO_2 offsetting silicate weathering CO_2 drawdown in the region, which suggests *sulphide-carbonate weathering* may provide a negative feedback to tectonic uplift induced cooling.

(2) REE patterns in the dissolved and adsorbed phases (*labile REE*) of the rivers vary widely across the Cordilleran watersheds, and predictably reflect basin lithology. Main stem samples reflect mixtures of the tributaries, suggesting *labile REE* patterns are

conservative in the rivers. This supports using *labile REE* as a weathering and hydrographic tracer.

(3) $Kd_{REE}^{ads/dis}$ values in June (high water stage, average $\approx 1 \times 10^3$) are approximately 50 times lower than $Kd_{REE}^{ads/dis}$ values in October (low water stage, average $\approx 50 \times 10^3$), indicating a change in composition and source of the suspended particulate matter from recently eroded rock flour (alpine source) in June, to older alluvial soils (valley source with a higher percentage of clay minerals) in October. This seasonal shift indicates silicate weathering is dominantly occurring in the valley regions of the watersheds, while the alpine regions have high physical erosion rates and little to no silicate weathering. Also, because ~80% of the sediment transport in these rivers occurs during the late spring to early summer, this shows that the suspended particulate budget is dominated by current uplift and erosion, not remobilization of Pleistocene glacial till. This suggests uplift and erosion in the Canadian Cordillera is near steady state.

(4) Annual Hg export to coastal waters by these rivers is 11 x 10^3 kg·yr^{-1}, of which 6% (650 kg·yr^{-1}) is in labile phases (dissolved < adsorbed < organic bound). Mass balance indicates that 2.5 to 100% of this flux can be attributed to chemical weathering. However, the strong correlation between chemical weathering rates and Hg fluxes suggests that weathering is the dominant control (near to 100%) on Hg release and transport. The results also show that sulphide oxidation and Hg concentration in sulphide minerals has the greatest influence on the amount of Hg liberated by chemical weathering.

(5) As with the REE, seasonal variation in Hg concentrations and distribution exist. In June, labile Hg dominantly exists in the adsorbed phase, but dominantly in the organic bound phase in October, which indicates Hg has greater affinity to organic ligands than

direct adsorption to inorganic particulate surfaces. Also, mineral bound Hg concentrations are much higher in June than October. This change in Hg concentration between the alpine and low-land derived particulate suggests that the development of soil may be cause loss of Hg to the atmosphere.

Examiners:

TABLE OF CONTENTS

LIST OF TABLES

Chapter 1:

LIST OF FIGURES

Chapter 1:

Chapter 2:

Chapter 3:

Chapter 4:

.....

ACKNOWLEDGEMENTS

I thank Kevin Telmer, whose vision instigated this project; the members of my committee: Dante Canil, Maycira Costa, and Kathy Gillis for their assistance and advice; and Bernhard Mayer for insightful questions and helpful comments. This thesis has benefited markedly from the comments of all of my committee members. Also, chapter 2 has benefited from the comments and reviews of Suzanne Anderson, Jerome Gaillardet, Lee Kump and an anonymous reviewer.

I thank Sussi Arason who has not given up on me no matter how many deadlines I forget; Mike Sanborn, Jiangzhong Fan, Trayce Keith, Kristy Hooker, Cheryl Peters, Heather Woluschuck for support and assistance in the field and in the lab; Virginie Lorant for helping me keep perspective on the project; Hannah and Maya Collinson for helping me keep perspective on life; all of my friends and family, in particular my Mom (Jean) and my Dad (Dennis), who have supported me through all of my enterprises, hair-brained or otherwise; and my grandmother (Anne "Anne-Mum" Stevenson) who taught me the value of learning and of being fascinated by the world around me.

This thesis has also benefitted from the work of Moire Wadleigh, whose research provided key baseline data; and whose lab at Memorial University performed oxygen isotope analyses on my sulphate samples. Moire's passing is a great loss to the Canadian and the International scientific community.

Financial support for this project has been provided by the University of Victoria, NSERC, COMERN, the Geological Association of Canada, and the Geological Society of America.

1 Introduction

The research described in this thesis is the result of a comprehensive geochemical survey of the Fraser, Skeena and Nass river systems which drain the western Canadian Cordillera, British Columbia, Canada (figure 1.1, 1.2). The main objective of the study was to collect and interpret a comprehensive chemical and isotopic data set for these rivers. Multiple geochemical tracers are used to quantify natural inputs to the rivers by chemical weathering of rocks. The results are applied to global scale problems: (i) the controls on fluxes of the greenhouse gas carbon dioxide (CO_2) between the atmosphere and lithosphere – which is important for the long term evolution of the Earth's atmosphere; and, (ii) quantification of the release of mercury (Hg) into the Earth's surface environment by chemical weathering – which is important because of the high toxicity of Hg, and the fact that the natural cycle of this element is poorly understood.

Many workers have studied the linkages between tectonic uplift, climate, weathering, and ocean/atmosphere chemistry (Ruddiman, 1997 is a collection of papers on this topic). However, these studies have largely focused on the importance of the Himalayan uplift, while uplift and weathering within the Cordilleran orogenic belt, which spans the western margin of North and South America, has received comparatively little attention. An important contribution of this work is that it provides data on weathering rates and processes in three of the largest watersheds draining the Canadian Cordillera into the Pacific Ocean. These rivers were selected because their catchment areas represent the geological and physiographic diversity of the Canadian Cordillera.

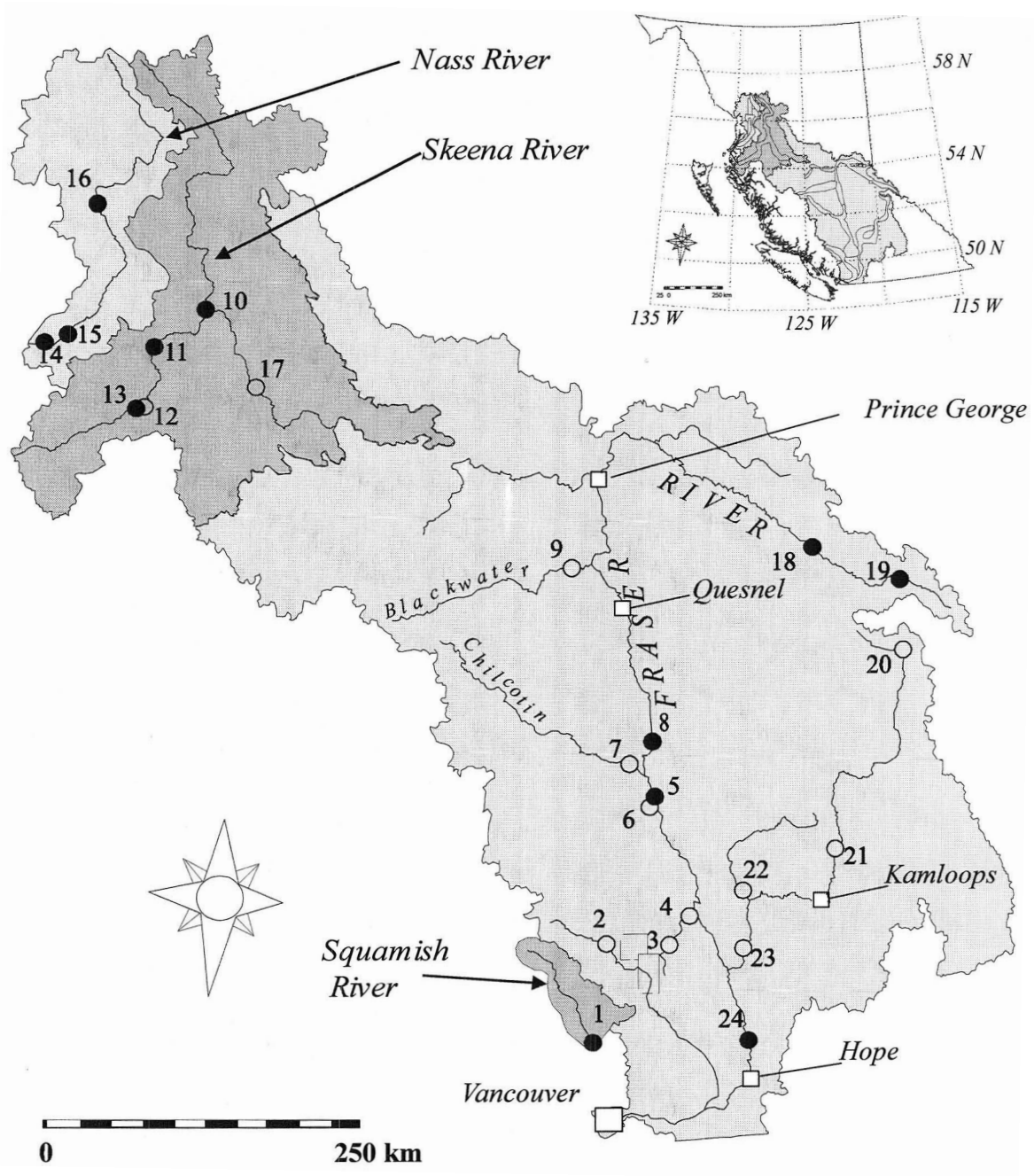

Figure 1.1 Fraser, Skeena and Nass watersheds, their main tributaries, and sample locations. The key to basin geology, location names, station numbers and sample numbers are given in Table 1.1. Station locations (latitude and longitude) are given in Appendix A. Closed circles mark main stem sample locations, open circles mark tributary sample locations.

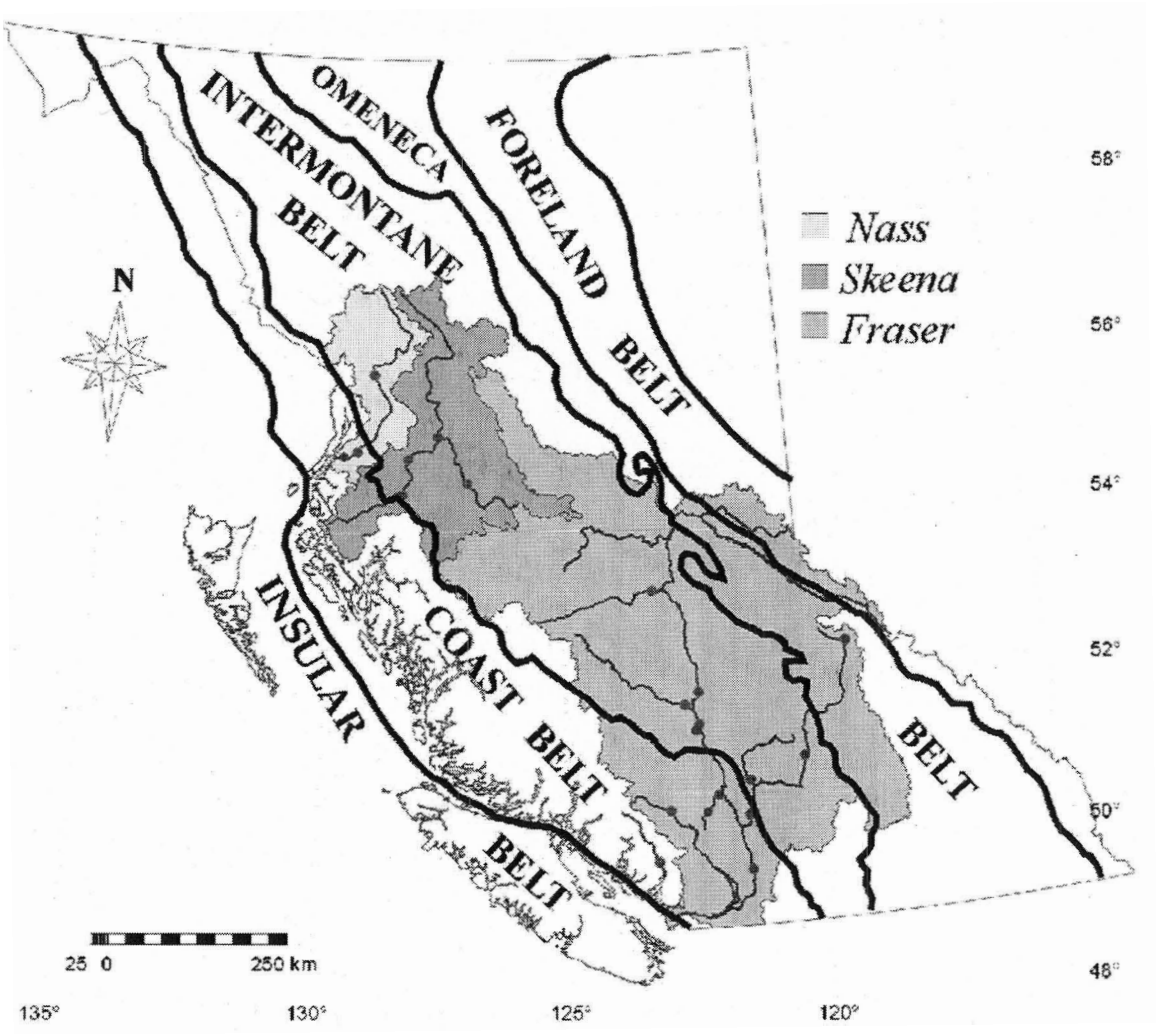

Figure 1.2 Map of the study area showing the major geological divisions (morphogeological belts) of the Canadian Cordillera.

Also, the Fraser, Skeena and Nass watersheds are largely pristine, with only limited population and industrial or agricultural activity within the catchments, and are three of the largest un-dammed rivers in North America. The closest large up-wind industrial centre is Japan, which means significant aerial transport of pollutants to these catchments is unlikely. Thus anthropogenic inputs to these rivers are minimal and relatively easy to constrain, which facilitates quantification of natural inputs.

1.1 PROJECT OBJECTIVES

The primary objectives of this project are to:

1. Provide new baseline geochemical data for the Fraser, Skeena and Nass river systems – dissolved major element concentrations, dissolved and suspended trace element concentrations, and stable isotopic ratios ($\delta^{13}C$ in dissolved inorganic carbon and $\delta^{34}S$ in dissolved sulphate).
2. Quantify watershed scale chemical weathering rates and associated fluxes of the greenhouse gas carbon dioxide (CO_2) between the lithosphere and the atmosphere/ocean within the Canadian Cordillera using the chemical and isotopic composition of river water.
3. Develop and implement methods to measure rare earth element (REE) concentrations and relative abundances (REE patterns) in river water and suspended particulate; assess the use of dissolved REE and REE adsorbed to suspended particulate as a geochemical tracer in river water; and, document REE delivery by rivers to the northeast Pacific Ocean by the Cordilleran rivers.

4. Develop methods to measure mercury (Hg) concentrations in river water and suspended particulate; determine the distribution of Hg between labile and refractory phases within the river water; quantify the natural release of Hg into the hydrosphere by chemical weathering; and, document Hg fluxes to the northeast Pacific Ocean by the Cordilleran rivers.

1.2 METHODOLOGY

The project objectives as listed above describe the sequence of data collection and analysis through the course of this project. A significant portion of this thesis has involved the development and application of new analytical techniques, thus practical descriptions of the methodology are given in each of the subsequent chapters as appropriate. Water and suspended particulate samples were collected from the Fraser, Skeena and Nass rivers, and major tributaries during two field campaigns, representing the peak (June) and trough (October) of the 2002 hydrograph. The samples were analysed for multiple major and trace components so that multiple chemical and isotopic tracers could be applied to interpreting river chemistry. This has allowed interpretations to a level of detail that would not have been possible using a less comprehensive data set. All sample preparation and analytical work was done at the University of Victoria, School of Earth and Ocean Sciences, except for the isotopic analysis of dissolved sulphate – $\delta^{34}S_{SO4}$ was measured at the University of Calgary, and $\delta^{18}O_{SO4}$ was measured at Memorial University.

1.2.1 Weathering Rates

Relative chemical weathering rates are determined and reported for major and tributary watersheds within the Canadian Cordillera. In order to make direct comparisons of weathering rates of different rock types, and between basins, bicarbonate (HCO_3^-) fluxes are used as a proxy of absolute weathering rate for the following processes:

Carbonate weathering by carbonic acid

$$CaCO_3 + H_2CO_3 \rightarrow Ca^{2+} + H_2O + 2HCO_3^- \quad (1)$$

Silicate weathering by carbonic acid

$$CaSiO_3 + 2H_2CO_3 \rightarrow Ca^{2+} + SiO_2 + H_2O + 2HCO_3^- \quad (2)$$

Carbonate weathering by sulphuric acid

$$CaCO_3 + \tfrac{1}{2}H_2SO_4 \rightarrow Ca^{2+} + \tfrac{1}{2}SO_4^{2-} + HCO_3^- \quad (3)$$

By using bicarbonate as a proxy of weathering rates, it is possible to determine and compare weathering rates of rock types where the mineralogy is known, or can be approximated, but the exact chemical composition is not known. The bicarbonate produced by these weathering processes is transported out of a watershed via river dissolved load. Thus the bicarbonate in river water ($HCO_{3\,river}^-$) is equal to the sum of bicarbonate produced by weathering carbonate minerals by carbonic acid ($HCO_{3\,Cc}^-$), silicate minerals by carbonic acid ($HCO_{3\,Sc}^-$) and of carbonate minerals by sulphuric acid ($HCO_{3\,SCW}^-$)

$$HCO_{3river}^- = HCO_{3Cc}^- + HCO_{3Sc}^- + HCO_{3SCW}^- \quad (4)$$

1.3 STUDY AREA

Water samples were collected from 12 rivers in the Canadian Cordillera, the Fraser, Skeena and Nass drainage basins during the peak (June) and trough (October) of the 2002 hydrograph. Dissolved concentrations of SO_4^{2-}, Cl^-, HCO_3^-, F^-, NO_3^-, Ca^{2+}, Mg^{2+}, Na^+, K^+, the $\delta^{13}C$ in dissolved inorganic carbon ($\delta^{13}C_{DIC}$), $\delta^{34}S$ in dissolved sulphate ($\delta^{34}S_{SO4}$), pH, temperature, conductivity, and charge balance from these samples are reported and described, along with mass balance calculations of chemical weathering rates in chapter 2. Rare earth element concentrations (dissolved and adsorbed to suspended particulate) are reported in chapter 3. In chapter 4, new data is reported on mercury concentrations in the dissolved phase, as well as the labile (adsorbed to mineral surfaces, and organic bound) and refractory (mineral bound) phases of the suspended particulate for the same samples.

1.3.1 Watershed Characteristics

The portions of the Fraser, Skeena and Nass Watersheds considered by this study drain a combined area of 280,000 km^2, with cumulative annual discharge averaging 4740 $m^3 \cdot s^{-1}$ (Environment Canada, 2001a). This represents approximately 0.2% of the global land mass, and 0.4% of the global annual river discharge to the oceans (Meybeck, 1979).

The hydrograph of the rivers draining the Canadian Cordillera is dominated by a pulse of water generated by snowmelt in late spring (Figure 1.3). Approximately 70% of the total discharge of these rivers occurs between May and August. Figure 1.3 illustrates the typical annual hydrograph for all of these rivers, which is also representative of the 2002 hydrograph.

A summary of watershed characteristics for the rivers sampled is given in Table 1.1. The Fraser River, and its tributary the Thompson River, are the largest rivers, and each traverses across the geological belts that make up the Canadian Cordillera. The remaining rivers are representative of various geological terranes of the Canadian Cordillera. A summary of the geology of each basin is also given in Table 1. 1.

1.3.2 Basin Geology

Except where noted, the following geological descriptions are taken from: Gabrielse and Yorath (1991), Wheeler and McFeely (1991), and Gabrielse et al. (1991). The Canadian Cordillera is a geologically complex region that makes up the northern portion of the western margin of North America. The transformation from a passive to an active margin is believed to have occurred in the Devonian, but the first hard evidence of subduction is the occurrence of Permian blue schists and eclogites (Monger, 1997). The Canadian Cordillera, an accretionary orogen, is typically described as a series of roughly north-south trending structural and lithological zones, or geomorphological belts. The eastern margin of the Canadian Cordillera is made up of ancestral passive margin carbonates and shales, ranging in age from Upper Proterozoic to Mesozoic, that have been thrust eastward onto the Continent. This is commonly known as the Rocky Mountain (Foreland) fold and thrust belt, and is a region of very high topography and relief, with many peaks exceeding 2500m. To the west is a belt of similarly high topography and relief (the Omenica belt), made up of highly metamorphosed sedimentary and igneous rocks that are intruded by granitic plutons.

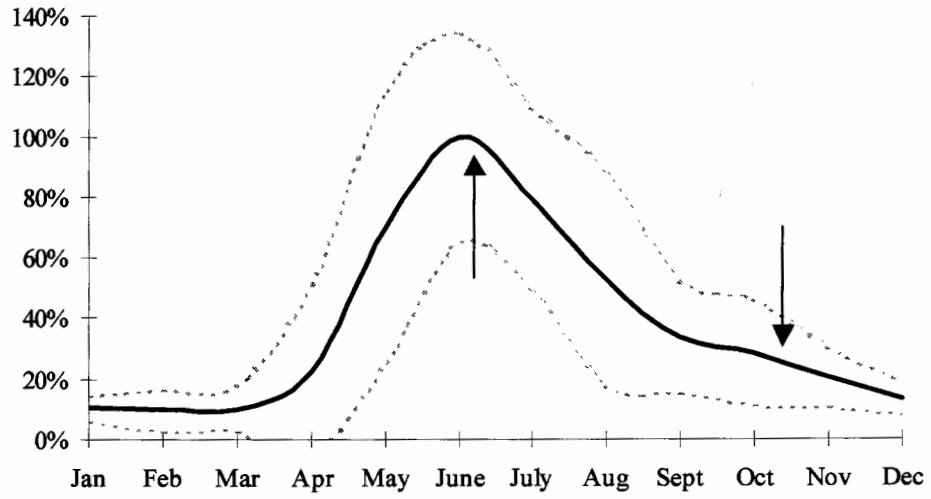

Figure 1.3 Average hydrograph of the Cordilleran Rivers expressed as % of maximum mean instantaneous discharge. The dashed lines represent the average ±2 standard deviations. Multiple year discharge data was taken from Environment Canada's HYDAT database (Environment Canada, 2001).

Table 1.1 Sample locations and key to station and sample numbers. Gauging stations refer to Environment Canada's (2001) hydrometric stations nearest to sample locations. Discharge data was obtained from Environment Canada. TSS is the suspended particulate measured at each station during the June and October 2002 field campaigns. Field duplicates are noted (dup), and the Fraser at Sheep Creek was sampled from the (W)est and (E)ast bank. Basin geology taken from Wheeler and Mcfeely (1991).

Station	Samples		River	gauging station	basin Area	mean annual discharge	June 2002 discharge	Oct 2002 discharge	TSS $mg \cdot l^{-1}$		Basin Geology
	June	Oct			km^2	$m^3 \cdot s^{-1}$	$m^3 \cdot s^{-1}$	$m^3 \cdot s^{-1}$	June	Oct	
1	101	201	Squamish at Cheekeye	08GA022	2330	237	545	80.9	50	7	arc volcanics, granitic intrusives, sedimentary rocks
2	102	202	Lillooet at Pemberton	08MG005	2160	124	321	49.6	12	33	
4	104	203	Cayoosh at Lillooet	08ME002	878	14.9	56.1	1.7	128	0.4	calcareous sediments, arc volcanics
5	105	--	Fraser at Gang Ranch	08MD013	146000	1520	5115	1360.8	124	--	transect of the Canadian Cordillera (see text)
7	107	205	Chilcotin at Farwell	08MB005	19300	101	238	58	89	6	neogene volcanics (andesites and basalts)
7	108	--	Chilcotin at Farwell (dup)	08MB005	19300	101	238	58	--	--	
8	109	206	Fraser at Sheep Cr (W)	08MC018	114000	1400	4500	1410	104	56	transect of the Canadian Cordillera (see text)
8	110	207	Fraser at Sheep Cr (E)	08MC018	114000	1400	4500	1410	151	65	
9	111	208	Blackwater	08KG001	12400	32.6	76.1	16.5	6	2	neogene volcanics (andesites and basalts)
10	112	209	Skeena at Hazelton	08EB003	25900	588	2680	550	135	7	arc volcanics, various marine and non-marine sediments
11	113	--	Skeena at Usk	08EF001	42200	--	4060	859	203	--	
12	114	210	Zymoetz at Terrace	08EF005	2980	105	450	105	177	7	arc volcanics, granitic intrusives
13	115	211	Skeena at Terrace	08EF001	42200	1016	4510	964	148	39	arc volcanics, various marine and non-marine sediments
13	116	212	Skeena at Terrace	08EF001	42200	1016	4510	964	138	40	
14	117	--	Nass at Greenville		--	--	--	--	107	--	
15	118	213	Nass at Canyon City	08DB001	18500	776	2590	722	116	610	
16	119	215	Nass at Meziadin		--	--	--	--	83	29	
17	120	216	Bulkley at Telkwa	08EE004	7360	134	617	103	61	4	arc volcanics
18	121	214	Fraser at McBride	08KA005	6890	196	732	135	33	32	Paleozoic shales and carbonates
19	122	217	Fraser at Tete Jaune	08KA007	1700	46	--	--	0	0	
20	123	218	N. Thompson Headwaters		--	--	--	--	23	4	Omenica metamorphic complex
21	124	219	N. Thompson at McLure	08LB064	19600	427	1620	188	14	2	Omenica metamorphic complex, neogene volcanics
23	126	221	Thompson at Spences Br	08LF051	54900	780	2650	348	13	2	transect of the Canadian Cordillera (see text)
24	127	222	Fraser at Alexandra	08MF005	217000	2710	9300	2160	26	59	
24	128	--	Fraser at Alexandra	08MF005	217000	2710	9300	2160	--	--	

The central regions of the Canadian Cordillera form the Intermontane Belt, meaning "between mountains". This belt has relatively low relief, and is a series of arc terranes of Late Triassic to Tertiary age that have been accreted onto the continental margin. The Intermontane Belt is composed of volcanic rocks of varying composition, and associated arc derived sediments, including clastics, shales, carbonates and cherts. This belt also contains significant Neogene back-arc flood basalts which are the dominant lithology in the Chilcotin and Blackwater watersheds. Further west are the coastal mountains, dominated by granitic intrusions, but also containing significant volcanic and sedimentary sequences. Some regions in the west have experienced considerable Quaternary volcanism, particularly the region drained by the Lillooet River. The most recent volcanic eruption in Canada occurred near the mouth of the Nass River at New Ayanish. Approximately 250 years ago 0.4 km^3 of basalt erupted, covering an area of 40 km^2, and killing approximately 2000 people (Brown, 1969).

1.4 STATUS OF PUBLICATIONS

Each of chapters 2, 3 and 4 of this thesis are intended as individual journal articles. Chapter 2, "On the role of sulphur in chemical weathering and atmospheric CO_2 fluxes: evidence from major ions, $\delta^{13}C_{DIC}$, and $\delta^{34}S_{SO4}$ in the rivers of the Canadian Cordillera" has been submitted to *Geochimica et Cosmochimica Acta*, and is now accepted for publication with minor revisions. Early in 2005, Chapter 3 "Dissolved and adsorbed rare earth element transport by rivers in the western Canadian Cordillera: influence of chemical versus physical erosion" will be submitted to *Chemical Geology*; and chapter 4, "Dissolved, adsorbed, organic bound and particulate mercury transport by

the Fraser, Skeena and Nass Rivers (British Columbia, Canada): the role of rock weathering" will be submitted to *Geochimica et Cosmochimica Acta*.

1.5 REFERENCES

Brown A. S. (1969) Ayanish lava flow, British Columbia. *Can. J. Earth Sci.* **6,** 1460-1468.

Environment Canada (2001) *Surface Water and Sediment Data* [HYDAT CD-ROM]. Atmospheric Environment Program, Water Survey of Canada, Environment Canada, Ottawa.

Gabrielse H. and Yorath C. J. (1991) Tectonic Synthesis. In *The Geology of the Cordilleran Orogen in Canada no. 4* (ed. H. Gabrielse and C. J. Yorath), pp. 677-705, Geological Survey of Canada.

Gabrielse H., Monger J. W. H., Wheeler J. O. and Yorath C. J. (1991) Tectonic Framework: Part A. Morphogeological belts, tectonic assemblages and terranes. In *The Geology of the Cordilleran Orogen in Canada no. 4* (ed. H. Gabrielse and C. J. Yorath), pp. 15-28, Geological Survey of Canada.

Meybeck M. (1979) Concentrations des eaux fluviales en éléments majeurs et apports en solution aux océans. *Rev. Geol. Dyn. Géogr. Phys.* **21,** 215-246.

Monger, J. W. H. (1997) Plate Tectonics and Northern Cordilleran Geology: An unfinished revolution. *Geoscience Canada* **24,** 189-198.

Ruddiman W.F. (ed.) (1997) *Tectonic Uplift and Climate Change*. Plenum, New York.

Wheeler J. O., McFeely P. (1991) Tectonic Assemblage Map of the Canadian Cordillera and Adjacent parts of the United States of America. Geological Survey of Canada, Map 1712a.

2 On the role of sulphur in chemical weathering and atmospheric CO_2 fluxes: evidence from major ions, $\delta^{13}C_{DIC}$, and $\delta^{34}S_{SO4}$ in the rivers of the Canadian Cordillera

2.1 OVERVIEW

Water samples from the Fraser, Skeena and Nass River basins of the western Canadian Cordillera were analysed for dissolved major element concentrations (HCO_3^-, SO_4^{2-}, Cl^-, Ca^{2+}, Mg^{2+}, K^+, Na^+), $\delta^{13}C$ of dissolved inorganic carbon (DIC), and $\delta^{34}S$ of dissolved sulphate in order to quantify chemical weathering rates and exchanges of CO_2 between the atmosphere, hydrosphere, and lithosphere. Weathering rates of silicates and carbonates were determined from major element stoichiometry and are consistent with $\delta^{13}C_{DIC}$ values (-9.8 to -3.7 ‰ $_{VPDB}$) produced by the following weathering reactions, in order of decreasing importance: (i) carbonate dissolution by carbonic acid (-8.2 ‰) > (ii) silicate dissolution by carbonic acid (-17 ‰) ≈ (iii) carbonate dissolution by sulphuric acid derived from the oxidation of sulphides (coupled *sulphide-carbonate weathering*) (+0.5 ‰). $\delta^{13}C_{DIC}$ values and mass balances illustrate that atmospheric equilibration does not significantly influence the isotopic composition of the rivers. The isotopic composition of dissolved sulphate (-8.9 to 14.1 ‰ $_{CDT}$) further supports this model. It reflects a dominantly sulphide source and is negatively correlated with $\delta^{13}C_{DIC}$, illustrating that sulphuric acid produced by the weathering of sulphides is dominantly neutralized by carbonates. These results illustrate that *sulphide-carbonate weathering* impacts the carbon isotopic composition of rivers. Comparison with data from the Ottawa and St. Lawrence River basins, however, illustrates that other factors such as landscape age (governed by tectonic uplift) and bedrock geology are probably important controls on the magnitude of *sulphide-carbonate weathering* – i.e. it is more significant in tectonically active areas where fresh sulphides are being more rapidly exposed to the surface.

Calculated DIC fluxes due to silicate weathering (63.6×10^3 mol C·km^{-2}·yr^{-1}) are equivalent to DIC fluxes due to *sulphide-carbonate weathering* (52.6×10^3 mol C·km^{-2}·yr^{-1}). Because, the latter transfers carbon to the atmosphere from the lithosphere (vice-versa for the first), this implies that *sulphide-carbonate weathering* provides a source of atmospheric CO_2 that offsets CO_2 drawdown caused by silicate weathering in this region.

Ultimately, the impact of *sulphide-carbonate weathering* on the atmosphere is dependant on the rate of coupled *sulphide-organic carbon deposition* in the ocean. On long time scales these two processes must be balanced, however, the two can be decoupled on time scales of ~$10^6 - 10^7$ years before marine concentrations of sulphate and calcium, and atmospheric concentrations of oxygen reach unreasonable limits. Sulphide based weathering of carbonates can therefore potentially impact atmospheric CO_2 budgets on time scales of millions to tens of millions of years. If *sulphide-carbonate weathering* is a significant process for other accretionary orogens found around the globe today and through the past (there is no reason to think otherwise), then it could, therefore, provide a previously unconsidered negative feedback to tectonically induced CO_2 drawdown and cooling, or a positive feedback for some global warming scenarios.

2.2 INTRODUCTION

One of the shortfalls in our ability to understand global climate evolution throughout Earth's history is the inability to quantify the natural sources and sinks of the greenhouse gas carbon dioxide (CO_2). The "missing sink" of atmospheric carbon (e.g. Tans et al., 1990; Schindler, 1999) is an example of this shortfall for recent times and short time scales – a period that is very rich in both direct information (e.g. emission rates of society; trapped gas bubbles in ice-cores) and high-quality proxy data such as the oxygen isotopic composition of high resolution marine sediments (Emiliani and Edwards, 1953; Emiliani,1955; Mix and Ruddiman, 1984). Determining the composition of the earth's atmosphere on longer time scales (geological) relies entirely on proxy data such as the isotopic composition of paleo-oceans as recorded in marine sediments (see Shackleton, 1985; 1987; Veizer et al. 1999 and references therein;), or at very long time scales, simply by evidence of the continued presence of water and life (Rankama, 1954; Mojzsis et al., 1996) – the argument being, that if liquid water and life existed, the atmosphere must have been of a suitable composition and temperature. As explained by Sagan and Mullen (1972) the presence of liquid water during earliest earth history, because the sun was 25% less luminous, requires a significantly different atmosphere than that we have today. These lines of evidence, although they are not direct measurements, establish boundary conditions for models of the composition of the atmosphere. The models are based on known processes such as volcanism, tectonism, ice-cover, primary productivity, others, and of course weathering rates, and are used to test how these processes interact and which are the most important for the evolution of the Earth's surface environment.

The core of many of these models (e.g. Berner and Kothavala, 2001) is the theory put forth by Walker et al. (1981). They proposed that a negative feedback between the chemical weathering rate of silicate minerals and atmospheric CO_2 concentration is the mechanism that regulates the greenhouse state of the atmosphere and thus maintains climate (temperature) stability. The premise of the feedback is that atmospheric CO_2 accumulation warms the atmosphere which accelerates the hydrological cycle due to the Clausius-Clapeyron relationship between temperature and the vapour pressure of water. At warmer temperatures, more precipitation causes faster chemical weathering of silicate minerals, which in turn draws down atmospheric CO_2 and cools the atmosphere.

This model is generally accepted, however serious questions remain despite the modelling efforts and some new high-quality databases on major river chemistry (e.g. Gaillardet et al., 1999; Galy et al., 1999) and its changes through time (Derry and France-Lanord, 1996). For example, Huh and Edmond (1999) claim that factors such as physical erosion rates driven by tectonic uplift, the geographic distribution of lithologies, frost shattering, and glaciation have a greater influence on chemical weathering rates than climate (see also Ruddiman, 1997). The snowball earth theory (Hoffman and Schrag, 2002) has clarified that the paleo-geography of the continents can be a dominant control on climate. It has recently been shown that the cycle of deposition/weathering of sulphide minerals on episodically exposed continental shelf regions could significantly impact the alkalinity budget of the oceans, and therefore the capacity of the oceans to absorb atmospheric CO_2 (Derry and Murray, 2004; Turchyn and Schrag, 2004).

A primary objective of this chapter is to demonstrate that another process can significantly impact atmospheric CO_2 on time scales similar to those proposed for the

silicate weathering feedback by Walker et al. (1981). Using the geochemistry of large rivers, chemical weathering of an accretionary orogen on the west coast of North America is investigated – the Canadian Cordillera. The results indicate an important weathering process to be the weathering of sulphide minerals (~pyrite) which releases sulphuric acid that is subsequently neutralized by weathering carbonate minerals. This process is called coupled "*sulphide-carbonate weathering*", henceforth SCW. The rate of SCW is determined by major ion stoichiometry and carbon isotope systematics.

SCW has the opposite effect on the atmosphere as silicate weathering – while silicate weathering consumes atmospheric CO_2 and transfers it to the lithosphere, SCW transfers CO_2 from the lithosphere to the atmosphere. Derry and Murray (2004) comment that changes in marine sulphate can change the oceans alkalinity budget, but importantly also point out that the impact is dependant on accompanying shifts in the concentrations of major cations. Ultimately, the amount of CO_2 released by SCW that remains in the atmosphere is determined by the rate of coupled "*sulphide-organic carbon sedimentation*" (SOCS) in the oceans. On long time scales, the geological record indicates the composition of the oceans and atmosphere has remained relatively constant (e.g. Garrels and Perry 1974; Kump, 1989) so the two must be equivalent (SCW=SOCS). However, controls on the two processes differ and are not directly linked (dominantly uplift, lithology, and climate for SCW; and ocean circulation, basin geometry, and trophism for SOCS), so it is probable that imbalances occur. The imperfect coupling of the carbon and sulphur cycles has long been known (Veizer et al., 1980; Kump, 1993). It has become all the more evident by the work of Paytan et al. (1998) whose high resolution comparison between seawater sulphate and marine carbonate carbon isotope

records reveals no clear systematic coupling between the sulphur and carbon cycles over one to several millions of years. Kurtz et al. (2003) also illustrate such a decoupling by showing that the ratio of the burial rate of pyrite sulphur to organic carbon has varied through the Cenozoic. Mass balance shows that the inorganic carbon in the atmosphere-ocean system can easily double without strongly impacting sulphate or calcium concentrations in the oceans or oxygen in the atmosphere. Variations in the rate of SCW can therefore potentially impact the composition of the atmosphere significantly.

In this chapter it is shown that in the case of the Canadian Cordillera, the magnitude of SCW is the same as that of silicate weathering, and so the transfer of CO_2 from the atmosphere to the lithosphere via the silicate weathering pathway (Walker et al., 1981) is potentially offset – depending on the rate of SOCS. The rate of SCW for different terrains and climates around the world will differ, however, the Canadian Cordillera is fairly representative of accretionary orogens and so, it is reasonable to expect SCW to be a significant process in other orogenies as well.

2.3 CHEMICAL WEATHERING AND THE CARBON CYCLE

Various methods have been developed to quantify silicate versus carbonate weathering rates using river chemistry. Some key examples include: mass balance approaches using dissolved major elements (e.g. Garrels and Mackenzie, 1971; Probst et al., 1994; Blum et al., 1998), an inversion method that uses dissolved major element ratios and dissolved $^{87}Sr/^{86}Sr$ (Negrel et al., 1993; Gaillardet et al., 1999), and isotopic methods that use dissolved $^{87}Sr/^{86}Sr$ composition (e.g. Stallard and Edmond, 1983; Palmer and Edmond, 1992; Edmond et al., 1995) or $\delta^{13}C$ of dissolved inorganic carbon (Telmer and Veizer, 1999). While these methods tend to return results of the same order

of magnitude, there is still no consensus on how silicate weathering rates can be determined from river chemistry. One reason is the dissolved composition of rivers is usually dominated by the dissolution products of carbonate minerals. This is even true in regions where carbonates are only present in small quantities (e.g. Drever and Hurcomb, 1986; Blum et al., 1998; Telmer and Veizer, 1999). The silicate weathering signal because it is only a minor component of the dissolved load of rivers, is therefore difficult to determine (low signal to noise ratio). For example, the $^{87}Sr/^{86}Sr$ method requires well defined end-member ratios. This works well in regions with large isotopic contrasts and pure end-members like the Guyana Shield (Stallard and Edmond, 1983) but in some systems such as the Himalayas, the common assumptions do not apply and so estimates are much less certain (Dalai et al., 2003; Oliver et al., 2003). To avoid these problems, two independent methods are used to apportion weathering to carbonate and silicate lithologies: (i) major element stoichiometry and (ii) carbon isotopes.

The use of carbon isotopes to identify weathering sources has been considered difficult because it is thought that equilibration with atmospheric CO_2 will obfuscate weathering signals. However, it appears that equilibration is a much slower process than the average residence time of water in rivers, perhaps because almost all rivers are over saturated with CO_2 relative to the atmosphere. For example, Telmer and Veizer (1999) found no evidence of atmospheric exchange in the Ottawa River and were able to effectively use carbon isotopes to separate carbonate and silicate weathering. As well, oceanographers frequently treat carbon isotopes as conservative tracers in estuaries and use them to separate terrestrial from marine water masses (Fry, 2002). Yang et al. (1996) found carbon isotopes in the headwaters of the St. Lawrence River to be isotopically

equilibrated with atmospheric CO_2 but these waters come from the great lakes which have residence time of hundreds of years. Within the St. Lawrence itself, Yang et al. (1996) found carbon isotopes to be conservative tracers of different water masses. As presented below, no evidence is found of atmospheric equilibration of dissolved inorganic carbon isotopes in the rivers of the Canadian Cordillera. Furthermore, carbon isotopes, unlike Sr isotopes, allow the rate of coupled sulphide-carbonate weathering (SCW) to be quantified.

2.3.1 Carbonic Acid Based Weathering

Simplified reactions and generalized minerals can be used to describe the relationship between chemical weathering and atmospheric CO_2:

$$CO_2 + H_2O + CaCO_3 \rightarrow 2HCO_3^- + Ca^{2+} \quad (1)$$

$$2CO_2 + 3H_2O + CaSiO_3 \rightarrow 2HCO_3^- + Ca^{2+} + H_4SiO_4 \quad (2)$$

Carbonic acid (formed by the dissolution of CO_2 in water) is most abundant in soils where the partial pressures of CO_2 are one or two orders of magnitude higher than in the atmosphere due to organic matter decay (Cerling et al. 1991). Because organic matter is composed of atmospheric carbon that has been fixed by photosynthesis, carbonic acid in soils can be considered as atmospheric CO_2. Both the above reactions therefore consume atmospheric CO_2. When the dissolved products of these reactions are transported to the oceans in river water, carbonate minerals are formed by the reverse of equation 1. Carbonate weathering followed by carbonate precipitation therefore simply represents the translocation of carbonate rocks on land to the sea. Since the residence time of bicarbonate (HCO_3^-) in the oceans is estimated to be 83,000 years (Berner and Berner,

1987), carbonate weathering and carbonate precipitation must be balanced on roughly the same time scale (~10^5 years). Carbonate weathering therefore has no impact on atmospheric CO_2 levels on times scales greater than 10^5 years. On shorter timescales, imbalances could occur that could, for example, cause accumulation or depletion in the atmosphere. When carbonates are precipitated from Ca-Mg silicate weathering products (sum equation 2 and reverse of equation 1), one of the two moles of CO_2 involved is transferred from the atmosphere to the lithosphere in the form of carbonate rocks. Garrels and Perry (1974) estimate the residence time of calcium carbonate in sedimentary rocks to be 356 million years (~10^8 years) although shorter times have also been used (e.g. Derry and France-Lanord, 1996, use 150 Ma). Silicate weathering could therefore impact atmospheric CO_2 levels at timescales as long as ~10^8 years.

However, rates of volcanism and estimated atmospheric CO_2 fluctuations in the Phanerozoic suggest balance between silicate weathering and carbonate recycling is attained on somewhat shorter time scales. During the Paleozoic, volcanic outgassing averaged $3.3 \pm 1.1 \times 10^{14}$ g C·yr^{-1} which is enough to double the mass of carbon in the atmosphere-ocean system (fluid carbon) in roughly 400,000 years (Holland, 1978). Berner (1998) and Berner and Kothvala (2001) claim that since the Devonian, the atmosphere has attained a maximum of roughly 5 times current CO_2 levels. This implies that volcanic outgassing (carbonate recycling) and silicate weathering are balanced on timescales of ~10^6 to 10^7 years.

The relationship between CO_2 drawdown and the weathering of Na and K silicates is less clear. Na^+ and K^+ can be involved in reverse weathering reactions which release CO_2 (e.g. Mackenzie and Kump, 1995); and they can be involved in basalt

alteration reactions (e.g. Humphris and Thompson, 1978; Hardie, 1983) possibly a source of Ca^{2+} to the oceans that is an indirect result of silicate weathering on land.

2.3.2 Sulphuric Acid Based Weathering

Coupled *sulphide carbonate weathering* has been shown to be an important chemical weathering process in many glacial environments (e.g. Anderson et al., 2000; Tranter et al., 2002) and is an important component of rock weathering at the catchment scale (Hercod et al., 1998). Others have commented on the significance of the contribution of sulphide oxidation to the chemical load of the Ganga-Brahmaputra and Yamuna rivers in the Himalayas (Galy and France-Lanord, 1999; Dalai et al., 2002a, b), and in western and northern Canadian river systems (Gaillardet et al., 2003; Millot et al., 2003). However, the impact on atmospheric CO_2 due to SCW has not been quantified, nor has it been considered in global carbon mass balances.

On timescales of 10^6 to 10^7 years (as per above) silicate weathering is proposed to provide a long-term sink for atmospheric CO_2 by transferring it to the carbonate reservoir (equation 3).

$$CaSiO_3 + CO_2 \rightarrow CaCO_3 + SiO_2 \quad (3)$$

Pyrite oxidation (equation 4) coupled with carbonate dissolution by sulphuric acid (equation 5), could be an important source of atmospheric CO_2 (net reaction: equation 6) on equivalent or shorter timescales.

$$\tfrac{1}{2} FeS_2 + \tfrac{15}{8} O_2 + H_2O \rightarrow \tfrac{1}{4} Fe_2O_3 + H_2SO_4 \quad (4)$$

$$H_2SO_4 + CaCO_3 \rightarrow Ca^{2+} + SO_4^{2-} + H_2O + CO_2 \quad (5)$$

$$\tfrac{1}{2}FeS_2 + CaCO_3 + \tfrac{15}{8}O_2 \rightarrow \tfrac{1}{4}Fe_2O_3 + Ca^{2+} + SO_4^{2-} + CO_2 \quad (6)$$

$$CO_2 + H_2O \rightarrow CH_2O + O_2 \quad (7)$$

$$\tfrac{1}{4}Fe_2O_3 + SO_4^{2-} + CH_2O + Ca^{2+} \rightarrow \tfrac{1}{2}FeS_2 + CaCO_3 + \tfrac{7}{8}O_2 + H_2O \quad (8)$$

On longer timescales, in order to attain steady-state ocean and atmosphere composition, the pyrite and carbonate weathering that occurs on land must be reversed in the oceans by sedimentation processes (e.g. Garrels and Perry, 1974). However, as discussed above, the residence time of HCO_3^- (0.083 Ma) is much shorter than the residence time of SO_4^{2-} (8.7 Ma) in seawater. Thus the removal of HCO_3^- from seawater by carbonate mineral formation (reverse of equation 1) is not directly coupled to the removal of SO_4^{2-} by pyrite formation. The implication is that, when coupled pyrite-carbonate weathering on land (equation 6) exceeds photosynthesis (equation 7; CH_2O represents simplified organic matter) and subsequent organic carbon driven pyrite deposition in the oceans (equation 8), there will be a net flux of CO_2 into the ocean-atmosphere system, and vice-versa. Using the residence time of SO_4^{2-} as a constraint, imbalances can conceivably occur on timescales of up to 10^7 years.

The magnitude of possible imbalances can be evaluated as follows: based on current ocean and atmosphere composition, if SCW provided enough carbon to double the combined ocean-atmosphere inorganic carbon reservoir (3.4×10^{18} mol, Garrels & Perry, 1974), marine concentrations of SO_4^{2-} and Ca^{2+} would increase from 28.9 to 31.2 mM and from 10.5 to 12.9 mM respectively; meanwhile, atmospheric oxygen (O_2) concentrations would decrease from 21 to 18%. Therefore, relatively small imbalances in the sulphur and oxygen cycles can lead to significant changes in atmospheric CO_2.

Precipitation of gypsum from seawater removes any limitations imposed by concentrations of marine SO_4^{2-} and Ca^{2+} leaving atmospheric O_2 as the singular most important constraint.

2.4 STUDY AREA

Water samples were collected from 12 rivers in the Canadian Cordillera, the Fraser, Skeena and Nass drainage basins, in June and October 2002 (Figures 1.1 and 1.2, chapter 1) Dissolved concentrations of SO_4^{2-}, Cl^-, HCO_3^-, F^-, NO_3^-, Ca^{2+}, Mg^{2+}, Na^+, K^+, the $\delta^{13}C$ in dissolved inorganic carbon ($\delta^{13}C_{DIC}$), pH, temperature, conductivity, and charge balance from these samples are reported. Cameron (1996) and Cameron et al. (1995), also investigated the geochemistry of the Fraser River system in the southern Canadian Cordillera. Using existing data from the ENVIRODAT database (Environment Canada, 1993) and new data, they report major anions and cations, dissolved trace and ultratrace elements, and the isotope ratios of O, H, S, C and Sr. They conclude that the control on chemistry is the diverse geological terranes of the various catchments and an overprinted anthropogenic signal but do not quantify this signal. Neither do they elaborate on chemical weathering rates. In terms of CO_2 fluxes, they only consider the instantaneous partial pressure of CO_2 in waters and state that this is due to the decay of vegetation on land and that it may be influenced by forestry practices. With this study, the existing databases are augmented with new data from different localities and focus on chemical weathering rates and mechanisms.

The portions of the Fraser, Skeena and Nass watersheds considered by this study drain a combined area of 280,000 km^2, with cumulative annual discharge averaging 4739 m^3/s (Environment Canada, 2001a). This represents approximately 0.2% of the global

land mass, and 0.4% of the global annual river discharge to the oceans (Meybeck, 1979). A detailed description of the study area is given in Chapter 1.

2.5 METHODS

Figure 2.1 is a flowchart illustrating the field and laboratory methods used to collect and analyse the water samples.

2.5.1 Field Methods

In June and October 2002, 47 river water samples were collected from 12 rivers during the peak (June) and trough (October) hydrograph.

Using a Hydrolab® "Quanta-G" multimeter, temperature, pH, specific conductivity, oxidation-reduction potential, and dissolved oxygen were measured *in-situ*. Bicarbonate alkalinity was measured within 10 minutes of sample collection by titration with 0.1600 N sulphuric acid, using a HACH® digital titrator. The precision and accuracy of this method, determined by replicate analyses of samples in the field, and by multiple analyses of a certified alkalinity standard, are better than ± 5 % in all cases.

2.5.2 Water Samples

Water samples were collected at a depth of approximately 30 cm in a clean 1 L HDPE bottle fixed to the end of a 2 m pole. Sample locations were chosen such that the main flow of the river could be reached using the sampling pole. Water was ladled into six clean 1 L HDPE bottles temporarily until the samples could be filtered. All samples were filtered on site through Millipore 0.45 μm HVLP polyvinyl filter membranes within one hour of collection except for samples: 122, 125, 127, and 128, which were stored in

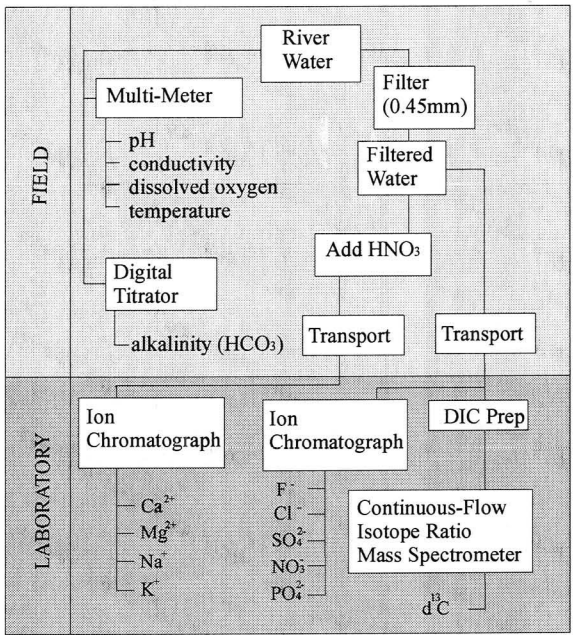

Figure 2.1 Flowchart of sample collection, preservation and analysis methods (modified from Telmer and Veizer, 1999).

the 1 L HDPE bottles with no head-space, in the dark, and at 4 °C until they could be filtered (within 24 hours of collection).

Cation and anion samples were stored in HDPE bottles. These bottles were previously unused, and were cleaned by rinsing several times with 18.2 MΩ deionized water (DI), soaking in DI for at least 24 hours, and then rinsing again with DI. Hall (1998) has shown that this procedure produces excellent blanks and in fact that rigorous acid cleaning can add contaminants to the bottles and/or lower recoveries due to surface reactions. Prior to filling, the bottles and caps were rinsed three times with filtered sample water. Cation samples were injected with concentrated (16 N) Anachemia Environmental Grade Nitric Acid so that the final acid strength in the samples was 0.08N. No preservative was added to the anion samples. Samples for $\delta^{13}C_{DIC}$ analysis were collected in pre-ignited 30 mL amber glass bottles with teflon lined caps (June sampling) and with polycone caps (October sampling). These bottles and caps were rinsed three times with filtered sample water before filling to overflowing with filtered water. $\delta^{13}C_{DIC}$ samples were collected in triplicate at each station. No preservative was added to the $\delta^{13}C_{DIC}$ samples. Samples for the determination of sulphur isotopes were collected in 1L glass bottles and acidified to pH 2 by addition of HCl. A small amount of $BaCl_2$ solution (saturated) was added to precipitate $BaSO_4$ which was then collected on Millipore 0.45 μm HA ashless filter membranes. All water samples were stored at 4°C in the dark from the time of collection to the time of analysis. Field blanks were collected using deionized water transported into the field. These samples were filtered, preserved, stored and analysed in the same manner as the regular samples. Concentrations in the field blank samples were below the limits of detection for all analytes.

2.5.3 Laboratory Analyses

Analyses were performed at the University of Victoria, School of Earth and Ocean Sciences except for sulphur isotopes which were determined at University of Calgary, Department of Physics and Astronomy, Isotope Science Laboratory.

Cations and Anions

Major dissolved cations (Na, K, Mg, Ca) and anions (F, Cl, SO_4, NO_3) were analysed using a Dionex DX-600 ion chromatograph. Instrumental precision was better than ± 6% for all species. Accuracy for the cations was determined by analysing SLRS-4 River water standard reference material (National Research Council of Canada). Results for the cations agreed with the certified values of SLRS-4 within 5% for all ions except Mg, which agreed within 10%.

Carbon and Sulphur Isotopes

All isotopic data are reported in the delta (δ) scale, which denotes a difference in the isotopic ratio in parts per thousand (‰) as compared to the isotopic composition of an accepted standard. Thus where R represents an isotopic ratio ($R = {}^{13}C / {}^{12}C$ in the case of carbon, and $R = {}^{34}S / {}^{32}S$ in the case of sulphur), $\delta = [(R_{sample} \div R_{standard}) - 1] \times 1000‰$. All carbon isotopic ratios ($\delta^{13}C$) are reported relative to the composition of Vienna Pee Dee Belmnite (vpdb), and the isotopic ratios of sulphur ($\delta^{34}S$) are reported relative to to Canyon Diablo Troilite (CDT).

$\delta^{13}C_{DIC}$ samples were prepared for analysis off line by the following method. For each sample, a 3mL aliquot of sample water was pipetted into a clean 10mL glass auto-sampler vial. The vial was sealed with a gas tight rubber septum. Immediately after sealing, the vial was flushed with pressurized helium to remove atmospheric carbon from

the vial. Ten drops of concentrated phosphoric acid was then injected into each vial to liberate the DIC as CO_2 gas. The samples were shaken and allowed to equilibrate overnight before $\delta^{13}C$ analysis using a Finnigan MAT delta plus XL isotope ratio mass spectrometer (IRMS) with Gasbench and TC/EA peripherals.

Precision and accuracy for the method was found to be better than ± 1 ‰ for all samples based on replicate analyses of samples, standards, and field duplicates. Because the samples were not treated with $HgCl_2$ in the field (as others have done, e.g. Telmer and Veizer, 1999) the samples were collected in triplicate. Six randomly selected samples were re-analysed after one month, and after two months of storage. The results after one and two months of storage agreed with the original results within ± 1‰ indicating that significant isotopic shifts between the time of collection and analysis did not occur. To test for atmospheric contamination during analysis, sample blanks were created by flushing empty vials with He, sealing them, then injecting them with phosphoric acid. Contamination was negligible in all cases.

$\delta^{34}S_{SO4}$ was measured on $BaSO_4$ using a Carlo Erba NA 1500 elemental analyzer interfaced to a VG Prism II Continuous Flow-Isotope Ratio Mass Spectrometry. $BaSO_4$ is scraped off filter membranes and packed into tin cups, which are dropped by auto sampler onto a quartz tube combustion column. Released gasses are swept by a helium carrier stream into a gas chromatograph to separate SO_2, CO_2 and NOx and then carried into the ion source of the mass analyzer. Precision and accuracy of these analyses were ±0.5‰, determined by comparison to internal lab standards and International Standards: NBS 127, IAEA S-1, IAEA S-2.

2.6 RESULTS

2.6.1 Major Elements and Charge Balance

Table 2 lists the analytical results for the Cordilleran waters and the calculated maximum, minimum, mean, median and standard deviation for each parameter. In general, the major element concentrations observed for the Cordilleran rivers follow the pattern $Ca^{2+}>Mg^{2+}>Na^{+}>K^{+}$ for the cations, and $HCO_3^{-}>>SO_4^{2-}>Cl^{-}>NO_3^{-}>F^{-}$, and are similar to the concentrations observed by others in these rivers (Cameron et al., 1995; Gaillardet et al., 2003). Comparison of the dissolved concentrations of these waters to the global major river data compiled by Gaillardet et al. (1999) shows the Cordilleran rivers to be moderately more dilute than the global averages.

Charge balance is listed in Table 2.1 as a percentage of the total ionic concentration:

$$Charge\_Balance = \left(\frac{(\Sigma cations(eq) - \Sigma anions(eq))}{(\Sigma cations(eq) + \Sigma anions(eq))} \right) \times 100\% \qquad (9)$$

where $\Sigma cations$ is the charge equivalent sum of Na^{+}, K^{+}, Mg^{2+}, Ca^{2+}, and $\Sigma anions$ is the charge equivalent sum of F^{-}, Cl^{-}, NO_3^{-}, SO_4^{2-}, and HCO_3^{-}. Because electro-neutrality is a thermodynamic requirement for all solutions, the charge balance can be used as an indicator of analytical quality. If *Σ positive charge (cations)* deviates from *Σ negative charge (anions)* by an amount that is greater than the analytical uncertainty, there must either be dissolved ionic species present that have not been accounted for, or an analytical

Table 2.1 The major chemistry, charge balance and δ13CDIC for the Fraser, Nass and Skeena rivers and their main tributaries, Canadian Cordillera, BC, Canada.

Stat no.	Sam no.	River	T °C	pH	SpC uS/cm	pCO_2 mbar	HCO_3^-	Na^+	K^+	Mg^{2+}	Ca^{2+}	F^-	Cl^-	SO_4^{2-}	NO_3^-	Chg Bal %	$\delta^{13}C$ vpdb ‰	$\delta^{34}S$ cdt ‰
										µmol/L								
		June Campaign																
1	101	Squamish Cheekeye	7.0	5.9	12	6.1	80	22	12	13	35	1	9	11	3	6.5	-9.8	
2	102	Lillooet Pemberton	9.3	6.8	35	2.6	235	52	26	29	121	2	14	55	4	1.3	-7.1	
3	103	Cayoosh Duffy Lk	7.0	7.3	33	0.9	265	45	19	31	121	5	20	33	5	1.1	-8.4	
4	104	Cayoosh Lillooet	7.2	7.5	59	1.2	518	47	25	50	257	4	16	67	4	0.8	-5.9	
5	105	Fraser Gang Ranch	13.6	8.3	94	0.3	1009	70	18	126	429	2	13	55	6	2.5	-7.6	
7	107	Chilcotin Farwell	13.7	7.9	60	0.5	586	87	24	84	228	3	8	71	ud	-0.2	-5.9	
7	108	ChilcotinFarwell(dup)	14.1	7.9	60	0.5	587	89	26	83	226	3	9	70	ud	-0.3	-5.9	
8	109	Fraser Sheep Cr(W)	13.2	8.2	90	0.4	1051	62	15	120	430	2	11	52	6	0.0	-7.5	
8	110	Fraser Sheep Cr(E)	13.3	8.3	91	0.4	1069	61	15	120	422	2	12	56	6	-1.8	-7.7	
9	111	Blackwater	17.8	8.4	104	0.3	1299	213	63	272	317	5	10	13	ud	4.1	-9.0	
10	112	Skeena Hazelton	7.1	7.7	48	0.6	446	43	9	56	211	2	4	55	3	1.8	-6.8	
11	113	Skeena Usk	7.7	8.2	47	0.2	472	43	11	53	201	2	4	49	3	-1.5	-7.1	
12	114	Zymoetz Terrace	5.9	8.6	37	0.1	418	33	11	33	167	2	5	18	3	-1.9	-7.1	
13	115	Skeena Terrace	8.1	8.3	48	0.1	452	45	12	55	213	2	5	48	3	3.0	-6.7	
13	116	Skeena Terrace	7.5	8.4	44	0.1	448	48	12	46	200	4	15	35	4	1.0	-7.8	
14	117	Nass Greenville	7.7	7.6	55	0.9	517	43	14	74	238	2	5	67	5	1.3	-7.3	
15	118	Nass Canyon City	7.6	7.8	59	0.6	540	44	10	77	250	2	5	76	5	0.3	-6.2	
16	119	Nass Meziadin	6.3	7.7	64	0.8	579	44	9	85	275	2	4	89	5	0.3	-6.2	
17	120	Bulkley Telkwa	8.3	7.9	39	0.4	408	44	11	41	178	2	6	27	2	2.3	-8.0	
18	121	Fraser McBride	9.2	8.5	91	0.2	881	26	15	145	413	2	6	123	5	0.6	-6.1	
19	122	Fraser Tete Jaune	10.1	9.0	100	0.1	1047	29	8	206	436	2	10	120	5	0.6	-5.5	
20	123	N.ThompsonHeadwat	8.5	8.3	52	0.2	474	16	27	46	248	2	4	66	10	0.7	-5.2	
21	124	N.Thompson McLu	10.5	7.9	50	0.4	469	38	20	53	229	3	6	46	7	3.9	-6.0	
23	126	Thompson Spences	12.5	8.3	61	0.2	611	70	24	71	263	3	14	53	6	1.5	-6.5	
24	127	Fraser Alexandra	12.5	8.5	79	0.2	979	59	19	96	367	2	11	56	5	-5.0	-7.4	
24	128	Fraser Alexandra	12.5	8.5	79	0.2	979	61	20	98	379	2	12	55	8	-3.6	-7.3	
		October Campaign																
1	201	Squamish Cheekeye	8.4	6.4	25	4.4	167	62	16	7	90	1	32	31	2	1.5	-5.9	3.2
2	202	Lillooet Pemberton	6.9	7.0	67	6.9	991	153	31	51	240	2	56	126	ud	-26.0	-4.1	1.6
4	203	Cayoosh Lillooet	9.3	7.7	115	1.4	1040	72	25	120	574	4	20	226	2	-1.1	-3.7	-8.9
7	205	Chilcotin Farwell	8.6	7.9	69	0.6	709	113	22	111	262	2	8	65	ud	1.9	-4.3	-2.2
8	206	Fraser Sheep Cr(W)	8.6	7.8	111	1.2	1215	93	12	169	525	1	62	93	4	0.8	-6.6	7.5
8	207	Fraser Sheep Cr(E)	8.6	7.8	111	1.3	1252	94	12	178	528	1	18	93	4	1.9	-6.4	7.8
9	208	Blackwater	7.6	8.5	146	0.5	2065	261	59	415	437	5	10	19	ud	-2.2	-8.0	8.0
10	209	Skeena Hazelton	5.0	7.8	75	0.8	718	59	5	83	325	1	4	112	3	-3.8	-4.8	-5.0
12	210	Zymoetz Terrace	6.9	7.4	52	1.5	583	95	12	178	529	1	4	39	2	39.0	-5.1	1.6
13	211	Skeena Terrace	7.8	7.4	56	1.5	583	43	7	49	255	1	5	46	2	-1.9	-4.9	-2.8
13	212	Skeena Terrace	7.8	7.4	56	1.5	583	45	7	52	261	1	6	56	2	-2.0	-5.3	-2.7
15	213	Nass Canyon City	6.9	7.7	75	0.6	473	49	11	84	303	1	10	98	4	9.8	-6.0	-4.0
16	215	Nass Meziadin	5.4	7.5	84	1.5	766	56	6	127	364	1	7	171	5	-3.6	-4.8	-4.7
17	216	Bulkley Telkwa	8.3	7.6	43	0.7	442	37	7	37	252	1	4	140	6	-8.2	-5.2	-0.3
18	214	Fraser McBride	6.3	7.7	99	1.3	905	28	10	172	440	1	6	39	ud	12.1	-4.7	9.2
19	217	Fraser Tete Jaune	6.8	7.7	117	1.6	1204	31	5	264	498	2	61	166	5	-1.4	-4.5	13.5
20	218	N.Thompson Headwa	5.3	7.6	73	1.0	673	15	27	62	336	1	3	107	7	-3.5	-4.4	14.1
21	219	N.Thompson McLu	10.9	7.8	69	0.8	696	46	20	73	321	2	7	67	4	0.6	-4.6	9.5
23	221	Thompson Spences	13.4	8.0	77	0.5	791	98	22	95	331	2	22	85	4	-0.8	-5.9	4.0
24	222	Fraser Alexandra	10.2	8.0	102	0.8	1126	93	15	154	475	1	17	81	4	2.1	-6.8	5.4
		Max	17.8	9.0	146	6.9	2065	261	63	415	574	5	62	226	10	39.0	-3.7	14.1
		Min	5.0	5.9	12	0.1	80	15	5	7	35	1	3	11	2	-26.0	-9.8	-8.9
		Median	8.3	7.8	66	0.6	599	49	15	83	269	2	9	61	4	0.6	-6.1	2.4
		Mean	9.1	7.9	70	1.1	726	65	17	101	309	2	13	72	4	0.7	-6.3	2.7
		Stdev	2.8	0.6	28	1.4	365	46	12	77	126	1	14	44	2	7.8	1.4	6.5

problem. The near zero charge balance for the Cordilleran samples indicates that the ionic constituents of these waters are well described by the major elements measured, except for samples 202 and 210.

Excess positive charge has been calculated for sample 210 collected from the Zymoetz River, October, 2002 suggesting these waters contain unaccounted anions. It has been shown that river waters can contain high concentrations of organic anions (dissociated organic acids) relative to the concentration of dissolved inorganic material, leading to a charge imbalance between inorganic cations and anions (Beck et al., 1974). This is a probable explanation for this sample.

Excess negative charge has been calculated for sample 202, collected from the Lillooet River, October, 2002. The upper Lillooet watershed (where the sample was collected) drains a hydrothermally active region with numerous documented hot and cold springs (Read, 1977). Thus it is possible that this water contains high concentrations of cations such as Li or Ba that are normally at low concentration and that were not measured. Analytical problems are ruled out because of the excellent results for all other samples and all standards including samples that bracketed these waters in the analytical run.

2.6.2 Dissolved Inorganic Carbon and $\delta^{13}C_{DIC}$

The concentration of Dissolved Inorganic Carbon (DIC) is the sum of the inorganic carbon species in a given solution:

$$DIC = [H_2CO_3^*] + [HCO_3^-] + [CO_3^{2-}] \quad (10)$$

$$[H_2CO_3^*] = [CO_{2(aq)}] + [H_2CO_{3(aq)}] \quad (11)$$

Both bicarbonate (HCO_3^-) and dissolved inorganic carbon (DIC) concentrations are reported in Table 2.1. The speciation of DIC is pH controlled (Stumm and Morgan, 1996). The pH range of the Cordilleran waters ranges from 5.9 for the June sample of the Squamish River (Sample 101) to 9.0 for the June sample of the Fraser River at Tete-Jaune (Sample 122), with an average of 7.9 for all of the samples. Therefore, bicarbonate (HCO_3^-) makes up more than 90% of the DIC in all cases, except for the Squamish River (HCO_3^- is 28% of the DIC in June, and 53% in October) and Lillooet River (HCO_3^- is 72% of the DIC in June, and 81% in October). The carbon isotopic signature of the DIC in the Cordilleran waters is therefore equivalent to that of dissolved HCO_3^- for all except the Squamish River.

The measured $\delta^{13}C_{DIC}$ values for the Cordilleran waters range from -3.7 to -9.8‰$_{vpdb}$, with the October samples being ~2‰ heavier than the June samples on average. Seasonal variability was greater in the smaller rivers such as Cayoosh Creek. The Thompson, Fraser and Blackwater Rivers were approximately 1‰ heavier in October than in June. The observed seasonal variability of $\delta^{13}C_{DIC}$ in the large rivers is similar to differences in field duplicates and sample splits thus can almost be treated as invariant.

The $\delta^{13}C_{DIC}$ values measured during this study are significantly heavier than $\delta^{13}C_{DIC}$ measured in the Ottawa River and tributaries (-17.4 to -7.3‰) (Telmer and Veizer 1999), and in the Rhine River and tributaries (-6.7 to -14.4‰) (Buhl et al. 1991; Flintrop et al., 1996). The Cordilleran $\delta^{13}C_{DIC}$'s are comparable to values measured in the Fraser River system (Cameron et al. 1995), the Danube River system (Pawallek and

Veizer 1994), the Ganga-Brahmaputra River system (Galy and France-Lanord, 1999) and the Indus River system (Karim and Veizer, 2000).

2.6.3 Dissolved Sulphate and $\delta^{34}S_{SO4}$

The natural sources of SO_4^{2-} in river water are cyclic salt in rainfall and weathering of the sulphur-rich minerals, pyrite, anhydrite and gypsum. Human activities (e.g. air pollution, mining, smelting of sulphidic ore, refining of petroleum, and chemical industries, such as the production of fertilizer with sulphuric acid) also contribute to the SO_4^{2-} content of river water. These multiple sources of sulphate can frequently be distinguished by their specific isotopic signatures. Sulphate derived from dissolution of evaporites typically has positive $\delta^{34}S$ values whereas sulphate derived from the oxidation of sulphides or from biogenic emissions may have strongly negative $\delta^{34}S$ (Pearson and Rightmire, 1980).

The $\delta^{34}S$ of sulphate in the Cordilleran river water samples ranges from -8.9 to +14.1‰$_{CDT}$. Since sulphur isotope fractionation between evaporitic sulphates (gypsum) and seawater is negligible (Nielsen, 1979), any sulphate in the Cordilleran rivers derived from gypsum dissolution should reflect that of ambient seawater at the time of the gypsum deposition. Based on the compilations by Holser and Kaplan (1966) and Kampschulte and Strauss (2004) and on the age distribution of rocks in the Canadian Cordillera, the average expected value for marine evaporites in the Canadian Cordillera is expected to be ~25‰$_{CDT}$. The values in the rivers are significantly lighter. They also are significantly lighter than values expected for modern marine sulphates which can be transported and deposited as aerosols (21‰$_{CDT}$; Wadleigh et al., 1996). They do however overlap partly with values for continental rain (+5 ‰$_{CDT}$) in central and southern Ontario

(Nriagu and Coker, 1978; Van Stempvoort et al., 1991) and with the long range continental precipitation end-member of +4 $‰_{CDT}$ estimated by Wadleigh et al. (1996). Values for $\delta^{34}S_{SO4}$ in precipitation measured in Northern Japan (-1 to +14$‰_{CDT}$, Motoyama et al., 2002) and California (+5.8‰ $_{CDT}$, Bao et al. 2003) are similar. These studies however, were carried out thousands of kilometres to the east or south and within the air masses that originate from North America's or Asia's huge industrial complexes. Values for precipitation for the west coast of Canada would be expected to be closer to a sea salt end-member because of the relative absence of industrial emissions – essentially zero for many areas. However, to make estimates and subsequent calculations conservative, $\delta^{34}S_{SO4}$ of +5$‰_{CDT}$ is used for atmospheric inputs. The magnitude of atmospheric sulphate input is estimated from median values of major element snow chemistry in the Cascade Mountains after Laird et al. (1986). This is further elaborated below.

After subtracting the atmospheric input from the values measured in the rivers, the residual value can then be divided between evaporite (+25$‰_{CDT}$) and sulphide end-members. The choice of a sulphide end-member is not straightforward because of the complicated physiological and ecological aspects of sulphur isotope fractionation during bacterial sulphate reduction (see Brüchert, 2004). Sedimentary sulphide isotope compositions ($\delta^{34}S_{sulphide}$) can easily range from -30 to +10$‰_{CDT}$. For example, the Sullivan mine in British Columbia (near the study area), one of the largest Sedex deposits in the world, has a range of $\delta^{34}S_{sulphide}$ values from -9.9‰ to +6.8$‰_{CDT}$ with many around 0$‰_{CDT}$ (Taylor and Beaudoin, 2000; Taylor 2004). Likewise, a range of isotopic values is produced by the weathering of granites (~ +10$‰_{CDT}$), volcanics (~+5$‰_{CDT}$), mafics

(~+1‰$_{CDT}$), and other rock types (see Holser and Kaplan, 1966). Using two end-member values of $\delta^{34}S_{sulphide}$ for isotopic mass balance calculations to determine the sources of sulphate in the rivers, a light (-25‰$_{CDT}$) and a heavy (0‰$_{CDT}$), apportions 44% and 82%, respectively, of sulphate in the rivers to sulphide weathering for the entire region, with the remainder coming from precipitation and from the dissolution of gypsum. Further below, however, constraints imposed by carbon isotope systematics are used to illustrate that the average isotopic composition of sulphides in the study area must be closer to 0‰$_{CDT}$ and therefore that ~79% of the non-atmospheric sulphate in the rivers originates from sulphide weathering. This is also supported by the fact that no evaporite deposits have been mapped within the watersheds considered by this study (Wheeler and McFeely, 1991).

2.7 CHEMICAL WEATHERING RATES

The mass balance of major elements transported out of a watershed in the dissolved load of rivers can be used to determine chemical weathering processes and rates. Major cations (Ca^{2+}, Mg^{2+}, Na^{+}, and K^{+}), and anions (Cl^{-}, HCO_3^{-}, SO_4^{2-}) are generally not significantly involved in secondary mineral formation in river water and can therefore be considered conservative. Thus, if mineralogy and the stoichiometry of dissolution is known, dissolved fluxes can be used to determine chemical weathering rates of catchment basin lithologies.

The mass balance calculations used here are based on those developed by Blum et al. (1998) to quantify silicate and carbonate weathering in the Himalayas, and subsequently modified by Anderson et al. (2000) to include the dissolution of carbonates by sulphuric acid, in order to quantify weathering rates and pathways in a glaciated

catchment in Alaska. Our calculations differ from those used by Anderson et al. (2000) since in this study, silica (SiO_2)is not included. This is because silica is not a conservative component of river water - silica has low solubility in surface waters, it is a nutrient and so can be removed from the water by biological activity, and dissolution of amorphous silica in sedimentary rocks can be an important source of silica in river waters that is not related to weathering of silicate rocks or CO_2 drawdown (e.g. Berner and Berner, 1987; Bluth and Kump, 1994). As well, here the isotopic composition of HCO_3^- ($\delta^{13}C_{DIC}$) is used to test the validity of the calculations, rather than $^{87}Sr/^{86}Sr$. $\delta^{13}C_{DIC}$ differentiates between three end-members – silicate weathering by carbonic acid (-17‰$_{vpdb}$), carbonate weathering by carbonic acid (-8.25‰$_{vpdb}$), and carbonate weathering by sulphuric acid (+0.5‰$_{vpdb}$) – whereas Sr isotopes distinguish only between carbonate and silicate weathering products regardless of the reaction pathway.

2.7.1 Cyclic salts and atmospheric inputs

In order to quantify chemical weathering contributions to river chemistry, natural atmospheric inputs and pollution inputs first need to be accounted for. In terms of pollution, because British Columbia is far removed from any major industrial centre (Japan is the closest down-wind industrial centre), it is highly unlikely that pollution sources significantly impact the major elements in these rivers.

Cameron et al. (1995) speculate that the dissolved Cl^- and SO_4^{2-} in the Fraser River downstream of Prince George as being significantly affected by effluent from pulp mills. However, other than an observed trend, no explanation or quantification of this input was given. Using recent estimates of pulp mill emissions, it is found that the volume of water flowing in the Fraser river (2710 m^3/s at Hope (Environment Canada,

2001a) – 30 km south of Station 24) is much too large for the major ion chemistry to be significantly impacted by the known pollution sources. Total inorganic pollutant emissions from pulp mills (1999-2001) within the Fraser Watershed (at Prince George, Quesnel, and Kamloops, Environment Canada, 2001b) could account for a maximum of 0.3% of the dissolved Cl^- and 0.1% of the dissolved SO_4^{2-} measured at station 24 on the Fraser River (samples 127, 128 and 222). This includes the low-water period of the hydrograph (sample 222) when effluent from the mills would be expected to have more impact on river chemistry. Also supporting this is the fact that the evolution of SO_4^{2-}, Cl^- and Na^+ concentrations in the Fraser River are minimal to undetectable moving downstream from Prince George and Quesnel. If these waters were affected by point source pulp mill effluent, they should become significantly more dilute moving downstream from the pollution source. Further, the chemistry can be well constrained without considering pollution sources. Thus it is concluded that local inputs from pulp mills are insignificant compared to the inputs from chemical weathering.

The concentrations of the major cations (Na^+, K^+, Mg^{2+}, Ca^{2+}) and of sulphate (SO_4^{2-}) have been corrected for atmospheric inputs using the ratios of these ions to chloride in snowfall. This method is similar to that employed by Stallard and Edmond (1981) but here estimates of precipitation chemistry are used rather than seawater ratios. This is more appropriate because the chemical composition of rainwater and cyclic aerosols does not maintain seawater ratios, but evolves as a function of distance from the ocean (e.g. Stallard, 1995). Precipitation chemistry was estimated from the median values of major element snow chemistry from a large survey made in the Cascade Mountains south of our study area by Laird et al. (1986). This snow should be similar to or more

concentrated than precipitation in the Canadian Cordillera because the Cordillera is less populated and more pristine and so estimates can be considered maximums. Using the molar ratios automatically accounts for increases in concentration caused by evapotranspiration which are commonly around 2 times (Telmer and Veizer, 2000). The calculation is as follows:

$$[X]_{atm} = [Cl]_{measured} \times ([X]/[Cl])_{precipitation} \quad (12)$$

where [X] represents the concentration of any element in the river water that can be contributed by atmospheric salts.

2.7.2 Rock types contributing to weathering products

Figure 2.2 compares the Cordilleran waters to end-member compositions for generalized rock types based on average compositions of granite, basalt, and carbonate (see Table 2.2). The Cordilleran waters are well described by the weathering of carbonate, basaltic and granitic rocks by carbonic acid, carbonate rocks by sulphuric acid, and to a lesser degree, basaltic and granitic rocks by sulphuric acid. It is not possible to quantitatively separate the contributions of basalt versus granite weathering in the presence of carbonates. The Cordilleran waters plot much closer to the end-member for basalt weathering by H_2CO_3 than that for granite weathering by H_2CO_3. Basalts are known to weather more rapidly than granites (Garrels and Mackenzie, 1971), and so it is reasonable to assume that the dissolution of basalts, rather than granites, is the dominant silicate weathering process in the study area. This is supported by the global importance of basalt weathering shown by Gaillardet et al. (1999). Figure 2.2 is an effective display

of the possible weathering pathways, however, to quantify these pathways, a mass balance approach is used.

2.7.2.1 Mass Balance

Chemical weathering rates of the generalized rock types in the Fraser, Skeena and Nass watersheds were quantified using the following steps.

Step 1. Atmospheric Input. Correct for atmospheric input of cyclic salts (equations 12 and 13) where $[X^*]$ is the corrected concentration of a dissolved element:

$$[X^*] = [X^{river}] - [X^{atm}] \tag{13}$$

Step 2. Apportion SO_4^* to sulphide and evaporite dissolution. This is done using $\delta^{34}S$ of the dissolved sulphate. First, the isotopic composition of non-atmospheric sulphate ($\delta^{34}S^*$) is calculated:

$$\delta^{34}S^* = (\delta^{34}S^{river} \cdot [SO_4^{river}] - \delta^{34}S^{atm}[SO_4^{atm}]) \div [SO_4^*] \tag{14}$$

$\delta^{34}S^{river}$, $[SO_4^{river}]$, $\delta^{34}S^{atm}$ and $[SO_4^{atm}]$ correspond to the isotopic compositions and concentrations of dissolved sulphate measured in the river samples, and that calculated for atmospheric precipitation (+5‰$_{CDT}$), respectively. The sulphate contributed from sulphide oxidation (SO_4^{pyr}) (dominantly pyrite) and gypsum dissolution (SO_4^{gyp}) to SO_4^* can be calculated by equations 15 and 16:

$$[SO_4^*] = [SO_4^{pyr}] + [SO_4^{gyp}] \tag{15}$$

$$\delta^{34}S^* \cdot [SO_4^*] = \delta^{34}S^{pyr} \cdot [SO_4^{pyr}] + \delta^{34}S^{gyp} \cdot [SO_4^{gyp}] \tag{16}$$

Table 2.2 Average composition of generalized bedrock types expressed in weight percent. Sources: (a) Wedepohl (1995); (b) average of Turekian and Wedepohl (1961) and Vinogradov (1962); (c) Turekian and Wedepohl (1961)

Rock type	Ca	Na	K	Mg
Granite(a)	0.8	1.8	3.1	0.4
Basalt(b)	7.2	2.8	0.1	4.6
Carbonate(c)	30.2	0.0	0.3	4.7

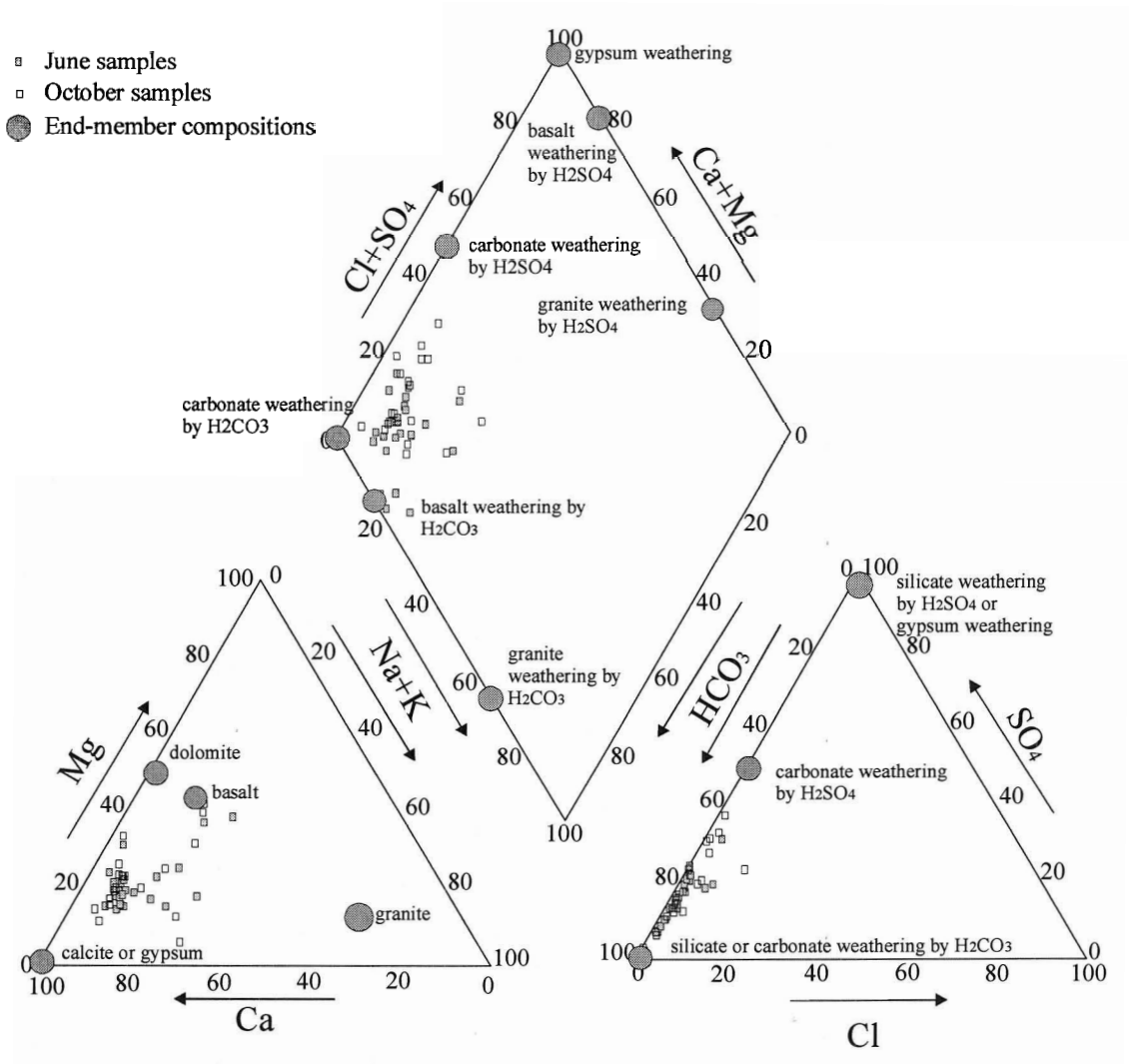

Figure 2.2 Piper diagram of the Cordilleran Waters illustrating contributions from weathering of major rock types by carbonic acid and sulphuric acid. Dominant chemical weathering contributions are carbonates by carbonic acid, carbonates by sulphuric acid and basalt by carbonic acid, with lesser contributions from the weathering of granites.

As explained in section 5.3, the isotopic end members of 0‰ and +25‰ CDT are used respectively for $\delta^{34}S^{pyr}$ and $\delta^{34}S^{gyp}$. Because $\delta^{34}S_{SO4}$ data was only obtained for the October 2002 samples, it is assumed that $\delta^{34}S_{SO4}$ in the rivers did not change significantly from June to October 2002, as is the case for $\delta^{13}C_{DIC}$, and for the relative concentrations of the major dissolved ions. Furthermore, the $\delta^{34}S_{SO4}$ values measured for this study correlate well to the values obtained by a previous survey of the Fraser River (Cameron et al., 1995), indicating that the isotopic composition of the Cordilleran rivers is relatively buffered. Ca^{2+} and Mg^{2+} coming from evaporite dissolution ($[Ca+Mg^{gyp}]$) are calculated as:

$$[Ca + Mg^{gyp}] = [SO_4^{gyp}] \tag{17}$$

Step 3. Carbonate Dissolution by Sulphuric Acid. Assume the acidity produced by pyrite oxidation is dominantly consumed by the dissolution of Ca and Mg carbonates (equation 4), a process that has been proven important in glacial and alpine catchments (e.g. Drever & Hurcomb 1986, Anderson et al. 2000). The Ca^{2+} plus Mg^{2+} in the rivers resulting from sulphuric acid dissolution of carbonates ($[Ca^{2+}+Mg^{2+}]_{Cs}$) is calculated as:

$$[Ca^{2+} + Mg^{2+}]_{Cs} = 2 \times [SO_4^{2-*}] \tag{18}$$

Similarly, the HCO_3^- resulting from the dissolution of carbonates by sulphuric acid ($[HCO_3^-]_{Cs}$) is calculated as:

$$[HCO_3^-]_{Cs} = 2 \times [SO_4^{2-*}] \tag{19}$$

Step 4. Silicate Dissolution by Carbonic Acid. Assume non-cyclic sodium (Na^{+*}) is dominantly derived from plagioclase dissolution, and non-cyclic potassium (K^{+*}) from potassium feldspar dissolution. As described in section 1.3.2, large portions of the Fraser,

Skeena and Nass watersheds are composed of arc derived rocks. These can be well represented by an intermediate plagioclase (An_{33}) with a Ca:Na ratio of 0.5. There are other possible sources of sodium and potassium, but this does not affect the stoichiometry of dissolution significantly. As well, the results are only moderately sensitive to the Ca:Na ratio chosen because Ca is much more concentrated in these rivers than Na. The Ca^{2+} resulting from silicate dissolution by carbonic acid ($[Ca^{2+}]_{Sc}$) is therefore calculated as:

$$[Ca^{2+}]_{Sc} = 0.5 \times [Na^{+*}] \quad (20)$$

Because charge balance must be maintained, anions and cations entering the water due to silicate dissolution by carbonic acid must be charge equivalent. Thus $[HCO_3^-]_{Sc}$ is calculated as:

$$[HCO_3^-]_{Sc} = [Na^{+*}] + [K^{+*}] + (2 \times [Ca^{2+}]_{Sc}) \quad (21)$$

Step 5. Carbonate Dissolution by Carbonic Acid. Assume that any remaining Ca^{2+} and Mg^{2+} is derived from the dissolution of carbonates by carbonic acid ($[Ca^{2+}+Mg^{2+}]_{Cc}$) (equation 1). The resulting HCO_3^- ($[HCO_3^-]_{Cc}$) is therefore:

$$[HCO_3^-]_{Cc} = 2 \times [Ca^{2+} + Mg^{2+}]_{Cc} \quad (22)$$

2.7.3 Mass Balance Results

Table 2.3 contains the results of the mass balance calculations, and Figure 2.3 summarizes these results for the Fraser, Skeena, and Nass rivers. Two main results are apparent: (i) carbonate dissolution by carbonic acid is the dominant chemical weathering process for most of the study area; and (ii) SCW (chemical weathering of carbonates by

sulphuric acid) is an important process in the watersheds ranging from 2 to 63% and averaging 19% of the HCO_3^- released (Table 2.3). SCW occurs at essentially the same rate as the weathering of silicates by carbonic acid, which on average produces 21% of the HCO_3^- (Table 2.3).

Uncertainty in the weathering mass balance results induced by sampling and analytical errors, and due to natural variability can be estimated from reproducibility of field duplicate samples. Duplicate samples were collected in June from the Chilcotin River (samples 107 and 108) and from the Fraser River (samples 127 and 128); and in October from the Skeena River (samples 211 and 212). Comparison of results for these samples (Table 2.3) shows that in all cases the results for the duplicates agree to within ± 20% in all cases, with many results being identical between duplicate samples.

2.7.4 Validation of Results

2.7.4.1 Carbon Isotopes

The isotopic signature of the HCO_3^- ($\approx\delta^{13}C_{DIC}$) provides an independent method of validating the mass balance results. $\delta^{13}C_{DIC}$ has been used to quantify the relative weathering rates of carbonate and silicate minerals in the Ottawa River basin (Telmer and Veizer, 1999). Similar to the Cordilleran waters, they show that in the Ottawa River system, DIC $\approx HCO_3^-$. They also show that the $\delta^{13}C_{DIC}$ of the Ottawa River system can be defined in terms of the mixing of two isotopic end-members (silicate dissolution by

Table 2.3 Atmospheric and chemical weathering contributions to the Cordilleran waters are listed as a percentage of the measured concentrations for each sample (mol%). Chemical weathering abbreviations are: carbonate weathering by sulphuric acid (Cs), silicate weathering by carbonic acid (Sc) and carbonate weathering by carbonic acid (Cc). For example, for sample 103, carbonate weathering by sulphuric acid contributes 35% of the measured Ca+Mg and 20% of the measured DIC (~HCO_3^-). Calculated (Calc.)and measured (Meas.) $\delta^{13}C_{DIC}$ show that carbon isotope systematics independently agree with these calculations (see text for explanation).

	Atmospheric Input			Gypsum Weathering		Sulphide-Carbonate Weathering			Silicate Weathering by H_2CO_3			Carbonate Weathering by H_2CO_3		$\delta^{13}C_{DIC}$	
Sample	Ca+Mg atm	Na+K atm	SO_4 atm	SO_4 gyp	Ca+Mg gyp	SO_4 pyr	Ca+Mg Cs	DIC Cs	Na+K Sc	Ca+Mg Sc	DIC Sc	Ca+Mg Cc	DIC Cc	Calc.	Meas.
	mol%													‰vpdb	
June Campaign															
101	20	16	24	7	2	69	31	19	84	18	57	29	35	-11.3	-9.8
102	11	12	8	4	1	88	65	41	88	15	48	8	10	-8.8	-7.1
103	15	20	19	0	0	81	35	20	80	11	32	39	45	-9.3	-8.4
104	6	14	7	0	0	93	40	24	86	6	19	47	56	-7.8	-5.9
105	3	10	7	0	0	93	18	10	90	6	14	73	81	-8.6	-7.6
107	3	4	3	0	0	97	44	23	96	13	32	40	42	-9.0	-5.9
108	3	5	4	0	0	96	44	23	95	14	33	40	42	-9.1	-5.9
109	2	9	6	30	3	63	12	6	91	5	12	78	81	-8.7	-7.5
110	2	10	6	30	3	64	13	7	90	5	12	76	77	-8.7	-7.7
111	2	2	23	26	1	50	2	1	98	18	37	78	70	-11.1	-9.0
112	2	5	2	0	0	98	40	24	95	8	20	50	60	-7.9	-6.8
113	2	5	3	0	0	97	37	20	95	8	20	52	56	-8.2	-7.1
114	3	7	7	6	1	87	16	8	93	8	17	74	71	-9.1	-7.1
115	2	5	3	0	0	97	34	20	95	8	21	56	66	-8.3	-6.7
116	7	16	13	0	0	87	25	13	84	8	20	61	66	-8.8	-7.8
117	2	6	2	0	0	98	42	25	94	6	18	49	60	-7.6	-7.3
118	2	6	2	0	0	98	45	27	94	6	17	47	56	-7.4	-6.2
119	1	4	1	0	0	99	49	30	96	6	16	44	55	-7.0	-6.2
120	3	7	7	0	0	93	23	13	93	9	23	64	69	-9.1	-8.0
121	1	10	1	37	8	62	27	17	90	2	7	61	78	-7.3	-6.1
122	2	17	2	57	11	41	15	9	83	2	5	71	87	-7.9	-5.5
123	1	5	2	56	13	43	19	12	95	2	12	64	80	-8.2	-5.2
124	2	6	4	37	6	59	19	11	94	6	19	66	80	-8.8	-6.0
126	5	10	8	15	2	77	25	13	90	9	24	59	65	-9.2	-6.5
127	3	9	6	20	2	74	18	8	91	6	13	71	67	-8.7	-7.4
128	3	9	6	20	2	73	17	8	91	6	13	72	70	-8.7	-7.3
October Campaign															
201	37	26	31	7	2	63	40	23	74	20	58	0	0	-12.0	-5.9
202	22	19	13	4	2	83	72	21	81	4	17	0	0	-7.4	-4.1
203	3	13	3	0	0	97	63	42	87	4	14	29	39	-5.6	-3.7
205	2	4	4	0	0	96	33	18	96	15	34	50	52	-9.6	-4.3
206	10	37	20	26	3	54	15	8	63	4	10	68	77	-8.4	-6.6
207	3	11	6	30	4	64	17	10	89	6	14	70	79	-8.7	-6.4
208	1	2	15	29	1	56	2	1	98	15	28	81	67	-10.7	-8.0
209	1	4	1	0	0	99	54	31	96	7	17	38	43	-6.9	-4.8
210	1	2	3	6	0	91	10	12	98	7	34	83	200	-9.0	-5.1
211	2	7	3	0	0	97	29	15	93	7	15	62	65	-8.2	-4.9
212	2	8	3	0	0	97	35	19	92	7	15	56	61	-7.9	-5.3
213	3	11	3	0	0	97	49	40	89	6	21	42	69	-6.9	-6.0
215	2	7	1	0	0	99	69	44	93	5	14	24	31	-5.3	-4.7
216	2	6	1	0	0	99	96	63	94	2	12	0	0	-2.4	-4.8
214	1	9	4	36	2	60	8	5	91	2	7	87	118	-8.3	-5.2
217	9	95	11	52	11	37	16	10	5	0	0	63	80	-7.3	-4.5
218	1	4	1	56	15	43	23	14	96	2	8	59	70	-7.7	-4.4
219	2	6	3	38	6	59	20	12	94	5	15	66	75	-8.5	-4.6
221	6	12	8	15	3	78	31	17	88	10	24	50	54	-8.9	-5.9
222	3	10	6	20	3	73	19	11	90	7	16	69	77	-8.7	-6.8

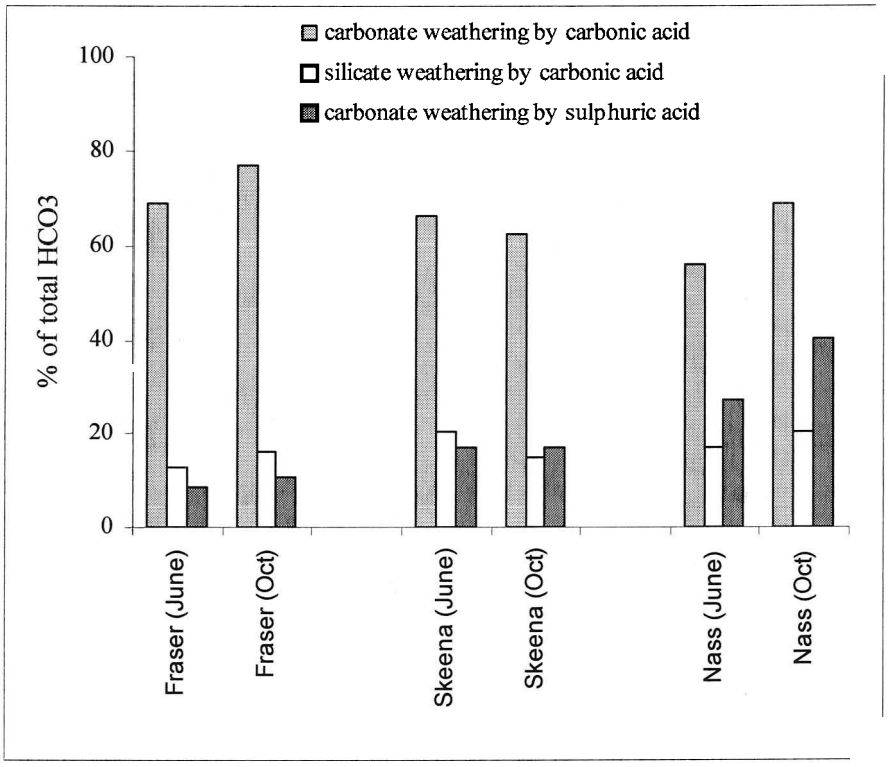

Figure 2.3 Relative DIC fluxes modeled for the Fraser, Skeena and Nass watersheds due to carbonate weathering by carbonic acid, carbonate weathering by sulphuric acid and silicate weathering by carbonic acid. The bicarbonate fluxes due to silicate weathering by carbonic acid and carbonate weathering by sulphuric acid are almost identical in the Fraser and the Skeena watersheds thus CO2 fluxes between reservoirs is small, while in the Nass watershed, sulphuric acid weathering of carbonates exceeds carbonic acid weathering of silicates.

carbonic acid, and carbonate dissolution by carbonic acid). For the Cordilleran waters, a third chemical weathering end-member must be defined (carbonate dissolution by sulphuric acid) in order to describe the $\delta^{13}C_{DIC}$. Using the isotopic end-members and the results of the mass balance calculations, it is possible to calculate an expected $\delta^{13}C_{DIC}$ for each sample. The expected $\delta^{13}C_{DIC}$ values can then be compared to the measured values to validate the mass balance calculations.

2.7.4.2 End-Member Definition.

The two dominant sources of carbon in groundwater DIC are from organic matter decay, and from carbonate mineral dissolution. Because river water is the surface expression of groundwater (Sklash et al., 1976) its $\delta^{13}C_{DIC}$ is similarly controlled. Carbonic acid forms in the soils by the dissolution of CO_2 derived from the decay of organic matter. Depending on pH, the equilibrium dissolution of this CO_2 into groundwater gives the resulting DIC a $\delta^{13}C$ of $-17 \pm \sim 5‰_{vpdb}$ (for a detailed description of this end-member definition see Telmer and Veizer, 1999). Carbonate minerals inherit the $\delta^{13}C$ of the DIC in the water from which they precipitate. Thus most carbonate rocks, which form in the oceans, will have a marine $\delta^{13}C$, which has remained close to $0‰_{vpdb}$ since the end of the Proterozoic (e.g. Veizer et al. 1999). Marine carbonate rocks of Paleozoic to Tertiary age have an average $\delta^{13}C$ of $\sim 0.5‰_{vpdb}$ (Faure, 1986). However, the age distribution representative of rocks in the Cordilleran could easily lead to a mean $\delta^{13}C$ closer to $+2‰_{vpdb}$ according to Veizer et al.'s (1999) recent compilation. To remain conservative, $\sim 0.5‰_{vpdb}$ is used.

Using these $\delta^{13}C$ values and the stoichiometry of dissolution (equations 1, 2 and 4), $\delta^{13}C_{DIC}$ end-members for this study are defined as: (i) the dissolution of one mole of

calcium or magnesium carbonate by carbonic acid involves one mole of dissolved soil CO_2 ($\delta^{13}C = -17‰_{vpdb}$), and one mole of carbonate from rocks ($\delta^{13}C = +0.5‰_{vpdb}$), producing an end-member of $\delta^{13}C_{DIC} = -8.25‰_{vpdb}$; (ii) The dissolution of silicate minerals by carbonic acid only involves carbon from soil CO_2 producing an end-member of $\delta^{13}C_{DIC} = -17‰_{vpdb}$; (iii) Carbonate dissolution by sulphuric acid involves only carbon in calcium or magnesium carbonate, resulting in a $\delta^{13}C_{DIC} = +0.5‰_{vpdb}$. The end-members as defined here are based on global data, and may not account for undocumented variability in the Canadian Cordillera.

2.7.4.3 Measured $\delta^{13}C_{DIC}$

Figure 2.4 plots the measured $\delta^{13}C_{DIC}$ in relation to major element ratios. The end-member compositions shown are defined by the stoichiometry of the dissolution reactions (equations 1, 2 and 4), and the isotopic end-members as described above. Figure 2.4 shows that the mass balance calculations based on major element ratios (Figure 2.2) agree well with the expected behaviour of carbon isotopes as defined by the end-members above. This illustrates that carbonate dissolution by carbonic acid is the dominant chemical weathering mechanism and that coupled sulphide carbonate weathering (SCW) strongly influences carbon isotopes in rivers.

2.7.4.4 Expected $\delta^{13}C_{DIC}$

An expected $\delta^{13}C_{DIC}$ can be calculated based on the mass balance results and the end-members described above by a three component mixing equation:

$$\delta^{13}C_{DIC} = (\%HCO_{3\,Sc}^{-} \times -17‰) + (\%HCO_{3\,Cc}^{-} \times -8.25‰) + (\%HCO_{3\,Cs}^{-} \times 0.5‰) \quad (23)$$

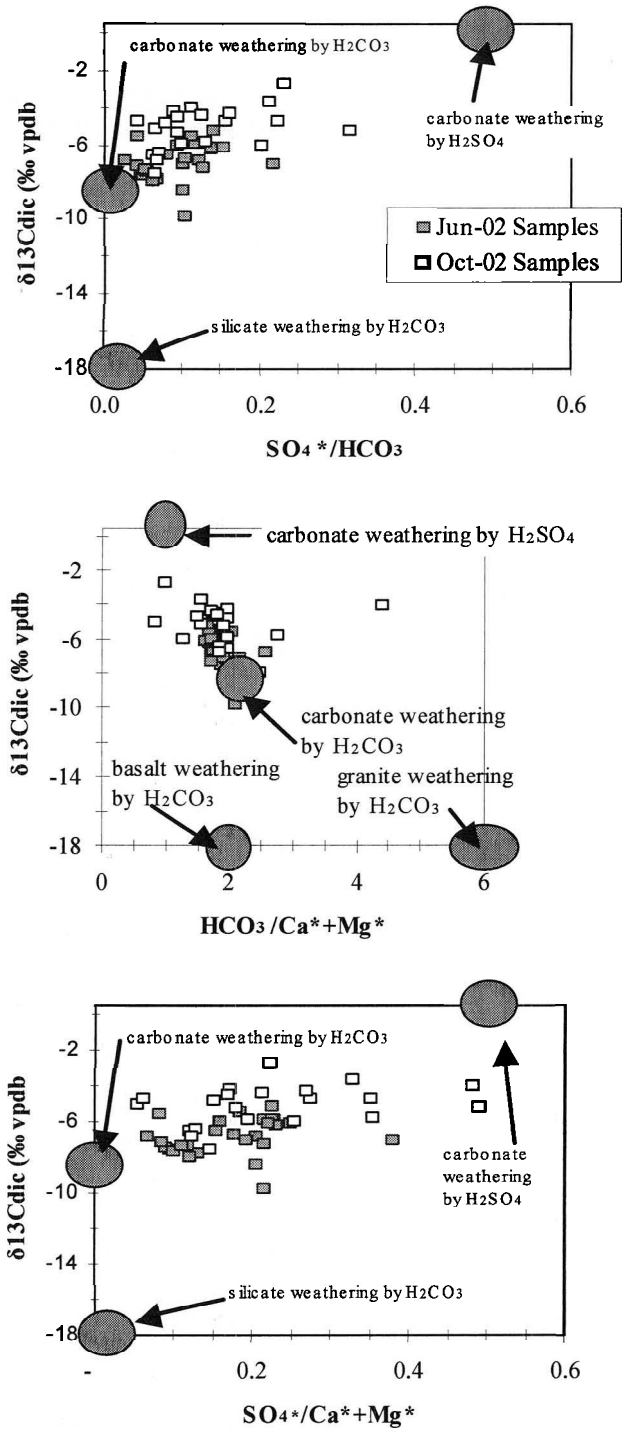

Figure 2.4 $\delta^{13}C_{DIC}$ versus ratios of major ions (corrected for atmospheric inputs) Ca*, Mg*, SO_4*, and HCO_3 in waters draining the Canadian Cordillera. Ideal water compositions, as described in the text, are shown to illustrate that most waters plot between compositions defined by carbonate dissolution by carbonic acid and coupled sulphide carbonate weathering, with an apparently smaller component of silicate weathering by carbonic acid.

Measured and calculated $\delta^{13}C_{DIC}$ for each sample are listed in Table 2.3. For most samples agreement between the measured and calculated $\delta^{13}C_{DIC}$ is very good with differences less than the uncertainty in the isotopic end-members and analytical results. Again this demonstrates that weathering rates and sources determined using $\delta^{13}C_{DIC}$ agree well with those determined from the major elements.

The calculated $\delta^{13}C_{DIC}$ values tend to be more negative than the measured values (the average difference is 1.9‰). Possible reasons are:

(1) Real isotopic end-members differ from theoretical ones. Notably, if the carbonate rock end-member were shifted to +2‰ PDB (very reasonable according to published data such as Veizer et al., 1999), then much better agreement between measured and calculated values is obtained. However, currently there are no data available to make better estimates.

(2) Dissolution of carbonates by sulphuric acid is underestimated. This could be the case if the amount of SO_4^{atm} or SO_4^{gyp} in the rivers has been overestimated. As described above, conservative estimates have been made for both parameters, and it is possible that either parameter has been over-corrected. Importantly, the calculated apportionment of SO_4^{2-} to evaporitic and sulphidic sources is sensitive to the $\delta^{34}S$ end member compositions used for SO_4^{atm}, SO_4^{gyp}, and SO_4^{pyr}. Changing the value of $\delta^{34}S^{atm}$ has little effect on the mass balance calculations (and $\delta^{13}C_{DIC}$) because the SO_4^{atm} is a small fraction of the SO_4^{2-} in most of the samples. The value of $\delta^{34}S^{pyr}$ is subject to the most uncertainty due to the possible broad range of sulphur isotopes in sulphides that have been observed. For this end member, $0‰_{CDT}$ was selected because it is representative of lithologies in the study area (Holser and Kaplan, 1966;

Taylor and Beaudoin, 2000).

(3) $\delta^{13}C_{DIC}$ is shifted by equilibration of DIC with atmospheric CO_2. Evidence against this is that (i) the flux of CO_2 across the water-air interface is uni-directional due to CO_2 overpressures inherited from soils; and (ii) DIC in isotopic equilibrium with atmospheric CO_2 has a $\delta^{13}C$ of approximately $0‰_{vpdb}$, but despite variable flow conditions and residence time for the different rivers, a dominantly atmospheric signal does not exist. As well, there is no observed relationship between flow conditions, residence time and $\delta^{13}C_{DIC}$. For example, the Thompson River at Spence's Bridge (station 23, samples 126 and 221) had $\delta^{13}C_{DIC}$ of -6.5 and $-5.9‰_{vpdb}$ in June and October, respectively. These values are equivalent to the mean $\delta^{13}C_{DIC}$ of all of the samples ($-6.2‰_{vpdb}$) even though the residence time of the Thompson water (which drains Kamloops and Shuswap Lakes) is much greater than that of the other rivers. This is supported by other work. Yang et al. (1996) saw atmospheric signals in St. Lawrence river water only because of very long (100 year) residence time of input waters in Lake Ontario, the main source of St. Lawrence water. However, none of the tributaries with shorter water residence times displayed these signals. Pawellek and Veizer (1994) attributed a downstream positive shift in the $\delta^{13}C_{DIC}$ of the Danube River to a combination of photosynthesis and atmospheric equilibration. However, re-interpretation of this data (Pawellek et al., 2002) shows this trend can be explained by the input of isotopically heavy DIC from the tributaries, and that the $\delta^{13}C_{DIC}$ of the Danube is conservative. Karim and Veizer (2000) attribute heavy (near $0‰_{vpdb}$) $\delta^{13}C_{DIC}$ values in streams draining high alpine (non-vegetated) Himalayan catchments to weathering by carbonic acid formed by dissolution of CO_2 directly from the

atmosphere into rainwater. This scenario is not an appropriate analogue to the Canadian Cordillera. Only the highest peaks and areas undergoing alpine glaciation are barren of vegetation and soil. No atmospheric signals were reported by Telmer and Veizer (1999) for the Ottawa River system, which has a water residence of roughly 3 months, similar to the fast flowing rivers in this study. Furthermore, $\delta^{13}C_{DIC}$ has effectively by used by marine biologists as a conservative tracer of water masses in marine estuaries (Fry, 2002), illustrating its conservative behaviour. Although, it is not possible to completely rule out atmospheric contamination, the close agreement of the expected and measured $\delta^{13}C_{DIC}$ values demonstrates that chemical weathering predictably controls the $\delta^{13}C_{DIC}$ in this study. As well, it is possible that in some cases other studies that have interpreted $\delta^{13}C_{DIC}$ as influenced by atmospheric equilibration have overlooked the role of sulphuric acid weathering of carbonates which imparts a similar signal but a more predictable one.

(4) Carbonic acid formed by dissolution of atmospheric CO_2 directly into water (i.e. not soil CO_2) has been underestimated as a weathering agent. Karim and Veizer (2000) attribute heavy (near $0‰_{vpdb}$) $\delta^{13}C_{DIC}$ values in streams draining high alpine (non-vegetated) Himalayan catchments to weathering by carbonic acid formed by dissolution of CO_2 directly from the atmosphere into rainwater. This scenario is not an appropriate analogue to the Canadian Cordillera where unvegetated areas are only a small fraction of the total.

(5) $\delta^{13}C_{DIC}$ values are affected by photosynthesis in the river water. Phytoplankton fix $^{12}CO_2$ preferentially over $^{13}CO_2$, leaving residual DIC ^{12}C depleted. As demonstrated by Telmer and Veizer (1999), signals that would be expected to covary with the

growth season are absent and the biomass required to alter the isotopic composition of DIC in the Ottawa River system would have to be unreasonably large. This is similarly the case for the Cordilleran rivers as mean $\delta^{13}C_{DIC}$ for October is heavier than for June. The heavier values in October are likely caused by more extensive water-rock interaction with isotopically heavy carbonates. This occurs because in June, snowmelt discharge peaks, and so residence time of water is reduced and the contribution of deeper groundwaters is relatively less. This is supported by higher TDS for October samples. Another contributor to the heavier $\delta^{13}C_{DIC}$ observed in October is the falling hydrograph. As the water table falls, more soil and rock will be exposed to oxidizing conditions, allowing for more sulphide oxidation within the weathering horizon. This is supported by a higher SO_4^{2-}:HCO_3^- ratio in October than in June (0.3 and 0.2 eq/eq, respectively).

(6) Other weathering reactions that are not accounted for may contribute to the measured $\delta^{13}C_{DIC}$. For example, significant acid production by the oxidation of reduced minerals other than sulphides (like magnetite), coupled with the weathering of carbonate minerals would cause the measured $\delta^{13}C_{DIC}$ to be less negative than the calculated $\delta^{13}C_{DIC}$. Also, the formation of metal carbonates like siderite would enhance equilibration of the $\delta^{13}C_{DIC}$ with carbonate $\delta^{13}C$, also causing the measured $\delta^{13}C_{DIC}$ to be less negative than the calculated $\delta^{13}C_{DIC}$. These processes are not accounted for, but since differences between the measured and calculated values are small, they can be secondary influences at most.

Table 2.4 Chemical weathering driven DIC fluxes for the Cordilleran watersheds. Carbon fluxes are listed as bulk annual DIC ($\sim HCO_3^-$) discharged from each watershed due to the three chemical weathering pathways, and as the amount discharged per square km per year.

	Total DIC fluxes			**DIC fluxes per km^2**		
	carbonate weathering by H_2CO_3	silicate weathering by H_2CO_3	carbonate weathering by H_2SO_4	carbonate weathering by H_2CO_3	silicate weathering by H_2CO_3	carbonate weathering by H_2SO_4
River	10^9 mol C·yr^{-1}			10^3 mol C·km^{-2}·yr^{-1}		
Fraser	62.6	12.1	8.0	288.4	55.9	36.7
Nass	7.6	2.3	3.9	411.3	124.2	212.7
Squamish	0.1	0.5	0.2	63.1	197.1	71.2
Skeena	10.2	2.9	2.7	241.5	69.1	63.2
Fraser Tributaries:						
Thompson	10.0	3.9	2.4	181.7	71.7	43.5
N. Thompson	3.5	1.3	0.8	180.3	64.1	42.4
Chilcotin	0.9	0.7	0.4	47.0	33.9	21.9
Blackwater	1.1	0.5	0.0	87.4	41.9	1.3
Lillooet	0.1	0.5	0.5	30.8	235.7	236.9
Cayoosh	0.2	0.1	0.1	174.2	60.6	117.2
Skeena Tributaries:						
Bulkley	0.8	0.3	0.5	113.2	46.8	68.5
Zymoetz	1.8	0.4	0.1	619.1	121.2	47.9

2.8 DIC FLUXES DUE TO CHEMICAL WEATHERING

Weathering driven DIC fluxes for the Cordilleran watersheds based on the mass balance results and discharge are listed in Table 2.4, and are calculated as follows:

$$DIC_{total} = \left([DIC]_{June} \times 0.7 + [DIC]_{October} \times 0.3\right) \times D \qquad (24)$$

Where DIC_{total} is the total annual flux of DIC for a given river; [*DIC*] are the measured concentrations of DIC during the June and October sampling campaigns; and *D* is the average annual water discharge based on historical hydrographic data collected by Environment Canada (2001a). The June and October DIC concentrations are weighted by multiplying by 0.7 and 0.3 respectively to represent the Cordilleran hydrograph. 70% of the water discharged by the Cordilleran rivers occurs during the summer months (Environment Canada, 2001a; also see Chapter 1 - Figure 1.3). It is assumed that the concentrations measured in June are representative of the typical summer (May to September) composition of these waters, and likewise that the concentrations measured in October are representative of the typical composition of these rivers during the remainder of the year.

For rivers where multiple locations were sampled, only the DIC flux from the point furthest downstream is given, since these samples represent an integration of the entire watershed. For the study area, atmospheric CO_2 drawdown by the chemical weathering of silicates is 17.8×10^9 mol C·yr^{-1}. Of this, 12.1×10^9 occurred in the Fraser basin, which agrees well with the 9.4×10^9 mol C·yr^{-1} determined by Gaillardet et al. (1999) for the Fraser River. The two independently determined fluxes may represent an estimate of the inter-annual variability of the calculation (22%).

The flux of DIC to the Pacific Ocean due to silicate weathering in the Fraser, Skeena and Nass watersheds is essentially equivalent to that due to sulphide-carbonate weathering (14.7×10^9 mol C/yr). The long-term fate of the DIC released by SCW depends on the rate of SOCS during the same time frame. The current rate of sulphide and carbonate deposition in marine sediments is unknown, however, since the magnitude of SCW is equivalent to that of silicate weathering, the flux of CO_2 to the atmosphere caused by SCW can potentially offset CO_2 drawdown due to silicate weathering during times of low SOCS.

CO_2 fluxes to the atmosphere can be calculated from the DIC fluxes shown in Table 2.4, based on the following: (i) that HCO_3^- entering the oceans is removed by carbonate precipitation according to the reverse of equation 1; (ii) half of atmospheric CO_2 fixed through silicate dissolution by carbonic acid is removed from the atmosphere/ocean by carbonate precipitation while the other half returns to the atmosphere; (iii) all of the atmospheric CO_2 fixed through carbonate dissolution by carbonic acid is returned to the atmosphere/ocean during subsequent carbonate precipitation; and (iv) sulphuric acid dissolution of carbonate minerals liberates half of the carbon dissolved to the atmosphere during carbonate precipitation. The long term fluxes of CO_2 between the fluid and solid reservoirs are therefore determined by the rates of dissolution of silicates by carbonic acid, the dissolution of carbonates by sulphuric acid, and as follows:

$$CO_{2CW} = \tfrac{1}{2}(CO_{2Cs}) - \left|\tfrac{1}{2}(CO_{2Sc}) + CO_{2Org}\right| \qquad (25)$$

where CO_{2CW} is the net flux of CO_2 between the atmosphere/ocean and carbonate rocks caused by chemical weathering, CO_{2Sc} is the carbon involved in silicate weathering by

carbonic acid (Equation 2), CO_{2Sc} is the carbon involved in SCW (Equation 6), and CO_{2Org} is the carbon involved in SOCS (Equation 7 and 8). A negative result for CO_{2CW} indicates a net transfer of CO_2 from the atmosphere to carbonate rocks (i.e. drawdown by silicate weathering is greater than release by pyrite-carbonate weathering) and vice-versa. Sulphides are weathered more easily than silicates, thus the rate of physical erosion may be an important determinant in controlling pyrite oxidation rates. It is likely that SCW is greatest in regions of high physical erosion, such as tectonically and glacially active regions like the Canadian Cordillera. This is evident by comparing the results from this study to data obtained for rivers from tectonically stable cratonic areas. Figure 2.5 plots $\delta^{13}C_{DIC}$ versus $\delta^{34}S_{SO4}$ for this study, the St. Lawrence River Basin (data from Yang et al., 1996), and for the Ottawa River Basin (data from Telmer, 1997). The negative correlation between $\delta^{13}C_{DIC}$ and $\delta^{34}S_{SO4}$ for the Cordilleran samples shows that sulphides are a significant contributor to weathering products in the tectonically active Cordilleran waters. A best fit line for the Cordilleran samples reflects a mix between atmospheric inputs of SO_4, where carbonate weathering by carbonic acid dominate the HCO_3^- inputs, and rivers with significant SCW occurring. The four Cordilleran samples to the upper right, collected from the headwater regions of the Fraser and North Thompson Rivers, are not included in the best fit determination. The $\delta^{34}S_{SO4}$ of these samples suggests evaporite inputs, although, as discussed previously, sulphides with strongly positive $\delta^{34}S_{SO4}$ can also occur. The relatively positive carbon isotope signatures suggest the latter. Data from the St. Lawrence and Ottawa basins show that $\delta^{34}S_{SO4}$ in those waters is invariant and therefore independent of $\delta^{13}C_{DIC}$. It almost exclusively reflects recorded atmospheric

composition around +5‰$_{CDT}$ (Nriagu and Coker, 1978), showing that SCW is not a dominant process in those tectonically stable and geologically mature terrains.

Other studies have noted the importance of SCW at local and regional scales in the tectonically active North American Cordillera and Himalayas (Galy and France-Lanord, 1999; Anderson et al., 2000; Dalai et al., 2002a, b; Gaillardet et al., 2003; Millot et al., 2003; Tranter et al., 2003), however, quantification of SCW at watershed scale has been problematic except in small catchments where dissolved sulphate can be easily accounted for. The dominance of SCW in tectonically active regions suggests that this process may provide a negative feedback to tectonically and glacially induced CO_2 drawdown and cooling. Or, alternatively, it could provide a positive feedback to global warming scenarios under which the hydrological cycle is accelerated. However, the global dataset is far from complete and there may be other important considerations. For example, the importance of SCW has also been documented in a region of Texas with very low physical erosion rates (Hercod et al., 1998). Global rates and controls on SCW will need to be more fully evaluated in order to determine the significance of this process.

Another factor to consider is the timescale on which coupled sulphide-carbonate weathering could affect atmospheric CO_2. Silicate weathering CO_2 drawdown is believed to offset geological inputs of CO_2 to the atmosphere (outgassing) on 10^6 year timescales (Walker et al., 1981). This is ultimately limited by the global silicate weathering rate. Because sulphide oxidation and carbonate weathering both occur more rapidly than silicate weathering, the relative contributions to atmospheric CO_2 caused by SCW could scale with rapid changes in physical erosion rates more so than silicate weathering rates.

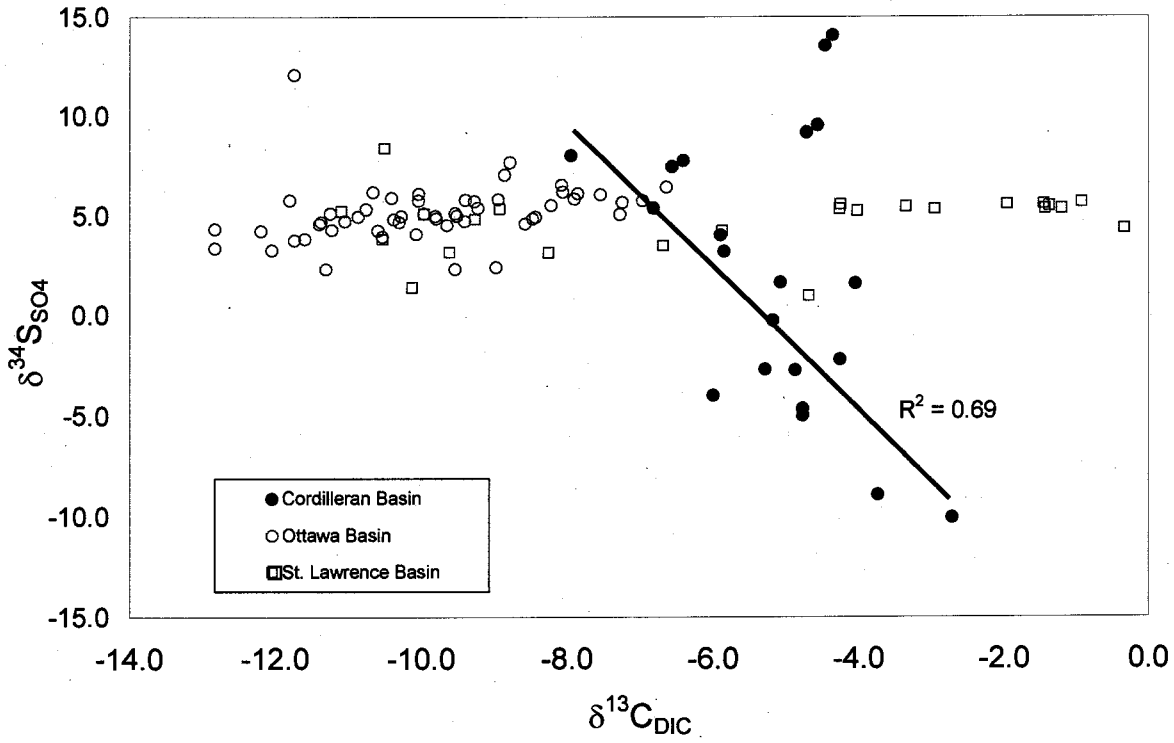

Figure 2.5 Isotopes of sulphur versus carbon in dissolved sulphate and dissolved inorganic carbon (DIC) for the Fraser, Skeena, and Nass River basins (Canadian Cordillera, this paper), Ottawa River Basin (from Telmer, 1997), and St. Lawrence River Basin (from Yang et al., 1996).

SCW would ultimately be limited by the drawdown of atmospheric oxygen (discussed by Derry and France-Lanord, 1996) and by the rate of carbonate precipitation in the oceans (residence time of HCO_3^- is on the order of 10^5 years). Following this line of reason, it is possible that continental glaciations such as those of the Pleistocene would increase SCW temporarily and that the modern signal measured in this study therefore does not approximate steady state but rather an ongoing adjustment to recent glaciation (J. Gaillardet, private communication). In other words, that the rate of SCW in the Cordilleran rivers may be an over-estimate and that its long term significance is less. The comparison between the Cordilleran rivers and those from the Canadian craton (Figure 2.5) suggest otherwise. The rivers draining the old and tectonically stable craton also experienced the Pleistocene glaciations but do not show significant SCW. This suggests that tectonic uplift is a key control. Clearly more data is needed to quantify this process.

2.9 CONCLUSIONS

Dissolved major element concentrations, $\delta^{13}C$ of dissolved inorganic carbon (DIC), and $\delta^{34}S$ of dissolved sulphate from the Fraser, Skeena and Nass River basins of the western Canadian Cordillera and were effectively used to quantify chemical weathering rates. Major element stoichiometry is consistent with $\delta^{13}C_{DIC}$ values produced by three weathering pathways: carbonate dissolution by carbonic acid, silicate dissolution by carbonic acid, and carbonate dissolution by sulphuric acid derived from the oxidation of sulphides (coupled *sulphide-carbonate weathering*). The first is dominant and the latter two occur at roughly the same rates. A variety of evidence illustrates that atmospheric equilibration does not significantly influence the isotopic composition of the rivers. The isotopic composition of dissolved sulphate reflects a sulphide source and is

negatively correlated with $\delta^{13}C_{DIC}$, illustrating that sulphuric acid produced by the weathering of sulphides is dominantly neutralized by carbonates, and that this is indeed a significant influence on the carbon isotopic composition of rivers. This result further demonstrates the potential for $\delta^{13}C_{DIC}$ to be used as a diagnostic tool to help constrain chemical weathering processes, and it may help provide a predictable explanation for the carbon isotopic composition of some previously published data.

Physical erosion rates, likely governed by tectonic uplift and also landscape history and climate, are likely to be important controls on the magnitude of *sulphide-carbonate weathering*. This is illustrated by a comparison with the tectonically stable Ottawa and St. Lawrence River basins, which do not exhibit a significant relationship between S and C isotopes.

DIC fluxes due to silicate weathering (63.6×10^3 mol $C \cdot km^{-2} \cdot yr^{-1}$) were determined to be very similar to those caused by SCW (52.6×10^3 mol $C \cdot km^{-2} \cdot yr^{-1}$). This implies that, SCW can be of a sufficient magnitude to significantly offset CO_2 drawdown caused by silicate weathering. Its impact will however depend on the rate of the balancing process, *sulphide-organic carbon deposition* (SOCS) in the ocean. Considering that the rate of SOCS has been shown to vary through time and that the processes that control it are different that those that control SCW, it seems plausible that imbalances in the SCW-SOCS cycle occur. Such imbalances could provide a previously unconsidered negative feedback to tectonically induced CO_2 drawdown and cooling, or conversely, a positive feedback for some global warming scenarios that lead to an accelerated hydrological cycle. Simple calculations show that SCW could double atmospheric CO_2 without strongly perturbing marine and atmospheric chemistry.

2.10 REFERENCES

Anderson S. P., Drever, J. I., Frost C. D. and Holden P. (2000) Chemical weathering in the foreland of a retreating glacier. *Geochim. Cosmochim. Acta* **64,** 1173-1189.

Bao H. and Reheis M.C. (2003) Multiple oxygen and sulfur isotopic analyses on water-soluble sulfate in bulk atmospheric deposition from the southwestern United States. *J. Geophys. Res.* **108 (D14),** 4430.

Beck K. C., Reuter J. H. and Perdue E. M. (1974) Organic and inorganic geochemistry of some coastal plain rivers of southeastern U.S. *Geochim. Cosmochim. Acta* **38,** 341-364.

Berner E. K. and Berner R. A. (1987) *The global water cycle: Geochemistry and environment.* Prentice-Hall, New Jersey.

Berner, R. A., 1998, The carbon cycle and CO_2 over Phanerozoic time: the role of land plants. *Phil. Trans. R. Soc. B* **353,** 75-82.

Berner, R. A. and Kothavala, Z. (2001) GEOCARB III: A revised model of atmospheric CO_2 over Phanerozoic time. *Am. J. Sci.* **301,** 182-204.

Blum J. D., Gazis C. A., Jacobson A. D. and Chamberlain C. P. (1998) Carbonate versus silicate weathering in the Raikhot watershed within the High Himalayan Crystalline Series. *Geology* **26,** 411-414.

Bluth G.J.S. and Kump L.R. (1994) Lithologic and climatologic controls of river chemistry. *Geochim. Cosmochim.* Acta **58,** 2341-2359.

Brown A. S. (1969) Ayanish lava flow, British Columbia. *Can. J. Earth Sci.* **6,** 1460-1468.

Brüchert V. (2004) Physiological and ecological aspects of sulphur isotope fractionation during bacterial sulphate reduction. In *Sulfur Biogeochemistry – Past and Present* (eds. J.P. Amend, K.J. Edwards and T.W. Lyons). Geological Society of America Special Paper **379.** pp. 1-16.

Buhl D., Neuser R. D., Richter D. K., Riedel D., Roberts B., Strauss H. and Veizer J. (1991) Nature and nurture: environmental isotope story of the river Rhine. *Naturwissenschaften* **78,** 337-346.

Cameron E. M. (1996) Hydrogeochemistry of the Fraser River, British Columbia: seasonal variation in major and minor components. *J. Hydrol.* **182,** 209-225.

Cameron E. M., Hall G. E. M., Veizer J. and Krouse H. R. (1995) Isotopic and elemental hydrochemistry of a major river system: Fraser River, British Columbia, Canada. *Chem. Geol.* **122,** 149-169.

Cerling T. E., Solomon D. K., Quade J. and Bowman J. R. (1991) On the isotopic composition of carbon in soil carbon dioxide. *Geochim. Cosmochim. Acta* **55,** 3403-3405.

Dalai T. K., Krishnaswami S. and Sarin M. M. (2002a) Major ion chemistry in the headwaters of the Yamuna river system: Chemical weathering, its temperature dependence and CO_2 consumption in the Himalaya. *Geochim. Cosmochim. Acta* **66,** 3397-3416.

Dalai T. K., Singh S. K., Triveldi J. R. and Krishnaswami S. (2002b) Dissolved rhenium in the Yamuna river system and the Ganga in the Himalaya: role of black shale weathering on the budgets of Re, Os, and U in rivers and CO_2 in the atmosphere. *Geochim. Cosmochim. Acta* **66,** 29-43.

Dalai T.K., Krishnaswami S. and Kumar A. (2003) Sr and $^{87}Sr/^{86}Sr$ in the Yamuna River System in the Himalaya: Sources, fluxes, and controls on Sr isotope composition. *Geochim. Cosmochim. Acta* **67**, 2931-2948.

Derry L.A. and France-Lanord C. (1996) Neogene Himalayan weathering history and river $^{87}Sr/^{86}Sr$; impact on the marine Sr record. *Earth Planet. Sci. Lett.* **142,** 59-74.

Derry L.A. and Murray R.W. (2004) Continental margins and the sulfur cycle. *Science* **303,** 1981-1982.

Drever J. I. and Hurcomb D. R. (1986) Neutralization of atmospheric acidity by chemical weathering in an alpine drainage basin in the North Cascades Mountains. *Geology* **14,** 221-224.

Edmond J. M., Palmer M. R., Measures C. I., Grant B. and Stallard R. F. (1995) The fluvial geochemistry and denudation rate of the Guayana Shield in Venezuela, Columbia, and Brazil. *Geochim. Cosmochim. Acta* **59,** 3301-3325.

Emiliani C. and Edwards G. (1953) Tertiary ocean bottom temperatures. *Nature,* **171**, 887-888.

Emiliani C (1955) Pleistocene temperatures. *J. Geol.* **63**, 538-578.

Environment Canada (Digital) (1993) In: *Envirodat Water Quality Database*. Inland Waters Directorate, Water Quality Branch, Environment Canada, Ottawa.

Environment Canada (2001a) *Surface Water and Sediment Data* [HYDAT CD-ROM]. Atmospheric Environment Program, Water Survey of Canada, Environment Canada, Ottawa.

Environment Canada (2001b) *National Pollutant Release Inventory (NPRI) Database*. Environment Canada, Ottawa.

Faure G. (1986) *Principles of Isotope Geology*. Wiley, Toronto.

Flintrop C., Hohlmann B., Jasper T., Korte C., Podlaha O. G., Scheele S. and Veizer J. (1996) Anatomy of pollution: rivers of North Rhine–Westphalia, Germany. *Am. J. Sci.* **261,** 58-98.

Fry B. (2002) Conservative mixing of stable isotopes across estuarine salinity gradients: A conceptual framework for monitoring watershed influences on downstream fisheries production. *Estuaries* **25,** 264-271.

Gabrielse H. and Yorath C. J. (1991) Tectonic Synthesis. In *The Geology of the Cordilleran Orogen in Canada no. 4* (eds. H. Gabrielse and C. J. Yorath). Geological Survey of Canada. pp. 677-705

Gabrielse H., Monger J. W. H., Wheeler J. O. and Yorath C. J. (1991) Tectonic Framework: Part A. Morphogeological belts, tectonic assemblages and terranes. In *The Geology of the Cordilleran Orogen in Canada no. 4* (eds. H. Gabrielse and C. J. Yorath). Geological Survey of Canada. pp. 15-28.

Gaillardet J., Dupré B., Louvat P. and Allègre C. J. (1999) Global silicate weathering and CO_2 consumption rates deduced from the chemistry of large rivers. *Chem. Geol.* **159,** 3-30.

Gaillardet J., Millot R. and Dupré B. (2003) Chemical denudation rates of the western Canadian orogenic belt: the Stikine terrane. *Chem. Geol.* **201,** 257-259.

Galy A., and France-Lanord C. (1999) Weathering processes in the Ganges-Brahmaputra basin and the riverine alkalinity budget. *Chem. Geol.* **159,** 31-60.

Galy A., France-Lanord C., and Derry L.A. (1999) The strontium isotopic budget of Himalayan rivers in Nepal and Bangladesh. *Geochim. Cosmochim. Acta.* **63,** 1905-1925.

Garrels R. M. and Mackenzie F. T. (1971) *Evolution of Sedimentary Rocks*. W.W. Norton & Company, New York.

Garrels R.M. and Perry E.A. Jr. (1974) Cycling of carbon, sulfur and oxygen through geologic time. In: *The Sea Vol. 5* (ed. E.D. Goldberg). Wiley. pp. 303-336.

Hall G. E. M. (1998) Cost-Effective Protocols for the Collection, Filtration and Preservation of Surface Waters for Detection of Metals and Metalloids at ppb ($\mu g \cdot l^{-1}$) and ppt ($ng \cdot l^{-1}$) Levels. Aquatic Effects Technology Evaluation Program (Task Force on Water Quality Issues). CANMET, Ottawa.

Hardie L. A. (1983) Origin of $CaCl_2$ brines by basalt-seawater interaction: Insights provided by some simple mass balance calculations. *Contrib. Mineral. Petrol.* **82,** 205-213.

Hercod D.J., Brady P.V. and Gregory, R. T. (1998) Catchment-scale coupling between pyrite oxidation and calcite weathering. *Chem. Geol.* **151,** 259-276.

Hoffman P.F. and Schrag D.P. (2002) The snowball Earth hypothesis; testing the limits of global change. *Terra Nova.* **14,** 129-155.

Holland H.D. (1978) *The Chemistry of the Atmosphere and the Oceans*. Wiley, New York.

Holser W.T. and Kaplan I.R. (1966) Isotope geochemistry of sedimentary sulfates. *Chem. Geol.* **1,** 93-135.

Huh Y., and Edmond J.M. (1999) The fluvial geochemistry of the rivers of Eastern Siberia: III. Tributaries of the Lena and Anabar draining basement terrain of the Siberian Craton and the Trans-Baikal Highlands. *Geochim. Cosmochim. Acta* **63,** 967-987.

Humphris S. E. and Thompson G. (1978) Hydrothermal alteration of basalts by seawater. *Geochim. Cosmochim. Acta* **42,** 107-125.

Kampschulte A. and Strauss H. (2004) The sulfur isotopic evolution of Phanerozoic seawater based on the analysis of structurally substituted sulfate in carbonates. *Chem. Geol.* **204,** 255-286.

Karim A. and Veizer J. (2000) Weathering processes in the Indus River Basin: implications from riverine carbon, sulphur, oxygen, and strontium isotopes. *Chem. Geol.*, **170,** 153-177.

Kump L.R. (1989) Chemical stability of the atmosphere and ocean. *Palaeogeogr. Palaeoclimatol. Palaeoecol.* **75,** 123-136.

Kump L.R. (1993) The coupling of the carbon and sulfur biogeochemical cycles over Phanerozoic time. In *Interactions of C, N, P and S Biogeochemical Cycles and Global Change* (eds. R. Wollast, F.T McKenzie and L. Chou). NATO ASI Ser. I, **4,** Springer-Verlag. pp. 475-490.

Kurtz A.C., Kump L.R., Arthur M.A., Zachos J.C. and Paytan A. (2003) Early Cenozoic decoupling of the global carbon and sulfur cycles. *Paleoceanography*, **18**, 1090.

Laird L. B., Taylor H. E., and Kennedy V. C. (1986) Snow chemistry of the Cascade-Sierra Nevada Mountains. *Environ. Sci. Technol.* **20,** 275–290.

Mackenzie F. T. and Kump L. R. (1995) Reverse weathering, clay mineral for oceanic element cycles. *Nature* **270,** 586-587.

Meybeck M. (1979) Concentrations des eaux fluviales en éléments majeurs et apports en solution aux océans. *Rev. Geol. Dyn. Géogr. Phys.* **21,** 215-246.

Meybeck M. (1987) Global chemical weathering of surficial rocks estimated from river dissolved loads. *Am. J. Sci.* **287,** 401-428.

Millot R., Gaillardet J., Dupré B. and Allègre C.J. (2003) Northern latitude chemical weathering rates: clues from the Mackenzie River Basin, Canada. *Geochim. Cosmochim. Acta* **67,** 1305-1329.

Mix A.C. and Ruddiman W. F. (1984) Oxygen-isotope analyses and Pleistocene ice volumes. *Quaternary Res.* **21**, 1-20.

Mojzsis S. J., Arrhenius G., McKeegan K. D., Harrison T. M., Nutman A. P. & Friend C. R. L. (1996) Evidence for life on Earth before 3,800 million years ago. *Nature*, **384**, 55-59.

Monger, J. W. H. (1997) Plate Tectonics and Northern Cordilleran Geology: An unfinished revolution. *Geoscience Canada* **24,** 189-198.

Motoyama R., Yanagisawa F., Akata N., Suzuki Y., Kanai Y., Kojima T., Kawabata A. and Ueda A. (2002) Sulfur isotope ratios of coals used in East Asia. *Journal of the Japanese Society of Snow and Ice* **64,** 49-58.

Negrel P., Allegre, C. J., Dupre, B. and Lewin E. (1993) Erosion sources determined by inversion of major and trace element ratios and strontium isotopic ratios in river water: The Congo Basin case. *Earth Planet. Sci. Lett.* **120,** 59-76.

Nielsen H. (1979) Sulfur Isotopes. In *Lectures in Isotope Geology* (eds. E. Jäger and J. Hunziker). Springer. pp. 283-312.

Nriagu J.O. and Coker R.D. (1978) Isotopic composition of sulfur in precipitation within the Great Lakes Basin. *Tellus* **30,** 365-375.

Oliver L., Harris N., Bickle M., Chapman H., Dise N. and Horstwood M. (2003) Silicate weathering rates decoupled from the $^{87}Sr/^{86}Sr$ ratio of the dissolved load during Himalayan erosion. *Chem. Geol.* **201**, 119-139.

Palmer M. R. and Edmond J. M. (1992) Controls over the stontium isotope composition of river water. *Geochim. Cosmochim. Acta* **56,** 2099-2111.

Pawellek F. and Veizer J. (1994) Carbon cycle in the upper Danube and its tributaries: $\delta^{13}C_{DIC}$ constraints. *Israel J. Earth Sci.* **43,** 187-194.

Pawellek F., Frauenstein F. and Veizer J. (2002) Hydrochemistry and isotope geochemistry of the upper Danube River. *Geochim. Cosmochim. Acta* **66,** 3839-3854.

Paytan A., Kastner M., Campbell D. and Thiemens M.H. (1998) Sulfur isotopic composition of Cenozoic seawater sulfate. *Science* **282,** 1459-1462.

Pearson F.J.Jr. and Rightmire C.T. (1980) Sulphur and oxygen isotopes in aqueous sulphur compounds. In *Handbook of environmental isotope geochemistry; Volume 1, The terrestrial environment, A.* (eds. P. Friz and J.C. Fontes). Elsevier. pp. 227-258.

Probst J. L., Mortatti J. and Tardy Y. (1994) Carbon river fluxes and weathering CO_2 consumption in the Congo and Amazon river basins. *Appl. Geochem.* **9,** 1-13.

Rankama K. (1954) The isotopic constitution of carbon in ancient rocks as an indicator of its biogenic or nonbiogenic origin. *Geochim. Cosmochim. Acta,* 5, 142-152.

Read P. B. (1977) Meager Creek volcanic complex, southwestern British Columbia. *Geol. Survey of Canada Paper* **77-1A,** 277-281.

Ruddiman W.F. (ed.) (1997) *Tectonic Uplift and Climate Change.* Plenum, New York.

Sagan C. and Mullen G. (1972) Earth and Mars: evolution of atmospheres and surface temperatures. *Science* **177,** 52-56.

Schindler D.W. (1999) Carbon cycling: The mysterious missing sink. *Nature* **398,** 105-107.

Shackleton, N.J. (1985) Oceanic carbon isotope constraints on oxygen and carbon dioxide in the Cenozoic atmosphere. In *The Carbon Cycle and Atmospheric CO2: Natural Variations Archean to Present, Geophys. Momgr. Ser.* **32** (eds E. T. Sundquist and W. S. Broecker). AGU, Washington, D.C. pp. 412-417.

Shackleton N.J. (1987) The carbon isotope record of the Cenozoic: History of organic carbon burial and of oxygen in the ocean and atmosphere. In *Marine Petroleum Source Rocks* (eds J. Brooks and A. J. Fleet). Geological Society, London. pp. 423-434.

Sklash M. G., Farvolden R. N. and Fritz P. (1976) A conceptual model of watershed response to rainfall, developed through the use of oxygen-18 as a natural tracer. *Can. J. Earth Sci.* **13,** 271-283.

Stallard R. F. (1995) Tectonic, environmental and human aspects of weathering and erosion: a global review using a steady-state perspective. *Ann. Rev. Earth Planet. Sci.* **23,** 11-39.

Stallard R.F. and Edmond J.M. (1981) Geochemistry of the Amazon; 1, Precipitation chemistry and the marine contribution to the dissolved load at the time of peak discharge. *J. Geophys. Res.* **86,** (C10) 9844-9858.

Stallard R.F. and Edmond J.M. (1983) Geochemistry of the Amazon 2. the influence of geology and weathering environment on the dissolved load. *J. Geophys. Res.* **88,** (C14) 9671-9688.

Stumm W. and Morgan J. J. (1996) *Aquatic Chemistry: Chemical Equilibria and Rates in Natural Waters* (Third Edition). John Wiley and Sons Inc. New York.

Taylor B.E. and Beaudoin G. (2000) Sulphur isotope stratigraphy of the Sullivan Pb-Zn-Ag deposit, B.C.; evidence for hydrothermal sulphur, and bacterial and thermochemical sulphate reduction. In *The geological environment of the Sullivan Deposit, British Columbia.* (eds. J.W. Lydon, T. Hoy, J.F. Slack, M.E. Knapp). Special Publication, Geological Association of Canada. Mineral Deposits Division 1. pp. 696-719.

Taylor B.E. (2004) Biogenic and thermogenic sulfate reduction in the Sullivan Pb-Zn-Ag deposit, British Columbia (Canada): Evidence from micro-isotopic analysis of carbonate and sulphide bedded ores. *Chem. Geol.* **204,** 215-236.

Tans P.T., Fung I.Y. and Takahashi T. (1990) Observational constraints on the global atmospheric CO_2 budget. *Science* **247,** 1431-1438.

Telmer K. (1997) *Biogeochemistry and water balance of the Ottawa River Basin.* Ph.D. Thesis, University of Ottawa.

Telmer K. and Veizer J. (1999) Carbon fluxes, pCO_2 and substrate weathering in a large northern river basin, Canada: carbon isotope perspectives. *Chem. Geol.* **159,** 61-86.

Telmer K. and Veizer J. (2000) Isotopic constraints on the transpiration, evaporation, energy, and gross primary production budgets of a large boreal watershed: Ottawa River basin, Canada. *Global Biogeochem. Cy.* **14,** 149-165.

Tranter M., Huybrechts P., Munhoven G., Sharp M. J., Brown G. H., Jones I. W., Hodson A. J., Hodgkins R. and Wadham J. L. (2002) Direct effect of ice sheets on terrestrial bicarbonate, sulphate and base cation fluxes during the last glacial cycle: minimal impact on atmospheric CO_2 concentrations. *Chem. Geol.* **190,** 33-44.

Turchyn A.V. and Schrag D.P. (2004) Oxygen isotope constraints on the sulfur cycle over the past 10 million years. *Science* **303,** 2004-2007.

Turekian K. K. and Wedepohl K. H. (1961) Distribution of the elements in some major units of the Earth's crust. *Geol. Soc. Am. Bull.* **72,** 175-191.

Van Stempvoort D.R., Wills J.J. and Fritz P. (1991) Aboveground vegetation effects on the deposition and cycling of atmospheric sulfur: chemical and stable isotope evidence. *Water Air Soil Poll.* **60,** 55-82.

Veizer J., Holser W.T. and Wilgus C.K. (1980) Correlation of 13C/12C and 34S/32S secular variations. *Geochim. Cosmochim. Acta* **44,** 579-587.

Veizer J., Ala D., Azmy K., Bruckschen P., Buhl D., Bruhn F., Carden G. A. F., Diener A., Ebneth S., Godderis Y., Jasper T., Korte C., Pawallek F., Podlaha O. G. and Strauss H. (1999) $^{87}Sr/^{86}Sr$, $\delta^{13}C$ and $\delta^{18}O$ evolution of Phanerozoic seawater. *Chem. Geol.* **161,**
59-88.

Vinogradov A. P. (1962) Srednie soderzhaniya khimicheskikh elementov v glavnykh tipakh izverhennykh gornykh porod zemnoi kory. *Geokhimiya* **7,** 555-571.

Wadleigh M.A., Schwarcz H.P. and Kramer J.R. (1996) Isotopic evidence for the origin of sulphate in coastal rain. *Tellus* **48B,** 44-59.

Walker J. C. G., Hays P. B. and Kasting J. F. (1981) A negative feedback mechanism for the long-term stabilization of Earth's surface temperature. *J. Geophys. Res.* **86,** (c10) 9776-9782.

Wedepohl K.H. (1995) The composition of the continental crust. *Geochim. Cosmochim. Acta* **59,** 217-239.

Wheeler J. O., McFeely P. (1991) Tectonic Assemblage Map of the Canadian Cordillera and Adjacent parts of the United States of America. Geological Survey of Canada, Map 1712a.

Yang C., Telmer K. and Veizer J. (1996) Chemical dynamics of the "St. Lawrence" riverine system: δD_{H2O}, $\delta^{18}O_{H2O}$, $\delta^{13}C_{DIC}$, $\delta^{34}S_{sulphate}$, and dissolved $^{87}Sr/^{86}Sr$. *Geochim. Cosmochim. Acta.* **60,** 851-866.

3 Dissolved and adsorbed rare earth element transport by rivers in the western Canadian Cordillera: influence of chemical versus physical erosion

3.1 OVERVIEW

Dissolved rare earth elements (REE), REE adsorbed to suspended particulate matter, and distribution coefficients of REE between the adsorbed and dissolved phases ($Kd_{REE}^{ads/dis}$) were measured in three of the largest river systems draining the western Canadian Cordillera into the Pacific Ocean (Fraser, Skeena and Nass). The results are used to interpret chemical and physical weathering processes within these watersheds, and to measure dissolved and adsorbed REE fluxes to the Pacific Ocean.

Prior to analysis by inductively coupled plasma mass spectrometry (ICP-MS), dissolved (< 0.45 μm) REE were concentrated using an iminiodiacetate resin; and, adsorbed REE were extracted from suspended particulate with 1 N ammonium acetate. Relative abundances of the REE (REE patterns) are found to have proportional distribution between the dissolved and adsorbed phases which is consistent for all of the samples. Thus adsorbed REE patterns can serve as a proxy for dissolved REE patterns, which eliminates the need for concentration procedures and large sample sizes required to measure dissolved REE. In this paper, the sum of the dissolved and adsorbed REE are considered (labile REE).

The REE patterns are found to vary across the Cordillera, and reflect basin lithology. Chondrite normalised labile La/Yb ratios (La_n/Yb_n) range from 2.4 to 13.2. The labile REE composition of the Fraser River near the mouth represents a mixture of inputs from individual tributaries, indicative of the conservative nature of the labile REE. Furthermore, there is sufficient variability in labile REE patterns between watersheds to support the development of labile REE as a chemical weathering or hydrological tracer.

$Kd_{REE}^{ads/dis}$ values in June (high water stage, average ≈ 1000) are approximately 50 times lower than $Kd_{REE}^{ads/dis}$ values in October (low water stage, average ≈ 50000). This indicates a change in the composition of the suspended particulate matter, suggesting a shift in particulate source from recently eroded rock flour (alpine source) in June, to alluvial soils (valley source) in October, which have developed over the Holocene and have greater proportion of clay minerals and therefore higher adsorptive capacity.

This shift indicates that silicate weathering (and CO_2 drawdown) is occurring in the valley regions of the watersheds (relatively low physical erosion rates), while the alpine regions have high physical erosion rates and little to no silicate weathering. This means that silicate weathering in the Canadian Cordillera is not directly coupled to physical erosion. This also shows that the suspended particulate budget of the Cordilleran rivers is dominated by current uplift and erosion, rather than remobilization of material eroded during Pleistocene glaciation, which suggests that the erosional regime in the Canadian Cordillera is approaching steady state.

3.2 INTRODUCTION

Physical and chemical erosion of continental material not only shapes the Earth's surface but also modulates the chemistry of the oceans and atmosphere, thereby directly influencing the Earth's surface environment (e.g. Garrels and Mackenzie, 1971; Garrels and Perry, 1974; Walker et al., 1981; Holland et al., 1986). Recently, earth scientists have become increasingly aware of intimate coupling between climate, tectonics, and erosion (e.g. Hoffman and Grotzinger, 1993). Walker et al. (1981) proposed a negative feedback between silicate weathering rates and atmospheric CO_2 has been responsible for regulating the greenhouse state of the atmosphere, and maintained climate stability over much of the earth's history. This has spurred many researchers to measure chemical and physical erosion rates globally (e.g. Meybeck, 1987; Milliman and Meade 1983; Summerfield and Hulton, 1994; Gaillardet et al., 1999 and many others) in order to quantify the interactions and feedbacks between these processes (Ruddiman, 1997 is a compilation of papers on this subject). An important motivation to study erosional processes and rates stems from the need to quantitatively understand the natural controls on these processes and how they interact with other Earth Systems so that perturbations due to human activities can be assessed and moderated, and to place recent observations into long-term perspective.

Conversion of bedrock into soil occurs through a combination of physical and chemical breakdown (weathering) of the bedrock material. Erosion refers to the process of transport of the weathered material from its source either as dissolved (chemical erosion) or particulate matter (physical erosion). Incongruent chemical weathering of silicate and sulphide minerals releases some of the constituent ions into solution,

providing nutrients for biota, and ultimately to be transported by river water as dissolved load. Other elements remain as components of secondary minerals which form the weathering residuum (regolith), a major component of soil. Other minerals, such as carbonates and evaporites weather congruently, which means that all of their component ions are dissolved and no secondary minerals are formed. In chapter 2 of this thesis, the chemical weathering pathways that are important in the Canadian Cordillera are described and quantified. These are, in order of decreasing importance: (i) carbonate weathering by carbonic acid > (ii) silicate weathering by carbonic acid ≈ (iii) coupled sulphide-carbonate weathering. These weathering pathways can be represented by equations 1 to 3:

carbonate (calcite) weathering by carbonic acid:

$$CO_{2(aq)} + H_2O_{(l)} + CaCO_{3(calcite)} \rightarrow 2HCO^-_{3(aq)} + Ca^{2+}{}_{(aq)} \quad (1)$$

silicate (albite) weathering by carbonic acid:

$$2CO_{2(aq)} + 3H_2O_{(l)} + 2NaAlSi_3O_{6(albite)} \rightarrow$$
$$2HCO^-_{3(aq)} + 2Na^+_{(aq)} + 4SiO_{2(aq)} + Al_2Si_2O_5(OH)_{4(kaolinite)} \quad (2)$$

coupled sulphide-carbonate weathering:

$$\tfrac{1}{2}FeS_2 + CaCO_3 + \tfrac{15}{8}O_2 \rightarrow \tfrac{1}{4}Fe_2O_3 + Ca^{2+} + SO^{2-}_4 + CO_2 \quad (3)$$

The absolute and relative rates of these reactions are important for the long term (> 10^5 years) evolution of the oceans and the atmosphere because they are a major source of ions to the oceans, and they involve important components of the atmosphere, O_2 and CO_2. Although carbonate weathering by carbonic acid (equation 1) converts CO_2 into bicarbonate (HCO_3^-), this weathering pathway does not influence the long term CO_2 budget of the atmosphere because it is balanced by carbonate deposition in the oceans

(the reverse of equation 1) on timescales equal to or less than 10^5 years. Silicate weathering (equation 2) can draw down atmospheric CO_2 on 10^5 year and greater timescales, because coupling of silicate weathering (equation 2) with carbonate deposition in the oceans (reverse of equation 1) facilitates sequestration of half of the CO_2 consumed by equation 2 into carbonate minerals in marine sediments. Coupled sulphide-carbonate weathering (equation 3) can provide a long term (> 10^5 years) source of CO_2 and sink of O_2 due to the disparity in marine residence times of SO_4^{2-} (~10^7 years, Berner and Berner, 1987) and HCO_3^- (~10^5 years, Berner and Berner, 1987). The long residence time of SO_4^{2-} in the ocean means that equation 3 can be balanced by pyrite deposition (which consumes CO_2 and liberates O_2, Garrels and Perry, 1974) on 10^7 year timescales, but on shorter timescales CO_2 can build in the atmosphere and O_2 be drawn down (see chapter 2 for a full discussion of this topic).

Chemical weathering and physical erosion rates are commonly measured by measuring the dissolved and particulate burden of rivers. This is possible because ~90% of the products of continental weathering and erosion that are transported to the ocean are transported by rivers (Garrels and Mackenzie, 1971). Under steady-state weathering conditions, the rate of supply of fresh bedrock by tectonic uplift is balanced by the rate of removal of material by chemical and physical erosion. Steady-state weathering also implies that the rate of conversion of bedrock into soil by chemical and physical weathering is balanced by erosion (physical removal of regolith), which means that soil depth and composition remains constant with respect to time. Current weathering and erosion rates that are measured using river fluxes can be accurately integrated over geological timescales only if the system in question is currently at steady state. Because

river measurements represent a snapshot in geological time, steady state must be assumed or inferred from other lines of evidence.

Interpretation of the chemical signal contained in rivers is further complicated multiple sources of the major elements. As well, the dissolved major element and strontium isotopic composition of rivers is almost always dominated by the products of carbonate dissolution, even when carbonate is present in trace amounts in the local bedrock (e.g. Drever and Hurcomb, 1986; Blum et al., 1998; Telmer and Veizer, 1999). Thus the silicate weathering signal is often only a minor to trace component of the bulk river chemistry, and therefore difficult to measure. This is important for our ability to understand climate/weathering feedbacks because only silicate weathering is responsible for long term ($>10^5$ yr) atmospheric CO_2 drawdown.

In this paper, the rare earth element (REE) signal in rivers is explored as a tracer of weathering and erosion. As part of a geochemical survey of three large watersheds of the western Canadian Cordillera (Fraser, Skeena and Nass) dissolved REE and REE adsorbed to suspended particulate (adsorbed REE) have been analysed in major rivers and tributaries. The sum of the dissolved and adsorbed REE (hereafter "labile REE") should be representative of REE liberated into solution by chemical weathering in the watershed. It is shown that the labile REE reflect the bedrock lithology for each watershed, and that the relative abundances of REE are conservative in the rivers so that downstream samples represent mixtures of the upstream sources (tributary waters). Seasonal changes in the distribution of REE between the dissolved and adsorbed phases of the rivers is shown to reflect both physical and chemical erosion style in the Canadian

Cordillera, and gives evidence that erosion in this system is currently approaching steady state.

3.2.1 Rare Earth Elements in River Water

Chemical weathering exposes all of the component ions of a mineral (trace and major alike) to a set of conditions that facilitates either dissolution into the aqueous phase or incorporation into secondary minerals such as clay or oxide minerals. The ions that do go into solution do not always remain as free dissolved ions, but can adsorb to particulate surfaces. REE are known to have a high affinity for adsorption onto particulate surfaces (Elderfield et al., 1990). The combination of dissolved and adsorbed REE in river water should be representative of the REE released into solution by bedrock weathering for a given catchment. The physical and chemical properties of REE make them excellent geochemical tracers, however their behaviour in aqueous systems remains poorly understood (McLennan, 1989).

In general, REE are incompatible elements during anatexis (partial melting of crustal or mantle rock), with decreasing incompatibility moving across the lanthanide group from La to Lu (e.g. McLennan, 1989). This means a melt generated by anatexis will be enriched in REE compared to the residual material, with preferential enrichment of light rare earth elements (LREE) over heavy rare earth elements (HREE). Because the evolution of continental crust involves recycling and re-melting of crustal rocks REE patterns can be used as an index of crustal evolution, and compositional maturity, where evolved rocks have higher LREE / HREE ratios than un-evolved rocks (e.g. McLennan, 1989).

Unique to the REE as a group of elements is their chemical similarity, which allows the relative abundances of REE to be preserved through metamorphic and weathering/erosion processes. Thus REE patterns can be used to determine provenance and petrogenetic history of sedimentary and igneous rocks (Taylor and McLennan 1985, McLennan 1989, Condie 1991). It has been shown that REE patterns in weathered material are essentially unchanged from the original unweathered source rock (Nesbitt 1979) but there are conflicting reports as to whether chemical weathering can produce dissolved REE with the same relative abundances as the source (McLennan 1989 reviews this topic). These two conclusions are somewhat contradictory, which reflects the poor understanding of REE in the exogenic cycle. The potential for dissolved REE patterns to be used as a chemical weathering tracer remains untested primarily because of the difficulty in analysing REE at typical ambient concentrations in natural waters (generally low to sub $ng \cdot kg^{-1}$ (ppt), e.g. Hall et al., 1995). This paper contributes new dissolved REE data for the Cordilleran Rivers, and presents a new method for determining dissolved REE patterns through analysis of REE adsorbed to suspended particulate matter.

3.3 STUDY AREA

Water samples were collected from 12 rivers in the Fraser, Skeena and Nass drainage basins, draining the western Canadian Cordillera, in June and October 2002. Dissolved concentrations of SO_4^{2-}, Cl^-, HCO_3^-, F^-, NO_3^-, Ca^{2+}, Mg^{2+}, Na^+, K^+, the $\delta^{13}C$ in dissolved inorganic carbon ($\delta^{13}C_{DIC}$), $\delta^{34}S$ in dissolved sulphate ($\delta^{34}S_{SO4}$), pH, temperature, conductivity, and charge balance from these samples are reported and described, along with mass balance calculations of chemical weathering rates in chapter

2. Here we present dissolved and adsorbed REE data for the same samples. See chapter 1 for a complete description of the watershed characteristics and basin geology.

3.4 METHODS

3.4.1 Sample Collection

During the peak (June) and trough (October) of the 2002 hydrograph, 49 water and suspended particulate samples (including field duplicates and blanks) were collected from 14 rivers draining the Fraser, Skeena and Nass watersheds. The water samples were filtered in the field through pre-weighed Millipore 0.45 μm HVLP polyvinyl filter membranes, and collected in clean HDPE bottles that were pre-rinsed with filtered water. These samples were preserved by injecting concentrated (16 N) Environmental Grade Nitric Acid so that the final acid strength in the samples was 0.06 N. A detailed description of the water sampling and preservation technique is given in chapter 2. Figure 3.1 is a flowchart of the sample preparation and analytical methods used.

Suspended particulate samples were collected by collecting the sediment laden filter membranes. On return to the lab, the sediment laden filters were dried in a desiccator at room temperature in the dark. The total suspended sediment concentration (TSS) was estimated by determining the mass (dry weight) of sediment captured per litre of water filtered. All drying, weighing and subsequent handling of the sediment samples was conducted under clean (class 100) conditions.

3.4.2 Reagent Preparation

All reagents used for sample preparation and for cleaning procedures were prepared with ultra pure reagents and with 18.2 MΩ (deionized) water.

3.4.3 Dissolved REE Concentration

In order to bring the REE to a level that could be reliably quantified by quadrapole ICP-MS analysis (LOD for Lanthanide elements is typically around 1 to 10 $ng \cdot kg^{-1}$ ($1\ ng \cdot kg^{-1} = 1$ ppt)), the samples were concentrated using a modified DIONEX ion chromatograph fitted with a CC-1 concentrator column packed with an iminiodiacetate resin. This method has advantages over evaporative concentration methods because it eliminates elements like chlorine and barium that can produce mass interferences on the REE during analysis by ICP-MS. The steps of the automated sample preparation is described here:

1. A fixed volume of filtered sample water is buffered on-line to pH 5.5 with ammonium acetate, and loaded onto the CC-1 column.
2. The alkali (Li, Na, K, Rb, Cs) and alkaline earth (Be, Mg, Ca, Sr, Ba. Ra) cations are eluted from the column to waste with ammonium acetate.
3. Ammonium acetate is rinsed from the column with deionised water.
4. The REE (and transition elements) that have been retained on the column are eluted in a small volume of 1.0 N nitric acid into a clean vial.

Concentration of the dissolved REE is achieved by loading a large volume of sample onto the CC-1 column and then eluting the REE into a much smaller volume of 1.0 N nitric acid. For this study, 88 mL of each sample was loaded onto the CC-1 and eluted in 8 mL of 1.0 N nitric acid giving 11 times concentration. All calibration standards and blanks were treated the same as the samples. The resulting concentrated solutions were then quantitatively injected with an internal standard (containing Be, Sc, Ge, In, Tl, Th), and analysed by ICP-MS.

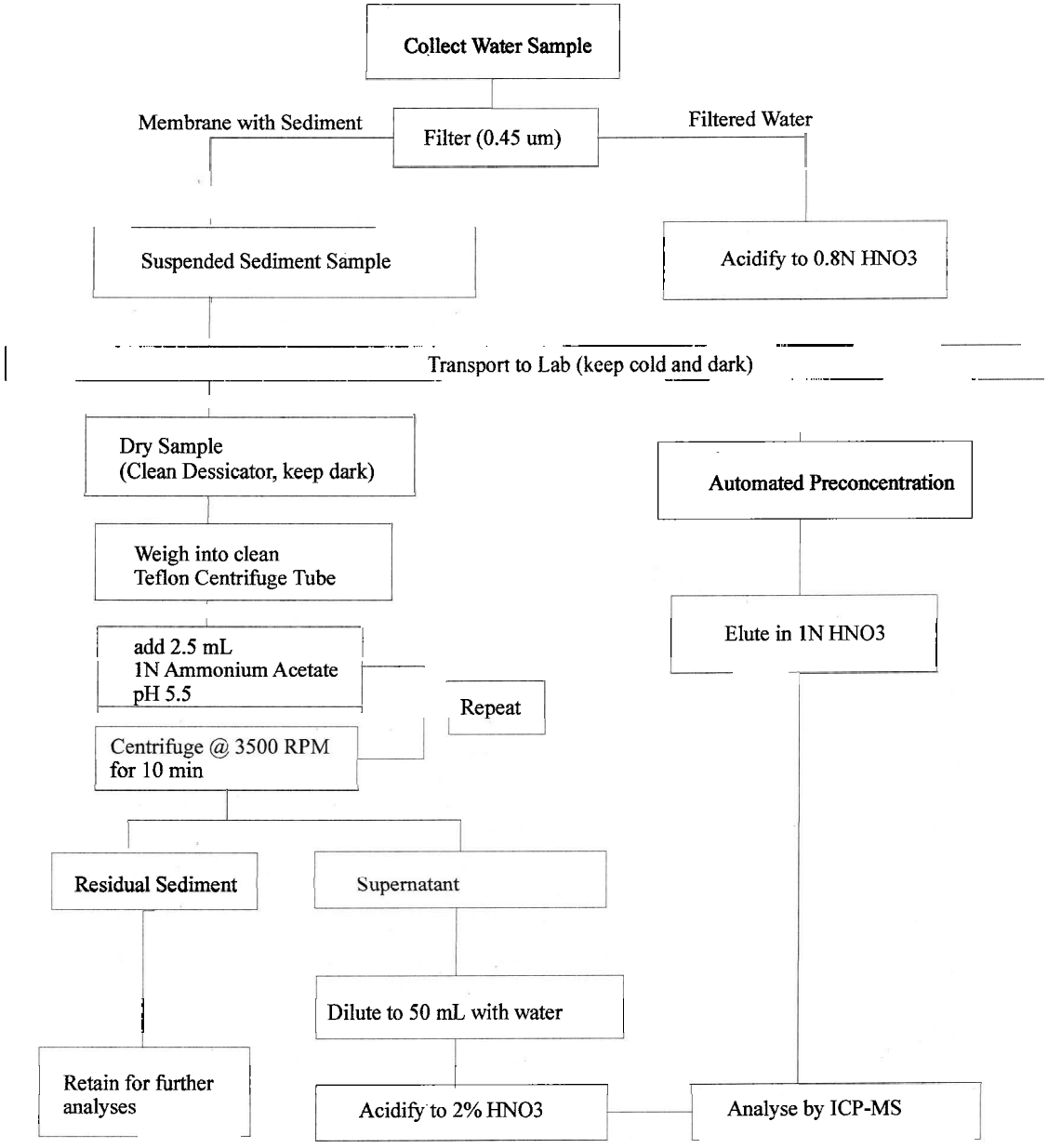

Figure 3.2 Flowchart showing the sample preparation and analysis procedures used to determine labile REE in the Cordilleran Rivers.

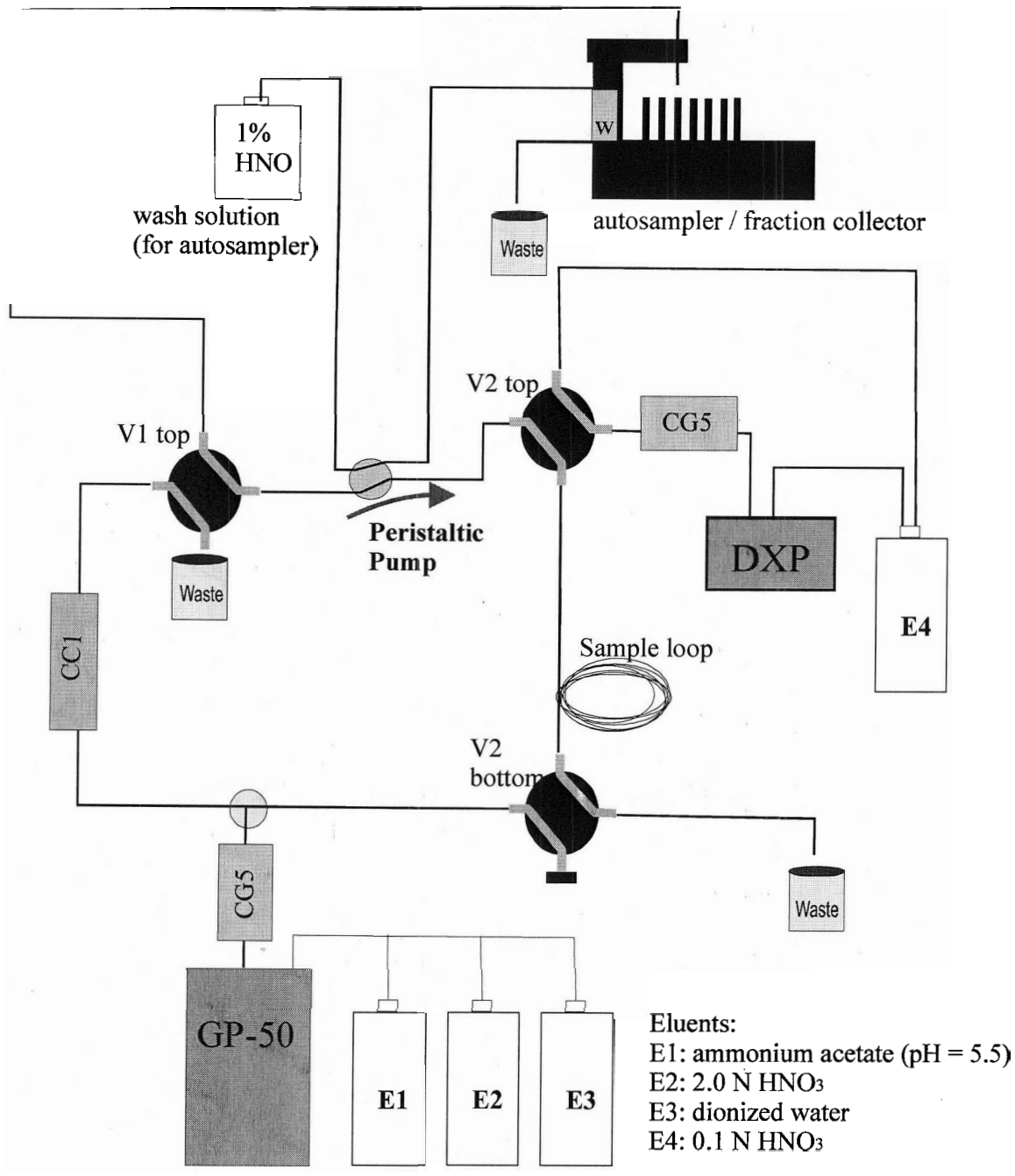

Figure 3.2 Schematic diagram of the automated REE concentration system showing two dual stack valves (V1, V2), four eluent bottles (E1 to E4), one gradient pump (GP-50), one isocratic pump (DXP), one peristaltic pump, 1% HNO3 (wash solution for autosampler probe)

A detailed description of this method is given by Hall et al. (1995). Figure 3.2 is a schematic diagram of the concentration system used for this work. Appendix D gives the details of the GP-50 gradient pump program and the AIM 1250 autosampler program. This system differs from the one used by Hall et al. in that our setup used a combination autosampler/fraction collector (AIM 1250 autosampler) instead of separate units to sip un-concentrated sample and deliver concentrated solution. Also, our system uses a peristaltic pump to load the sample into a sample loop prior to loading the sample onto the CC-1 with the DXP pump rather than directly pumping the sample onto the column. The advantage of using a sample loop is that the amount of sample loaded onto the column can be precisely determined (by the number of times the sample loop is loaded) and is not dependant on pump flow stability. A further advantage of using the sample loop is that while the sample loop is being loaded, the CC-1 column can be rinsed with ammonium acetate buffer to remove Group I and II elements. This minimizes the risk of overloading the column with cations which could inhibit the retention of analyte elements. A disadvantage of using a sample loop is that more sample is consumed than if it were directly pumped onto the CC-1. About 5 mL of sample is lost each time the loop is loaded. It would be possible to reduce this volume, but not to entirely eliminate it.

We used a 22 mL sample loop made from NO-OX tubing (double layered tubing with a teflon inner tube and a plastic outer sheath), which was loaded four times for each sample. The entire concentration procedure takes about 60 minutes for each sample. The samples were processed in batches of 8 (1 blank, 1 standard, 6 samples).

3.4.4 Adsorbed REE Extraction

The adsorbed REE are defined as REE adsorbed to surfaces of suspended particulate material in river water, and are in equilibrium (i.e. are exchangeable with) ions in solution. Thus an extraction method designed to liberate only weakly bound REE into solution was devised. This extraction is based on common protocols for determining exchangeable cations in porous media (e.g. Fetter, 1994; Langmuir, 1997). Here the extraction was performed with ultra pure 1N ammonium acetate solution buffered to pH 5.5. This is a cation exchange extraction, where the ammonium ions (NH_4^+) preferentially bond to adsorption sites on the particulate surfaces, thereby displacing adsorbed cations (including REE) into solution. Because the pH is buffered to 5.5 (weakly acidic), and the duration of the extraction is short (two extractions of 30 minutes each), there should be no dissolution of minerals. Thus the elements that go into solution should be representative of REE that are weakly adsorbed to particle surfaces only.

Particulate samples were transferred quantitatively into clean Teflon centrifuge tubes by scraping the material off the filters with a clean plastic spatula (weighing the material removed from the filter); or, in cases where there was not enough material on the filter to quantitatively scrape an aliquot off, the entire filter membrane was placed into a clean centrifuge tube. Selected samples were prepared by both methods (scraping and whole membrane extraction). Analytical results agreed within method precision.

The exchangeable REE were extracted as follows: 2.5 mL of 1N ammonium acetate (pH 5.5) was added to each centrifuge tube. The tubes were then shaken vigorously for about 15 s, followed by gentle mixing for 30 min using a mechanical mixer. Samples were then centrifuged at 3500 rpm for 10 min, and the supernatant

extracted into a clean HDPE bottle using a fresh pipette tip (trace metal certified) for each sample. The extraction was repeated twice in order to ensure that all of the exchangeable material was extracted. The extracted supernatant was diluted to ~50 mL with 18 MΩ deionized water, and acidified to 2% v/v with 16N HNO_3. These samples were then spiked with internal standard and analysed by ICP-MS.

3.4.5 Analysis

All of the samples were analysed for REE at the University of Victoria using a VG PQII+S quadrupole ICP-MS fitted with a concentric nebuliser and cool water jacketed spray chamber. Instrumental drift corrections were made based on variations in the sensitivity of Indium and Thorium (added to each sample in the internal standard). Indium and Thorium were used for this correction because their masses (115 and 232 amu respectively) bracket the analyte masses. External calibration standards were prepared from NIST traceable pure element standard solutions, and made up in the same matrix as the analyte samples. For both the exchangeable REE and the dissolved REE, procedural and field blanks returned values below instrumental detection. Analyte elements were undetectable in all blanks.

Table 3.1(A) Labile REE concentrations ($ng \cdot kg^{-1}$) for the Cordilleran rivers (June Campaign). "ud" denotes analytes below method limit of detection.

Station	Sample	Y	La	Ce	Pr	Nd	Sm	Eu	Gd	Tb	Dy	Ho	Er	Tm	Yb	Lu
1	101	46	43	76	12	51	11	3	10	2	9	2	6	1	5	1
2	102	126	100	194	29	123	28	7	28	4	25	5	16	2	15	2
4	104	95	46	79	16	73	19	6	21	3	19	4	11	2	11	2
5	105	99	78	144	21	88	21	6	23	4	20	4	12	2	11	2
7	107	50	34	77	11	48	12	3	13	2	12	2	6	1	6	1
7	108	78	61	140	20	87	21	6	22	3	20	4	11	1	9	1
8	109	108	96	180	27	105	28	9	29	8	27	8	17	8	19	16
8	110	132	112	220	30	123	28	7	29	5	26	5	14	2	12	2
9	111	106	48	72	16	75	18	4	21	3	19	4	13	2	14	2
10	112	201	120	254	41	195	53	17	60	9	50	9	24	3	18	3
11	113	190	92	183	31	151	42	14	46	7	40	8	21	3	17	2
12	114	232	92	175	31	148	40	13	46	7	44	9	24	3	22	3
13	115	251	146	305	50	227	62	20	70	11	58	11	28	4	23	4
13	116	190	89	170	29	141	39	12	44	7	40	8	21	3	19	3
14	117	120	53	121	19	95	29	9	33	5	27	5	12	2	9	1
15	118	97	40	90	15	72	22	7	25	4	21	4	10	1	7	1
16	119	52	15	27	6	28	9	3	11	2	10	2	5	1	4	1
17	120	194	75	118	25	120	32	10	37	6	34	7	21	3	19	3
18	121	90	144	203	36	142	28	6	29	4	22	4	10	1	8	1
19	122	37	80	69	19	73	13	2	13	2	9	1	4	ud	2	ud
20	123	109	134	189	36	139	29	6	31	5	24	4	11	1	9	1
21	124	99	128	147	31	122	25	5	24	4	21	4	12	2	11	2
23	126	89	86	115	23	92	20	5	20	3	18	4	11	2	10	2
24	127	106	100	189	27	115	26	7	28	4	24	5	13	2	12	2
24	128	78	56	93	15	65	16	4	17	3	16	3	9	1	9	1
max		251	146	305	50	227	62	20	70	11	58	11	28	8	23	16
min		37	15	27	6	28	9	2	10	2	9	1	4	1	2	1
median		106	86	144	25	105	26	6	28	4	22	4	12	2	11	2
mean		119	83	145	25	108	27	8	29	5	25	5	14	2	12	2
stdev		58	36	66	10	46	13	4	15	2	13	2	6	1	6	3

Table 3.1(B) Dissolved REE concentrations ($ng \cdot kg^{-1}$ (ppt)) for the Cordilleran rivers (October Campaign). "ud" denotes analytes below method limit of detection.

Station	Sample	Y	La	Ce	Pr	Nd	Sm	Eu	Gd	Tb	Dy	Ho	Er	Tm	Yb	Lu
1	201	18	17	32	5	20	4	1	4	1	3	1	2	ud	2	ud
2	202	39	32	63	9	37	8	2	8	1	7	2	4	1	4	1
4	203	13	5	5	1	7	2	ud	2	ud	2	ud	1	ud	1	ud
7	205	22	14	30	5	20	5	1	5	1	5	1	3	ud	3	ud
8	206	102	97	159	24	101	23	6	25	4	21	4	12	2	10	2
8	207	139	150	278	40	160	36	9	37	6	32	6	17	2	15	2
9	208	33	15	21	5	21	5	1	6	1	6	1	4	1	4	1
10	209	100	46	52	17	74	25	10	29	8	26	8	16	8	17	16
12	210	75	27	36	9	44	12	4	15	2	14	3	9	1	8	1
13	211	100	46	67	15	70	20	6	23	4	21	4	12	2	10	2
13	212	149	75	137	24	115	30	9	34	5	31	6	17	2	14	2
15	213	317	195	437	61	275	74	23	81	13	75	14	38	5	29	4
16	215	72	25	35	11	45	17	7	20	6	18	6	10	4	9	5
18	214	154	220	262	55	216	43	9	46	7	36	6	17	2	12	2
20	218	154	211	267	54	212	43	9	47	7	36	6	16	2	12	2
21	219	39	45	51	11	45	9	2	9	1	8	2	4	1	4	1
23	221	30	30	26	7	28	6	1	6	1	6	1	3	1	4	1
24	222	169	154	269	41	169	39	10	42	7	36	7	20	3	17	3
max		317	220	437	61	275	74	23	81	13	75	14	38	8	29	16
min		13	5	5	1	7	2	1	2	1	2	1	1	1	1	1
median		87	46	58	13	57	18	6	21	4	19	4	11	2	9	2
mean		96	78	124	22	92	22	7	24	4	21	5	11	2	10	3
stdev		77	74	126	20	81	19	5	21	4	18	3	9	2	7	4

Table 3.2(A) Adsorbed REE dry weight concentrations ($\mu g \cdot kg^{-1}$ (ppb)) for the Cordilleran rivers (June Campaign). "ud" denotes analytes below method limit of detection.

Station	Sample	Y	La	Ce	Pr	Nd	Sm	Eu	Gd	Tb	Dy	Ho	Er	Tm	Yb	Lu
1	101	49	53	112	15	60	13	5	13	2	10	2	6	2	5	2
2	102	115	86	154	24	95	22	9	22	4	19	4	10	2	9	2
4	104	131	64	99	19	87	24	10	28	4	22	4	12	2	10	2
5	105	190	157	330	43	167	42	14	45	7	35	7	19	3	15	3
7	107	138	73	164	22	108	28	9	30	5	25	5	13	1	10	1
8	109	190	161	333	42	172	41	13	44	7	35	7	18	2	15	2
8	110	262	227	479	58	239	57	17	62	9	48	9	25	3	19	3
9	111	422	276	405	85	386	93	25	101	14	79	15	42	5	35	5
10	112	120	56	99	17	86	25	13	30	4	23	4	10	1	6	ud
12	114	177	71	129	21	104	31	16	35	5	31	6	15	2	12	2
13	115	127	58	102	18	88	26	14	31	4	23	4	11	1	7	1
13	116	152	68	118	21	98	29	15	33	5	28	5	13	1	9	1
14	117	129	44	84	15	76	24	13	30	5	23	4	10	1	6	1
15	118	102	34	68	12	60	21	11	25	4	20	3	8	1	5	1
16	119	111	37	77	13	66	23	11	26	4	21	4	9	1	6	1
17	120	70	33	58	10	45	14	5	14	2	12	2	6	ud	4	ud
18	121	323	555	936	135	487	98	21	99	14	68	12	30	3	19	3
20	123	99	123	180	30	118	26	5	27	4	20	3	8	ud	6	ud
21	124	103	135	171	32	120	28	7	27	4	19	3	9	ud	7	ud
23	126	116	123	226	32	128	28	8	29	4	21	4	11	ud	9	ud
24	127	363	354	682	93	356	86	26	91	14	70	13	35	4	27	4
max		422	555	936	135	487	98	26	101	14	79	15	42	5	35	5
min		49	33	58	10	45	13	5	13	2	10	2	6	1	4	1
median		129	73	154	22	104	28	13	30	4	23	4	11	2	9	2
mean		166	133	238	36	150	37	13	40	6	31	6	15	2	12	2
stdev		98	129	226	32	119	25	6	26	4	19	3	10	1	8	1

Table 3.2(B) Adsorbed REE dry weight concentrations ($\mu g \cdot kg^{-1}$ (ppb)) for the Cordilleran rivers (October Campaign). "ud" denotes analytes below method limit of detection.

Station	Sample	Y	La	Ce	Pr	Nd	Sm	Eu	Gd	Tb	Dy	Ho	Er	Tm	Yb	Lu
1	201	1014	861	1547	237	857	202	64	199	32	144	32	81	14	81	15
2	202	2374	1635	3249	493	1796	411	107	441	68	351	70	195	29	180	30
7	205	1906	940	2012	317	1249	351	109	375	59	294	63	169	24	135	23
8	207	2355	2197	4314	601	2139	534	147	587	93	453	87	235	31	183	29
9	208	2553	1625	2449	491	2095	511	141	576	88	418	95	242	41	202	42
13	211	1078	542	1087	168	676	200	72	234	36	190	37	90	13	76	12
13	212	3728	1814	3805	615	2556	753	261	903	134	674	132	361	50	272	47
15	213	2018	785	1482	235	953	302	118	369	61	317	62	155	19	106	15
17	216	2971	1204	2039	402	1698	512	178	594	99	505	95	252	37	192	32
21	219	4675	5213	7362	1319	4614	1046	270	1176	174	858	164	392	54	293	53
23	221	3489	3383	5285	911	3250	778	205	804	125	638	125	322	48	263	46
24	222	2325	1820	3616	502	1813	462	137	508	80	409	78	198	26	160	26
max		4675	5213	7362	1319	4614	1046	270	1176	174	858	164	392	54	293	53
min		1014	542	1087	168	676	200	64	199	32	144	32	81	13	76	12
median		2364	1630	2849	492	1805	487	139	542	84	414	82	217	30	181	29
mean		2540	1835	3187	524	1975	505	151	564	87	438	87	225	32	179	31
stdev		1058	1312	1832	323	1112	251	67	283	42	206	39	98	14	72	14

Table 3.3(A) Labile REE concentrations (ng REE per kg water (ppt)) for the Cordilleran rivers (June Campaign). "ud" denotes analytes below method limit of detection.

Sample	Y	La	Ce	Pr	Nd	Sm	Eu	Gd	Tb	Dy	Ho	Er	Tm	Yb	Lu
101	2.5	2.7	5.6	0.8	3.0	0.7	0.3	0.7	0.1	0.5	0.1	0.3	0.1	0.3	0.1
102	14	11	19	2.9	12	2.7	1.1	2.7	0.4	2.3	0.5	1.3	0.2	1.1	0.2
104	17	8.2	13	2.5	11	3.1	1.3	3.5	0.5	2.8	0.6	1.5	0.2	1.3	0.2
105	24	19	41	5.3	21	5.2	1.7	5.6	0.9	4.4	0.9	2.3	0.3	1.8	0.3
106	70	45	99	14	58	15	4.8	15	2.5	13	2.5	6.9	1.0	6.1	1.0
107	12	6.5	15	2.0	9.7	2.5	0.8	2.7	0.4	2.2	0.4	1.1	0.1	0.9	0.1
109	20	17	35	4.3	18	4.3	1.3	4.6	0.7	3.7	0.7	1.9	0.2	1.6	0.2
110	40	34	73	8.8	36	8.7	2.6	9.3	1.4	7.3	1.3	3.7	0.4	2.8	0.4
111	2.6	1.7	2.5	0.5	2.4	0.6	0.2	0.6	0.1	0.5	0.1	0.3	0.0	0.2	0.0
112	16	7.5	13	2.3	12	3.4	1.8	4.0	0.6	3.1	0.5	1.4	0.1	0.9	ud
114	31	13	23	3.8	18	5.4	2.8	6.2	1.0	5.4	1.0	2.7	0.3	2.1	0.3
115	19	8.7	15	2.6	13	3.9	2.1	4.6	0.7	3.5	0.6	1.6	0.2	1.1	0.1
116	21	9.3	16	2.8	14	4.0	2.1	4.6	0.7	3.8	0.7	1.8	0.2	1.3	0.2
117	14	4.7	9.0	1.6	8.1	2.6	1.4	3.2	0.5	2.5	0.5	1.1	0.1	0.7	0.1
118	12	4.0	7.9	1.3	7.0	2.4	1.2	2.9	0.4	2.3	0.4	0.9	0.1	0.6	0.1
119	9.2	3.1	6.4	1.1	5.5	1.9	0.9	2.2	0.3	1.7	0.3	0.7	0.1	0.5	0.1
120	4.2	2.0	3.5	0.6	2.8	0.8	0.3	0.9	0.1	0.7	0.1	0.4	ud	0.3	ud
121	11	18	31	4.5	16	3.3	0.7	3.3	0.5	2.3	0.4	1.0	0.1	0.6	0.1
123	2.3	2.8	4.1	0.7	2.7	0.6	0.1	0.6	0.1	0.5	0.1	0.2	ud	0.1	ud
124	1.4	1.8	2.3	0.4	1.6	0.4	0.1	0.4	0.0	0.3	0.0	0.1	ud	0.1	ud
126	1.5	1.6	2.9	0.4	1.6	0.4	0.1	0.4	0.0	0.3	0.0	0.1	ud	0.1	ud
127	9.3	9.1	17	2.4	9.1	2.2	0.7	2.3	0.3	1.8	0.3	0.9	0.1	0.7	0.1
max	70	45	99	14	58	15	4.8	15	2.5	13	2.5	6.9	1.0	6.1	1.0
min	1.4	1.6	2.3	0.4	1.6	0.4	0.1	0.4	0.0	0.3	0.0	0.1	0.0	0.1	0.0
median	13	7.9	14	2.3	10	2.6	1.2	3.1	0.5	2.3	0.4	1.1	0.2	0.8	0.1
mean	16	11	21	3.0	13	3.3	1.3	3.7	0.6	2.9	0.6	1.5	0.2	1.1	0.2
stdev	16	11	24	3.1	13	3.2	1.1	3.4	0.5	2.9	0.6	1.5	0.2	1.3	0.2

Table 3.3(B) Labile REE concentrations (ng REE per kg water (ppt)) for the Cordilleran rivers (October Campaign). "ud" denotes analytes below method limit of detection.

Sample	Y	La	Ce	Pr	Nd	Sm	Eu	Gd	Tb	Dy	Ho	Er	Tm	Yb	Lu
201	6.7	5.7	10.3	1.6	5.7	1.3	0.4	1.3	0.2	1.0	0.2	0.5	0.1	0.5	0.1
202	78	54	106	16	59	13	3.5	14	2.2	11.5	2.3	6.4	1.0	5.9	1.0
205	11	5.6	11.9	1.9	7.4	2.1	0.6	2.2	0.3	1.7	0.4	1.0	0.1	0.8	0.1
207	154	144	282	39	140	35	10	38	6.1	30	5.7	15	2.0	12	1.9
208	5.2	3.3	5.0	1.0	4.2	1.0	0.3	1.2	0.2	0.8	0.2	0.5	0.1	0.4	0.1
211	42	21	42	6.5	26.3	7.8	2.8	9.1	1.4	7.4	1.4	3.5	0.5	3.0	0.5
212	148	72	151	24	101	30	10	36	5.3	27	5.2	14	2.0	11	1.9
213	1232	479	905	144	582	185	72	225	37	193	38	95	12	65	9.4
216	11.9	4.8	8.1	1.6	6.8	2.0	0.7	2.4	0.4	2.0	0.4	1.0	0.1	0.8	0.1
219	10.1	11.2	15.9	2.8	9.9	2.3	0.6	2.5	0.4	1.8	0.4	0.8	0.1	0.6	0.1
221	5.7	5.5	8.7	1.5	5.3	1.3	0.3	1.3	0.2	1.0	0.2	0.5	0.1	0.4	0.1
222	138	108	215	30	108	27	8.1	30	5	24	4.6	12	1.5	9.5	1.5
max	1232	479	905	144	582	185	72	225	37	193	38	95	12	65	9.4
min	5.2	3.3	5.0	1.0	4.2	1.0	0.3	1.2	0.2	0.8	0.2	0.5	0.1	0.4	0.1
median	27	16	29	4.7	18	5.0	1.8	5.8	0.9	4.7	0.9	2.3	0.3	1.9	0.3
mean	153	76	147	23	88	26	9.1	30	4.9	25	4.9	13	1.6	9.1	1.4
stdev	345	135	256	40	163	52	20	63	10	54	11	26	3.3	18	2.6

Table 3.4 Labile REE fluxes measured near the mouths of the Fraser, Skeena, Nass and Squamish Rivers.

	Y	La	Ce	Pr	Nd	Sm	Eu	Gd	Tb	Dy	Ho	Er	Tm	Yb	Lu
kg/yr															
Fraser	4099	3315	6553	907	3308	836	247	913	143	731	138	355	46	285	44
Skeena	1359	649	1280	210	910	270	110	320	48	246	47	124	16	93	15
Nass	9252	3588	6784	1078	4394	1398	552	1705	281	1460	283	711	88	487	70
Squamish	28	27	52	7.6	28	6.4	2.3	6.4	1.1	4.8	1.1	2.7	0.6	2.6	0.6
TOTAL	14738	7579	14669	2202	8641	2510	911	2944	474	2442	469	1193	150	868	131
g/km2/yr															
Fraser	19	15	30	4	15	4	1	4	1	3	1	2	0.2	1	0.2
Skeena	32	15	30	5	22	6	3	8	1	6	1	3	0.4	2	0.4
Nass	500	194	367	58	238	76	30	92	15	79	15	38	5	26	4
Squamish	12	12	22	3	12	3	1	3	0.5	2	0.5	1	0.3	1	0.3
TOTAL	53	27	52	8	31	9	3	11	2	9	2	4	1	3	0.5
Uncertainty in REE Fluxes (from Skeena Field Duplicates)															
+/- %	55%	55%	59%	59%	57%	56%	47%	57%	58%	56%	57%	62%	65%	62%	69%

3.5 ANALYTICAL RESULTS

3.5.1 Labile REE concentrations

Dissolved and adsorbed REE concentrations are listed in table 3.1(A and B) and table 3.2(A and B) respectively. The range of dissolved REE concentrations are well represented by La and Lu as end-members of the lanthanide elements, with dissolved La concentrations ranging from 5 to 220 $ng \cdot kg^{-1}$ and dissolved Lu ranging from 0.4 to 16.0 $ng \cdot kg^{-1}$. The range of dissolved REE concentrations in the Cordilleran rivers are similar to the range of dissolved REE concentrations determined by others in a number of the rivers from around the world (Goldstein and Jacobsen, 1988; Elderfield et al., 1990; Dupré et al., 1996; Sholkovitz et al., 1999), and agree well with a limited dataset of dissolved REE concentrations previously measured in the Skeena, Nass and Stikine Rivers (Gaillardet et al., 2003).

The Cordilleran rivers do not show a systematic variation in dissolved REE concentrations between the high (June) and low (October) stages of the hydrograph, however, this is not the case for adsorbed REE concentrations. The dry weight concentrations of adsorbed La ranged from 33 to 555 $\mu g \cdot kg^{-1}$ in June, and 542 to 5213 $\mu g \cdot kg^{-1}$ in October, with similar increases for all of the REE from June to October. However, the suspended load of the Cordilleran rivers is lower during the low stages of the hydrograph (Milliman, 1980), and so, the total concentration of labile REE (dissolved + adsorbed REE) per litre of water is similar for the high and low water stages (table 3.3). An exception is the Nass River at Canyon City which had higher labile REE concentrations in October (sample 213) than in June (sample 118). This can be explained

by a large storm event near the mouth of the Nass, causing high discharge and high sediment load at the time of sampling.

3.5.2 Labile REE Fluxes to British Columbia's Coastal Waters

Annual fluxes of labile REE delivered to the Pacific Ocean by the Fraser, Skeena, Nass and Squamish Rivers as kg REE per year, and as g REE per km^2 per year are listed in Table 3.4. Annual labile REE fluxes (REE_{total}) in kg per year are calculated as follows:

$$REE_{total} = \left([REE]_{June} \times 0.7 + [REE]_{October} \times 0.3\right) \times D \qquad (4)$$

[*REE*] represents the measured concentrations of labile REE during the June and October respectively, in $kg \cdot L^{-1}$. *D* is the average annual water discharge based on historical hydrographic data collected by Environment Canada (2001). The June and October concentrations are weighted by multiplying by 0.7 and 0.3 respectively to represent the Cordilleran hydrograph. 70% of the water discharged by the Cordilleran rivers occurs during the summer months (Environment Canada, 2001a; also see Chapter 1 - Figure 1.3). It is assumed that the concentrations measured in June are representative of the typical summer (May to September) composition of these waters, and likewise that the concentrations measured in October are representative of the typical composition of these rivers during the remainder of the year. These estimates are based on labile REE concentrations measured in samples collected closest to the mouths of these rivers

Table 3.4 shows that the labile REE flux from the Nass River far exceeds that from the other rivers, both in total magnitude (kg per year) and per km^2. This is likely due to excessively high labile REE concentrations measured near the mouth of the Nass River during the October campaign (sample 213). This sample was collected during a large storm event that resulted in the lower regions of the Nass watershed being in full flood at

the time of sampling, and causing high erosion rates of the soil in the area. The effect of this storm event illustrates the potential significance of temporally isolated events on river fluxes to the oceans.

The Squamish catchment (2330 km^2) is very small in comparison to Fraser, Skeena and Nass (277700 km^2 cumulatively), however it is included in this study as an example of a small coastal catchment draining directly into the Pacific Ocean. Along the coast of British Columbia, there are numerous small rivers (by area) that drain the coastal mountains directly into the Pacific Ocean. The total cumulative catchment area of these rivers is similar to the area drained by the Fraser, Skeena and Nass systems, also, the coastal rivers are characterized by high runoff and high suspended load (Milliman and Syvitski, 1992) thus their total particulate fluxes are likely of a similar or greater magnitude as the larger systems. The logistics of sampling these numerous and remote rivers is beyond the scope of the current study, however, it is important to note that the true labile REE delivery to British Columbia's coastal waters may be more than double the amounts measured for the Fraser, Skeena and Nass Rivers.

3.5.3 Labile REE Distribution Between Dissolved and Adsorbed Phases in Cordilleran Rivers

Adsorption of ionic species to particulate surfaces serves to lower the free energy of a system (Stumm and Morgan, 1996). Adsorbed ions help to satisfy excess charged sites that exist on the surfaces of suspended particulate. Exchange of ionic species between the dissolved and adsorbed phases is an equilibrium process:

$$M^{+}_{(aq)} \leftrightarrow M^{+}_{(ads)} \quad (5)$$

The distribution between the two phases can therefore be written as an equilibrium constant, in this case called the distribution coefficient ($Kd_{REE}^{ads/dis}$):

$$Kd_{M}^{ads/dis} = [M]_{ads}/[M]_{dis} \quad (6)$$

The measured $Kd_{REE}^{ads/dis}$ are listed in Table 3.5.

The $Kd_{REE}^{ads/dis}$ decrease from La to Lu for each sample, which reflects the increased solubility of the HREE compared to the LREE (Elderfield et al., 1990). There is high variability of the magnitudes of $Kd_{REE}^{ads/dis}$ between all samples, and there is at least an order of magnitude shift for most stations between the June and October samples. Table 3.5 shows the October $Kd_{REE}^{ads/dis}$ values (average ≈ 50000) to be about 50 times higher than the June $Kd_{REE}^{ads/dis}$ values (average ≈ 1000).

Importantly, the relative $Kd_{REE}^{ads/dis}$ between the REE are conservative. This is demonstrated by Figure 3.3, which shows the linear relationship between the distribution coefficients of many of the REE pairs. This shows that the REE patterns are predictably different between the dissolved and adsorbed phases for all of the Cordilleran samples. The consistency of the REE patterns between the adsorbed and dissolved phases means that adsorption / desorption reactions or other processes within the river water are not significantly altering the labile REE patterns, and that the observed REE patterns are likely controlled by REE patterns of the source material (i.e. basin lithology).

The consistency of the relative distribution of the REE also shows that the REE patterns in the adsorbed phase can be used to deduce the REE patterns in the dissolved phase, and vice versa (Table 3.6). This has important practical aspects. Determination of dissolved REE involves complicated and expensive concentration techniques, such as the

method described in this paper, which require large sample volumes to be collected and preserved in ultra-clean conditions. Collection and preservation of large ultra-clean water samples is not always practical, particularly in remote regions. Determination of adsorbed REE by the method outlined in this paper is much easier to implement, requires much less investment in reagents, time and equipment, and requires as little as a few mg of suspended particulate matter. The results presented in this paper show that REE adsorbed to suspended particulate can serve as an adequate proxy for labile REE.

3.5.4 Labile REE Patterns

Selected REE parameters are listed in Table 3.6: chondrite normalized europium anomalies ($Eu/Eu^* = Eu_n \div (Sm_n \times Gd_n)^{0.5}$), cerium anomalies ($Ce/Ce^* = (3\times Ce_n) \div (2\times La_n + Nd_n)$), Nd_n/Sm_n and La_n/Yb_n. This table shows that these REE parameters are similar in the two phases, but not identical. In general, the adsorbed REE have slightly higher LREE enrichment (La_n/Yb_n from 4.0 to 19.2) than the dissolved REE (La_n/Yb_n from 2.2 to 12.7), and slightly lower Nd_n/Sm_n (0.9 to 1.3) than the dissolved REE (1.0 to 1.6). Both the dissolved and adsorbed REE show slightly negative cerium anomalies (Ce/Ce^* dissolved = 0.75 ± 0.14, Ce/Ce^* adsorbed = 0.80 ± 0.11) and slightly negative europium anomalies in the dissolved REE (Eu/Eu^* dissolved = 0.80 ± 0.11) but near flat europium anomalies in the adsorbed REE ($Eu/Eu^* = 1.03 \pm 0.27$).

Figure 3.4 (A) and (B) are the chondrite and PAAS (Post Achaean Australian Shale) normalized plots of the Cordilleran labile REE from the Fraser, Skeena, Nass and Squamish main stems. Values for chondrite and PAAS are taken from McLennan (1989). These plots show that the normalized REE patterns are similar but unique for each of the Cordilleran river systems. Figure 3.4 (A) shows that all of the Cordilleran samples have

significant enrichment of LREE over HREE compared to chondrite, reflecting a source more evolved than chondrite, which is typical of continental rocks. The PAAS normalized REE patterns (figure 3.4 (B)) display the middle REE enrichment that has been observed in other river waters (e.g. Goldstein and Jacobsen, 1988; Sholkovitz et al., 1999). The PAAS normalised labile REE are enriched in HREE over LREE compared to PAAS, indicating a source that is less evolved (more mafic) than the shale composite which represents evolved upper continental crust composition. This is supported by the mapped lithologies of the Canadian Cordillera which contains large provinces of Island Arc material and mafic volcanics (Wheeler and McFeely, 1991). Therefore, the bulk Cordilleran composition must be less compositionally mature than the PAAS shale composite.

3.5.5 Uncertainty in the labile REE fluxes and patterns

Comparison of measured labile REE concentrations (Table 3.3 A and B) in field duplicate samples collected from the Skeena River in June (115, 116) and October (211, 212) show that while there is good agreement between the measured labile REE concentrations in the two June samples, there is substantial difference between the two October samples. The variability in measured labile REE concentrations lead to uncertainty in the flux calculations of ± 50 to 70% (Table 3.4). Replicate analyses of individual samples returned results that agree within analytical precision (± 5%). This shows that the observed variability between the field duplicate samples reflects natural variability in labile REE concentrations, rather than problems with the extraction and analytical technique.

Importantly, the REE patterns are very reproducible between the field duplicate samples, even though the labile REE concentrations can be highly variable (Figure 3.5). This is consistent with REE in seawater, which have been shown to have highly variable concentrations, but conservative relative abundances (e.g. Elderfield et al., 1990).

Table 3.5 REE distribution coefficients between adsorbed and dissolved REE ($Kd_{REE}^{ads/dis} \times 10^3$) for the Cordilleran rivers. Values only calculated for samples with data for both dissolved and adsorbed REE.

Sample	Y	La	Ce	Pr	Nd	Sm	Eu	Gd	Tb	Dy	Ho	Er	Tm	Yb	Lu
							June Campaign								
101	1.1	1.2	1.5	1.3	1.2	1.2	1.9	1.2	1.5	1.2	1.4	1.0	1.8	1.0	1.5
102	0.9	0.9	0.8	0.8	0.8	0.8	1.2	0.8	0.8	0.7	0.7	0.7	0.7	0.6	0.6
104	1.4	1.4	1.3	1.2	1.2	1.2	1.7	1.3	1.2	1.1	1.1	1.0	1.0	0.9	0.9
105	1.9	2.0	2.3	2.0	1.9	2.0	2.4	2.0	1.8	1.8	1.7	1.6	1.3	1.4	1.1
107	2.8	2.1	2.1	2.0	2.2	2.3	2.8	2.3	2.2	2.1	1.9	2.0	1.5	1.8	1.3
109	1.8	1.7	1.8	1.5	1.6	1.5	1.3	1.5	0.8	1.3	0.8	1.1	0.3	0.8	0.1
110	2.0	2.0	2.2	1.9	2.0	2.0	2.4	2.1	2.0	1.9	1.8	1.8	1.4	1.5	1.4
111	4.0	5.7	5.6	5.3	5.2	5.1	6.2	4.9	4.5	4.1	3.5	3.1	2.5	2.6	2.0
112	0.6	0.5	0.4	0.4	0.4	0.5	0.8	0.5	0.5	0.5	0.4	0.4	0.3	0.3	--
114	0.8	0.8	0.7	0.7	0.7	0.8	1.2	0.8	0.7	0.7	0.7	0.6	0.5	0.5	0.5
115	0.5	0.4	0.3	0.4	0.4	0.4	0.7	0.5	0.4	0.4	0.4	0.4	0.3	0.3	0.3
116	0.8	0.8	0.7	0.7	0.7	0.7	1.2	0.8	0.7	0.7	0.6	0.6	0.5	0.5	0.5
117	1.1	0.8	0.7	0.8	0.8	0.8	1.5	0.9	0.9	0.9	0.9	0.8	0.6	0.7	0.7
118	1.0	0.9	0.8	0.8	0.8	0.9	1.5	1.0	1.0	0.9	0.9	0.8	0.7	0.7	0.6
119	2.1	2.6	2.8	2.4	2.3	2.5	3.6	2.3	2.4	2.1	1.9	1.7	1.3	1.5	1.2
120	0.4	0.4	0.5	0.4	0.4	0.4	0.6	0.4	0.3	0.4	0.3	0.3	--	0.2	--
121	3.6	3.8	4.6	3.7	3.4	3.5	3.7	3.4	3.3	3.1	2.9	2.9	2.4	2.5	2.2
123	0.9	0.9	1.0	0.8	0.9	0.9	0.9	0.9	0.8	0.8	0.8	0.7	--	0.7	--
124	1.0	1.0	1.2	1.0	1.0	1.1	1.3	1.1	1.0	0.9	0.8	0.8	--	0.6	--
126	1.3	1.4	2.0	1.4	1.4	1.4	1.7	1.4	1.2	1.2	1.1	1.0	--	0.9	--
127	3.4	3.5	3.6	3.4	3.1	3.3	3.9	3.3	3.1	3.0	2.7	2.6	2.1	2.2	1.8
Min	0.4	0.4	0.3	0.4	0.4	0.4	0.6	0.4	0.3	0.4	0.3	0.3	0.3	0.2	0.1
Max	4.0	5.7	5.6	5.3	5.2	5.1	6.2	4.9	4.5	4.1	3.5	3.1	2.5	2.6	2.2
Median	1.1	1.2	1.3	1.2	1.2	1.2	1.5	1.2	1.0	1.1	0.9	1.0	1.0	0.8	1.0
Mean	1.6	1.7	1.7	1.6	1.5	1.6	2.0	1.6	1.5	1.4	1.3	1.2	1.1	1.1	1.1
Stdev	1.1	1.3	1.4	1.3	1.2	1.2	1.4	1.1	1.1	1.0	0.9	0.8	0.7	0.7	0.6
							October Campaign								
201	55.1	51.8	49.0	50.7	42.2	47.8	57.2	50.1	59.0	41.7	43.3	36.7	38.4	36.8	33.1
202	60.2	50.7	51.2	55.8	48.3	52.3	53.7	56.7	55.2	48.5	45.6	45.1	39.4	40.5	34.2
205	87.4	65.2	67.1	69.7	62.2	72.2	75.2	72.6	77.1	61.3	66.5	60.0	62.0	52.5	0.0
207	17.0	14.6	15.5	15.2	13.4	14.9	16.4	15.7	16.1	14.3	14.6	13.9	13.5	12.4	13.0
208	77.8	110.7	119.1	106.5	98.0	93.8	118.9	94.1	100.4	70.9	72.3	58.4	64.8	45.7	54.1
211	10.8	11.8	16.3	11.3	9.7	10.0	11.1	10.2	10.0	9.2	8.8	7.8	8.2	7.4	7.5
212	25.0	24.1	27.8	25.2	22.2	24.7	28.0	26.4	25.1	21.9	22.1	21.7	23.1	19.3	22.7
213	6.4	4.0	3.4	3.9	3.5	4.1	5.2	4.5	4.5	4.2	4.4	4.1	3.9	3.6	3.7
219	118.4	115.0	144.5	119.3	103.4	115.0	139.7	125.6	124.5	109.9	106.7	90.7	90.7	75.5	82.1
221	118.2	114.2	204.5	132.5	114.5	133.9	151.5	126.0	141.0	112.7	106.0	92.3	90.7	74.7	80.2
222	13.8	11.8	13.4	12.3	10.7	11.8	13.6	12.2	12.1	11.4	11.0	10.0	9.0	9.3	9.0
Min	6.4	52.2	64.7	54.8	48.0	52.8	61.0	54.0	56.8	46.0	45.6	40.1	40.3	34.4	30.9
Max	118.4	43.8	64.7	46.7	41.1	45.4	53.8	45.4	48.5	39.1	37.8	32.1	32.4	26.1	29.5
Median	55.1	50.7	49.0	50.7	42.2	47.8	53.7	50.1	55.2	41.7	43.3	36.7	38.4	36.8	22.7
Mean	53.6	52.2	64.7	54.8	48.0	52.8	61.0	54.0	56.8	46.0	45.6	40.1	40.3	34.4	30.9
Stdev	42.4	43.8	64.7	46.7	41.1	45.4	53.8	45.4	48.5	39.1	37.8	32.1	32.4	26.1	29.5

Table 3.6 Comparison of selected REE parameters in the dissolved and adsorbed phases of the Cordilleran River waters. All values are normalised to chondrite (chondrite values taken from McLennan, 1989). Eu/Eu* and Ce/Ce* are the europium and cerium anomalies respectively.

	Dissolved REE				*Adsorbed REE*			
Sample	La_n/Yb_n	Nd_n/Sm_n	Ce/Ce*	Eu/Eu*	La_n/Yb_n	Nd_n/Sm_n	Ce/Ce*	Eu/Eu*
				June Campaign				
101	5.5	1.5	0.78	0.78	6.8	1.5	0.93	1.20
102	4.5	1.5	0.85	0.81	6.3	1.4	0.80	1.23
104	2.8	1.2	0.69	0.91	4.3	1.2	0.66	1.21
105	4.9	1.3	0.83	0.80	7.2	1.3	0.95	0.95
107	4.0	1.3	0.95	0.81	4.8	1.3	0.93	0.97
109	3.4	1.2	0.85	1.01	7.3	1.4	0.93	0.91
110	6.2	1.4	0.88	0.76	8.2	1.4	0.95	0.88
111	2.4	1.3	0.62	0.64	5.3	1.4	0.62	0.79
112	4.4	1.2	0.86	0.91	5.8	1.1	0.73	1.45
114	2.9	1.2	0.77	0.91	4.0	1.1	0.76	1.46
115	4.4	1.2	0.86	0.91	5.5	1.1	0.72	1.48
116	3.2	1.2	0.78	0.91	4.9	1.1	0.73	1.50
117	4.1	1.1	0.89	0.88	4.6	1.0	0.76	1.50
118	3.9	1.1	0.89	0.88	4.8	0.9	0.78	1.42
119	2.5	1.0	0.72	0.90	4.3	1.0	0.81	1.35
120	2.6	1.2	0.64	0.87	5.0	1.1	0.75	1.18
121	12.7	1.6	0.65	0.61	19.2	1.6	0.79	0.66
123	10.3	1.6	0.64	0.58	14.4	1.5	0.67	0.59
124	8.1	1.6	0.53	0.64	13.7	1.4	0.59	0.74
126	5.9	1.5	0.60	0.73	9.4	1.5	0.83	0.88
127	5.6	1.4	0.84	0.75	8.9	1.3	0.88	0.89
				October Campaign				
201	5.1	1.6	0.83	0.83	7.2	1.4	0.82	0.97
202	4.9	1.5	0.87	0.78	6.2	1.4	0.89	0.77
205	3.8	1.3	0.88	0.88	4.7	1.2	0.92	0.91
207	6.9	1.4	0.84	0.75	8.1	1.3	0.90	0.80
208	2.2	1.3	0.59	0.63	5.4	1.3	0.65	0.80
211	3.0	1.1	0.60	0.92	4.8	1.1	0.87	1.02
212	3.6	1.2	0.75	0.88	4.5	1.1	0.88	0.97
213	4.5	1.2	0.94	0.90	5.0	1.0	0.83	1.08
219	7.9	1.6	0.52	0.64	12.0	1.4	0.66	0.74
221	5.7	1.6	0.40	0.68	8.7	1.4	0.72	0.79
222	6.0	1.4	0.78	0.76	7.7	1.3	0.91	0.86
Min	2.2	1.0	0.40	0.58	4.0	0.9	0.59	0.59
Max	12.7	1.6	0.95	1.01	19.2	1.6	0.95	1.50
Mean	4.9	1.3	0.75	0.80	7.2	1.3	0.80	1.03
Med	4.4	1.3	0.78	0.81	6.0	1.3	0.81	0.96
Stdev	2.3	0.2	0.14	0.11	3.4	0.2	0.11	0.27

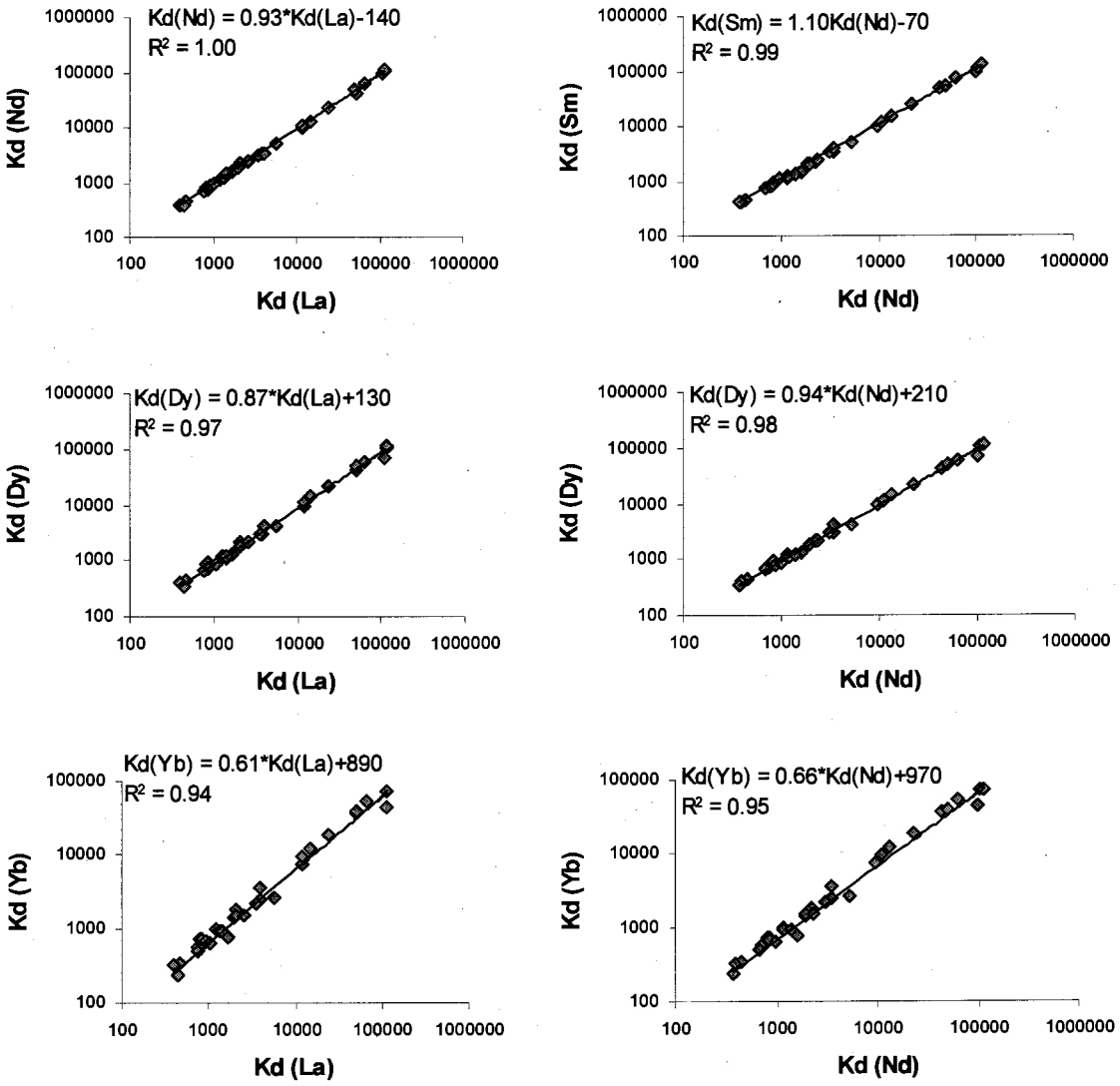

Figure 3.3 Distribution coefficients (adsorbed / dissolved) for selected REE pairs. This figure shows that the REE distribution between the dissolved and adsorbed phases are consistently proportional.

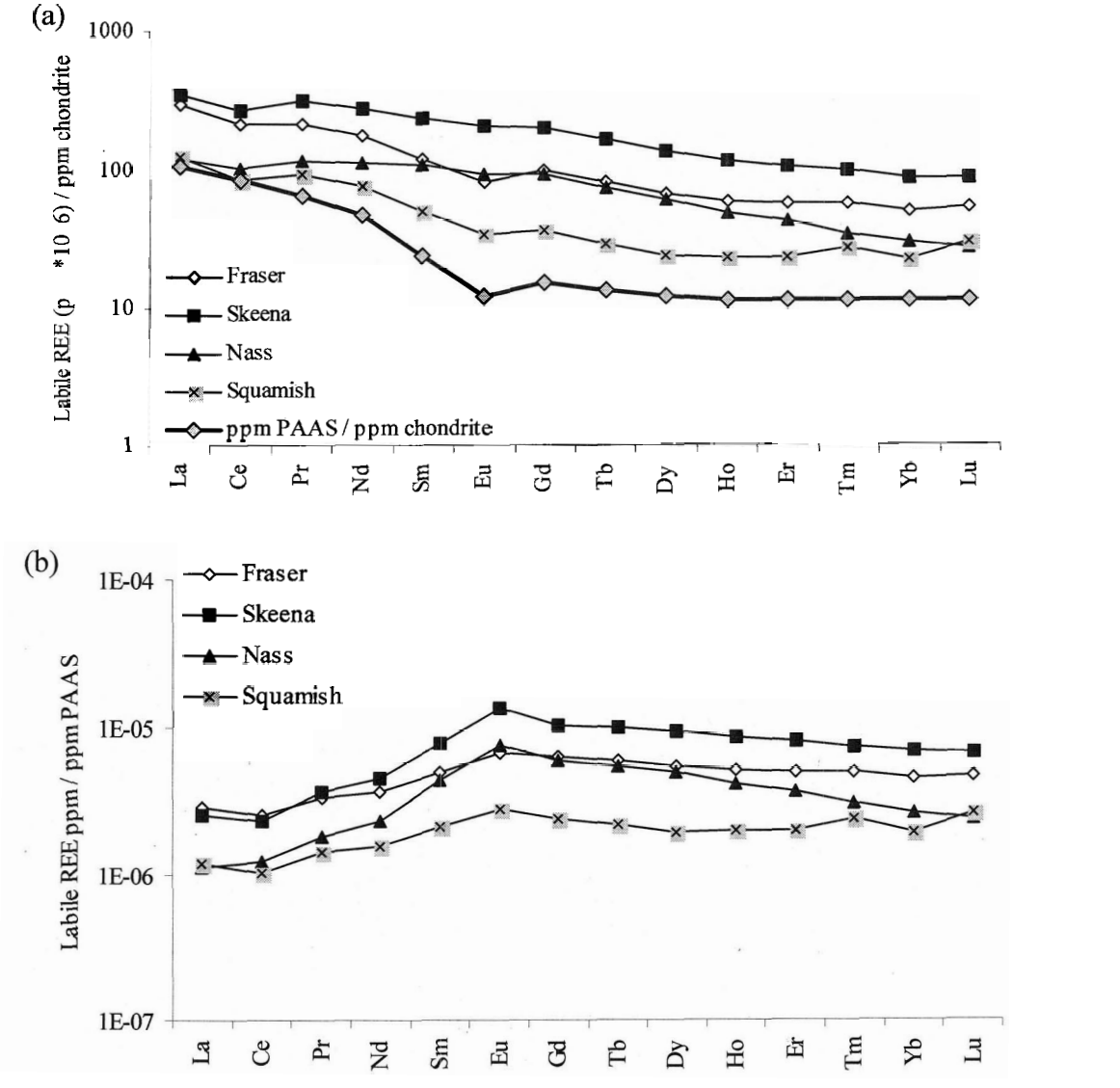

Figure 3.4 Chondrite and PAAS normalised labile REE for the Fraser, Skeena, Nass and Squamish rivers. The samples plotted are from the June 2002 sampling campaign, and from stations closest to the mouths of each river. This figure displays the variability of labile REE compositions within the Canadian Cordilleran river systems. Values for chondrite and PAAS taken from McLennan (1989).

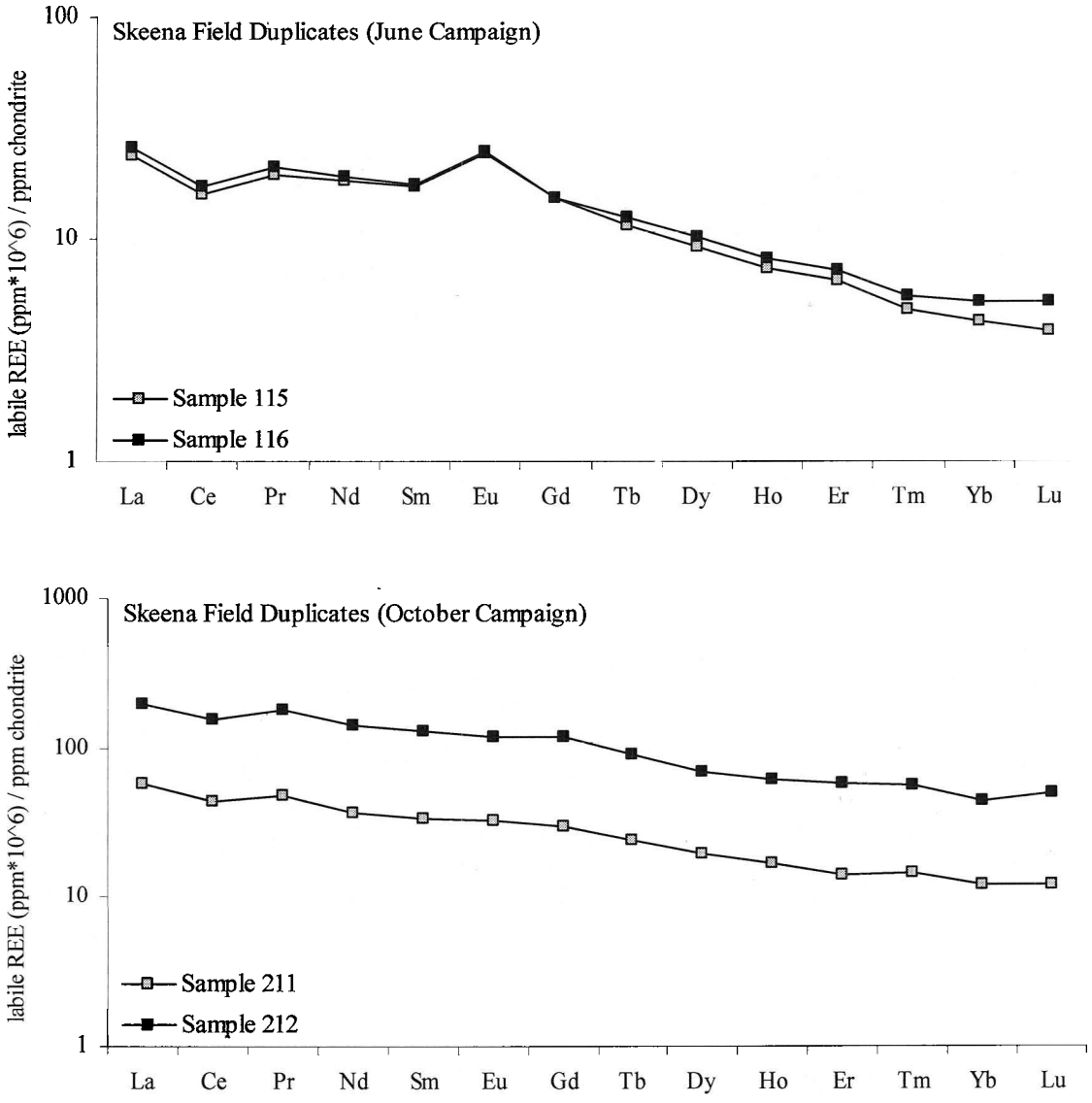

Figure 3.5 Comparison of the chondrite normalized labile REE plots for the field duplicate samples collected near the mouth of the Skeena River during the June and October field campaigns. This figure shows that the REE patterns are preserved between the duplicate samples even though there is substantial differences in the measured concentrations between the October duplicate samples.

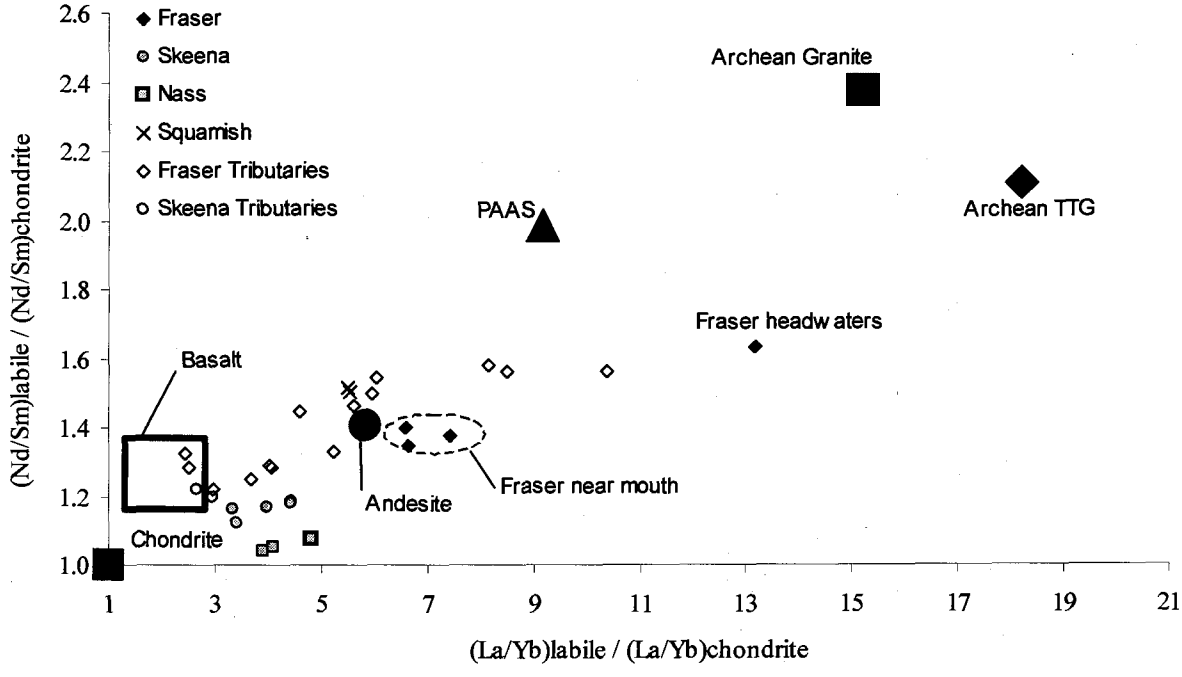

Figure 3.6 Chondrite normalized Cordilleran labile REE ratios. This plot shows the high degree of regional variability of the labile REE, and the distinct REE compositions of the different watersheds. The end members shown are REE compositions of typical crustal rocks (taken from McLennan, 1989 – PAAS, Andesite, Chondrite; and Condie, 1993 – Basalt, Archean Granite, Archean TTG (trondjhemite, tonalite, granodiorite) The labile REE of the Fraser river and tributaries represent a mixture between basalt, andesite and Archean granitoid compositions. The labile REE composition of the Skeena and Nass Rivers plot on separate vectors that indicate a mixture between granitic and chondritic rocks.

3.6 DISCUSSION

3.6.1 Lithological Control on Labile REE Patterns

The labile REE composition of the Cordilleran Rivers represents a mixture between basaltic and granitic compositions, with many of the rivers biased towards an andesitic to basaltic composition (Figure 3.6). Figure 3.6 shows that the labile REE compsotion of the individual rivers is generally representative of the basin (silicate) lithology for each watershed. This is strong evidence that the labile REE patterns are controlled by catchment lithology, and that fractionation during chemical weathering must be minor.

The Fraser River samples collected closest to the headwaters show a highly evolved REE composition similar to Archean granitoids. This is reflects the weathering of Paleozoic and older sedimentary rocks in the Foreland Belt (Rocky Mountains) that formed as a result of erosion of the Archean cratonic rocks to the East. Downstream the Fraser River mixes with tributary waters that drain watersheds underlain by mafic volcanics. These rivers (e.g. Blackwater and Chilcotin) show basaltic labile REE composition. As a result, the labile REE composition of the Fraser River near the mouth is roughly andesitic, and plots midway between the end members compositions of the headwaters and the basaltic tributaries. Since the Fraser River traverses a full transect of the Canadian Cordillera, and thus integrates the compositional complexity of that orogen, it is possible that the andesitic REE composition near the mouth of the Fraser represents the bulk composition of the Canadian Cordillera.

The downstream evolution of the Fraser River has been shown using the neodymium isotopic composition of suspended particulate, and the strontium isotopic

composition of the dissolved load (Cameron and Hattori, 1997). Consistent with the results presented here, Cameron and Hattori show that the headwater composition of the Fraser River reflects weathering and erosion of cratonic rocks.

The labile REE composition of the Skeena and Nass rivers plot on trends that are distinct from the Fraser system, and reflect a mixture between granitic rocks, and chondritic rocks, or some end-member that is LREE depleted compared to typical basalt. The mapped bedrock geology in the Skeena and Nass watersheds are dominated by intermediate to mafic arc volcanics and arc derived sediments (Wheeler and McFeeley, 1991). The labile REE composition of these rivers as displayed in figure 3.6, however, shows a trajectory towards a chondritic or even subchondritic REE composition. This suggests that there is a significant component of weathering of ultramafic rocks.

The labile REE compositions of the Cordilleran Rivers as presented in Figure 3.6 do show distinct separation in La_n/Yb_n and Nd_n/Sm_n between watersheds, and that these differences can be explained by silicate lithologies within the watersheds. This is important because the dissolution of carbonate rocks dominates chemical weathering in the Canadian Cordillera. This is due to the high solubility of carbonate minerals compared to silicate minerals, and has been observed in watersheds of all scales worldwide (see chapter 2 for a discussion of chemical weathering rates in the Canadian Cordillera). Importantly, only silicate weathering can provide a sink of atmospheric CO_2 on long timescales ($>10^5$ yr). Figure 3.6 shows that the labile REE in each watershed reflect the distribution of silicate rocks in spite of the consistently high rates of carbonate weathering. This means that labile REE may provide a chemical weathering tracer that is relatively insensitive to carbonate dissolution, and thus help to circumvent the difficulties

in determining silicate weathering rates due to the carbonate weathering signal that overwhelms the dissolved major elements, and strontium isotopes in river water.

As has been discussed above, the downstream evolution of the Fraser River labile REE which represents mixing of REE compositions of the waters derived from weathering evolved Foreland rocks (high La_n/Yb_n and Nd_n/Sm_n) with tributary waters derived from weathering mafic catchments as the river flows westward through the Cordillera, suggests that the labile REE are similarly conservative as strontium in the Cordilleran rivers, and similarly can resolve inputs to the rivers of waters derived from weathering of distinct lithologies, but with some distinct differences from strontium isotopes: (i) the labile REE appear to be insensitive to carbonate inputs, while the $^{87}Sr/^{86}Sr$ is easily dominated by carbonate weathering, and (ii) samples can be analysed for labile REE by quadrupole ICP-MS, an analytical tool that is more cost effective and more widely available than thermal ionization mass spectrometers (TIMS) or multi-collector ICP-MS required for isotopic analysis.

3.6.2 Cordilleran Erosion and the Seasonal Variation of $Kd_{REE}^{ads/dis}$

The seasonal changes in $Kd_{REE}^{ads/dis}$ observed in the Cordilleran rivers (table 3.4) can be explained by changes in the adsorptive capacity of the suspended particulate. Adsorptive capacity depends in the density of unsatisfied charged sites on the surface of the particulate matter, which is dominantly controlled by surface area (Langmuir, 1997). Therefore, adsorptive capacity is affected by factors such as grain size and shape (figure 3.7). Mineral composition affects surface charge of a particle primarily by controlling the morphology, and therefore surface area (Langmuir, 1997).

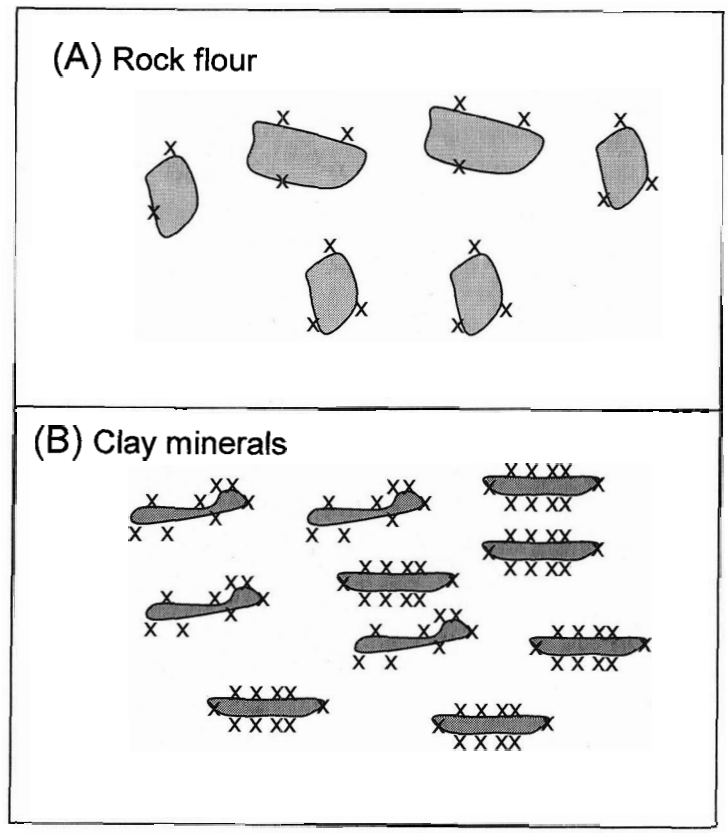

Figure 3.7 A portrayal of how particulate composition, which affects morphology and surface charge, and grain size affect the adsorptive capacity of suspended particulate matter. Adsorption sites are represented by "X". Rock flour (A), dominantly primary minerals like feldspars, micas and quartz has fewer adsorption sites than clay minerals (B).

The amount and size of particles a river is able to suspend and transport is directly proportional to the kinetic energy of the system (i.e. flow velocity + turbulence, e.g. Boggs, 1987). Thus at high discharge rates, there is an increasing capacity to suspend coarse and dense material that would normally be transported as bedload (a detailed description of sediment transport mechanisms is given by Boggs, 1987). The grain size distribution of the suspended particulate therefore depends on the stage of the hydrograph, with an increasing proportion of coarse grains during high flow. This means that during high flow the adsorption site to mass ratio of the suspended particulate matter drops due to the higher proportion of coarse grains. However, grain size distribution alone cannot explain the full magnitude of variation in $Kd_{REE}^{ads/dis}$ from June to October. All of the samples were collected from near the surface of the waters (at a depth of about 30 cm), where the relative concentration of sand-sized particles should be lower than at depth due to higher settling rate than for silt. Visual observation of the material captured by the filters showed a very low percentage of sand sized particles (< 5%) for all of the samples. This means that grain size distribution in the samples could not have varied enough to explain the variability in $Kd_{REE}^{ads/dis}$.

Figure 3.8 shows distinct trends in adsorbed REE concentration as a function of total suspended particulate concentration ($mg \cdot L^{-1}$) for the June and October samples, with a third trend followed by the Fraser River samples collected in June. This is again difficult to explain by changing grain size distribution alone. If all of the $Kd_{REE}^{ads/dis}$ variability was due only to grain size distribution differences, then a single trend would result. The slope of this trend should decrease with increasing discharge rate, due to the suspension of increasingly coarse particles. In fact, this is observed in the October

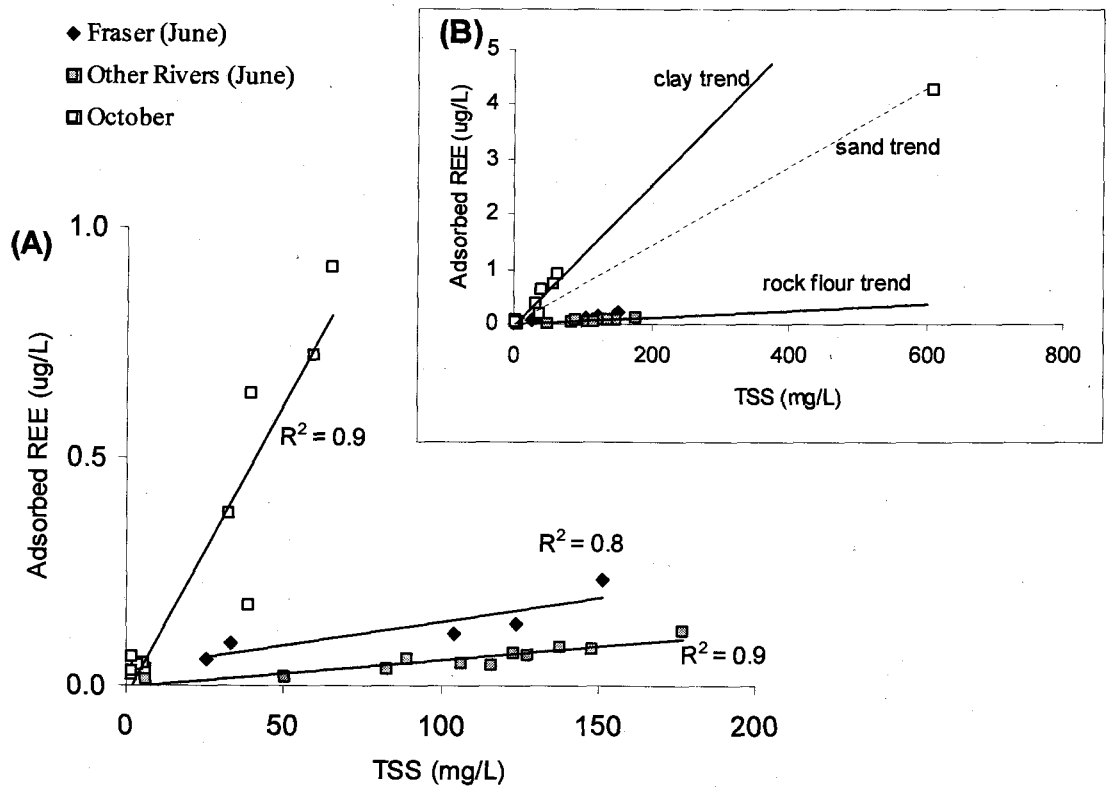

Figure 3.8 The relationship between adsorbed REE concentration and the concentration of suspended particulate in the Cordilleran rivers. The distinct trends for October versus June indicates a seasonal change in particulate composition. The June samples are dominated by unweathered rock flour, and the October samples dominated by soil based material with a higher proportion of clay minerals. (A) shows that the Fraser River in June has a distinct trend falling between the June and October trends defined by the other rivers. This is likely due to the larger size of the Fraser which causes the output to be less seasonally variable than the other rivers. The inset (B) includes the October Nass sample (high suspended load due to a storm event in October), which is shown to fall between the clay and rock flour trends, likely due to suspension of sand grains at high discharge.

samples (figure 3.8, open squares) where the low discharge/low suspended load samples plot on a line with a relatively high slope ("clay trend"), indicative of material with high adsorptive capacity). Projection of this line to the sample collected near the mouth of the Nass River in October (shown in figure 3.8 (B)), which had extremely high suspended load due to a large storm event during the October sampling, requires a line with lower slope ("sand trend"), indicative of the higher percentage of coarse grained particles present in this sample.

In contrast to the October samples, the June samples (figure 3.8, shaded squares) plot on a trend with a much lower slope ("rock flour trend"). This shows that the overall adsorptive capacity of the suspended particulate is lower in the rivers in June than in October independent of the concentration of particles in suspension. Since grain size distribution alone cannot account for the trends shown by figure 3.8, or for the seasonal variation in $Kd_{REE}^{ads/dis}$, it is concluded that the composition of the suspended particulate material must be different in June than in October.

The adsorptive capacity per unit mass of clay minerals (products of incongruent silicate weathering) is very high compared to finely ground primary minerals such as quartz or feldspar. This is primarily due to morphological differences between the clay and primary mineral particles (Langmuir, 1997). For example, one gram of illite or kaolinite particles will have about100 times more adsorption sites than a gram of quartz particles; other clay minerals, such as montmorillonite, can have as much as 6000-8000 as many adsorption sites as a comparable mass of quartz particles (Langmuir 1997). Thus, from the relative slopes of the trends plotted in figure 3.8, it is inferred that the October samples contain a higher modal percentage of clay minerals than the June

samples. Clay minerals form as a result of incongruent weathering of silicate minerals. Thus it can also be inferred from figure 3.8 that the June samples are derived from an unweathered source such as the rock flour currently being produced in the alpine regions of the watersheds, whereas the October samples are dominated by particulate derived from a source that has undergone significantly more silicate weathering.

Figure 3.8 (A) also shows that in June, the Fraser river samples (black diamonds) plot on their own trend that is distinct from the other June samples. The Fraser June trend has a slightly higher slope than the other rivers, which is closer to the October trend line, and indicates suspension of material with higher adsorptive capacity than the other rivers in June. This may be due to the larger size of the Fraser watershed, which means that the composition of material in suspension may be more buffered, and less susceptible to seasonal hydrographic variations as the other smaller rivers.

3.6.3 Seasonal Shift in Suspended Particulate Source?

The high alpine regions of the Canadian Cordillera are subject to alpine glaciation, intense weather and temperature shifts (leading to frost shattering), and have high topographic relief, with many slopes at or exceeding the angle of repose of loose rock. Physical weathering rates in these regions are very high, and chemical weathering is dominated by the coupled dissolution of pyrite and carbonates (Anderson et al. 2000, Tranter et al. 2002). Other workers have reported very low to negligible silicate weathering rates in glaciated alpine catchments (Anderson et al 2000, Sharp et al. 2002). Also, Alexander and Burt (1996) study of soils in a glacial catchment show that there is little evidence of clay mineral formation on surfaces exposed for less than a few hundred years. Thus particulate derived from recent alpine erosion (< 300 years ago) within the

Fraser, Skeena and Nass watersheds would likely contain little, if any clay minerals, which is consistent with the low adsorptive capacity for REE measured in the June suspended particulate samples.

Detritus produced by glacial action in the alpine regions is flushed out during the snowmelt event during late spring-early summer, which is the main feature of the Cordilleran hydrograph, as most of the water discharged by the Fraser, Skeena and Nass is during this snowmelt period (see figure 1.2, chapter 1). Milliman (1980) showed that approximately 80% of the sediment deposited on the Fraser River estuary is delivered during the snowmelt period. The fact that the adsorptive capacity of the suspended material is consistently low during the period when the alpine catchments are being flushed is strong evidence that (i) in June these rivers are dominated by sediment from the alpine regions and (ii) this material is freshly eroded as exemplified by the low adsorptive capacity.

During the low stage of the hydrograph, i.e. the remainder of the year, as represented by the October samples, the suspended matter in the rivers has significantly higher adsorptive capacity, indicative of a higher percentage of clay minerals. The source of sediment during the low stage of the hydrograph must be dominated by the alluvial plains and valley regions of the watersheds, since discharge from the alpine regions is minimal during the low stage of the hydrograph. Figure 3.9 illustrates the seasonal change in sediment source proposed here. The preferential production of clay minerals (silicate weathering) in the lowland regions is supported by others who have shown that silicate weathering in mountainous catchments is enhanced at low altitude by warmer

(a) High water period (snowmelt during late spring to early summer).

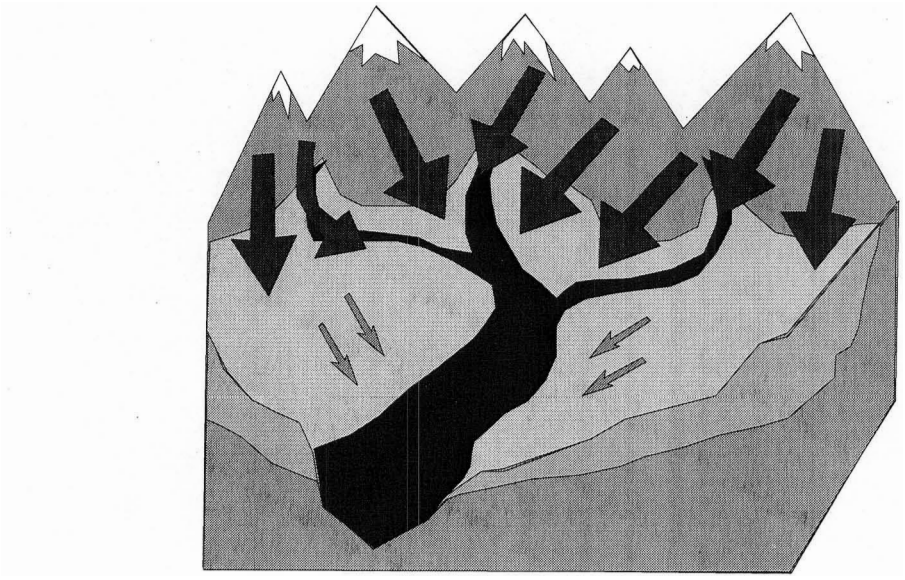

(b) Low water period.

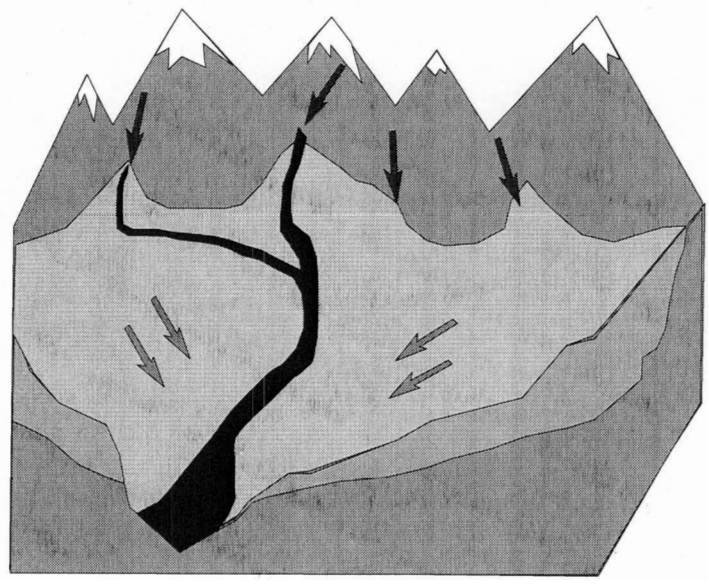

Figure 3.9 A diagram showing seasonal variation in particulate input to the Cordilleran rivers. Alpine derived material (shown by the black arrows) dominates during the high water stage of the rivers (A), whereas lowland derived sediment (shown by the grey arrows) is less variable, but proportionally more important during the low water stage (B).

temperatures (Drever and Zobrist, 1992), and by the action of plant by protecting fine soil material from erosion which increases water-rock interaction time, and by the production of high levels of CO_2 and organic acids in the soils due to plant respiration and decomposition of organic matter (Berner, 1992; Drever, 1994).

Most of the sediment is discharged from these rivers during the snowmelt period (~80%, Milliman, 1980), and is shown to be recently eroded, therefore, re-working of material eroded during Pleistocene glaciation, and subsequently stored within the Cordilleran basins, is only a minor component of the sediment load of the Cordilleran rivers. This contradicts previous work (Church and Slaymaker, 1989), and suggests that the Cordillera is currently at or near erosional steady state, and that the rate of export of sediment by the rivers largely reflects current uplift and erosion.

The fact that silicate weathering is dominantly occurring in the valley regions of the Cordilleran watersheds has important implications for the coupling between uplift and silicate weathering. The areas of highest physical erosion appear to be producing large volumes of detritus that is exported directly to estuarine and marine sedimentary basins without experiencing any significant amount of silicate weathering, and therefore no CO_2 drawdown. In contrast, the composition of particulate derived from the valley regions with relatively low rates of physical erosion shows evidence of clay mineral formation, and therefore silicate weathering. This is supported by work in the Mackenzie river system in northern Canada, where silicate weathering rates in the low lying regions are reported to be 3 to 4 times higher than in the regions of highest uplift and physical erosion (Millot et al., 2003). These results show that uplift and high physical erosion rates alone are not sufficient to drive high silicate weathering rates, and therefore global

cooling by CO_2 drawdown, as indicated by others (Raymo and Ruddiman, 1992; Edmond and Huh, 1997).

3.7 CONCLUSIONS

Concentrations of dissolved REE, REE adsorbed to suspended particulate, and $Kd_{REE}^{ads/dis}$ from the Fraser, Skeena and Nass river basins have been used to estimate labile REE mass fluxes to the ocean from these rivers. The REE patterns within the dissolved and adsorbed phases are consistent with basin lithology. The REE patterns in main stem samples also reflect mixing of tributary inputs, which suggests that the labile REE are conservative within the rivers. This supports the use of labile REE as a weathering and hydrographic tracer in rivers.

The relative $Kd_{REE}^{ads/dis}$ are proportional, independent of concentration. This proportionality between the $Kd_{REE}^{ads/dis}$ values can be used to predict dissolved REE patterns from the adsorbed REE, and vice versa. This means that adsorbed REE, which are easier to sample and to analyse, can serve as a proxy for dissolved REE.

A seasonal variability in $Kd_{REE}^{ads/dis}$ was observed in all samples, with high water samples (collected during the spring snowmelt driven freshet) had $Kd_{REE}^{ads/dis}$ approximately 50 times lower than low water samples. This can be explained by a seasonal compositional change in the mineralogy of the suspended particulate, from material with low adsorptive capacity during the high water stage to material with high adsorptive capacity during the low water stage. This appears to reflect a shift in particulate source from recently eroded unweathered rock (alpine source) during the spring snowmelt pulse, to alluvial soils developed over the Holocene during the

remainder of the year (valley source). This implies that chemical weathering of silicates (and CO_2 drawdown) is decoupled from physical erosion in the Canadian Cordillera, so that the highest silicate weathering rates are in the regions with low rates of physical erosion. This also implies that the suspended particulate budget of the Cordilleran rivers is dominated by current uplift and erosion, rather than remobilization of material eroded during Pleistocene glaciation, which suggests that the erosional regime within the Canadian Cordillera is approaching steady state.

3.8 REFERENCES

Alexander E.B. and Burt R. (1996) Soil development on moraines of Mendenhall Glacier, southeast Alaska. 1. The moraines and soil morphology. *Geoderma* **72,** 1-17.

Anderson S. P., Drever, J. I., Frost C. D. and Holden P. (2000) Chemical weathering in the foreland of a retreating glacier. *Geochim. Cosmochim. Acta* **64,** 1173-1189.

Berner E.K. and Berner R.A. (1987) *The Global Water Cycle: Geochemistry and environment*. Prentice-Hall, New Jersey.

Berner R.A. (1992) Weathering, plants, and the long-term carbon cycle. *Geochimica et Cosmochimica Acta* **56,** 3225-3231.

Blum J. D., Gazis C. A., Jacobson A. D. and Chamberlain C. P. (1998) Carbonate versus silicate weathering in the Raikhot watershed within the High Himalayan Crystalline Series. *Geology* **26,** 411-414.

Boggs S.Jr. (1987) *Principles of Sedimentology and Stratigraphy*. Merril, Ohio.

Cameron E.M., Hall G.E.M., Veizer J. and Krouse R.H. (1995) Isotopic and elemental hydrogeochemistry of a major river system: Fraser River, British Columbia, Canada. *Chemical Geology* **122,** 149-169.

Cameron E.M. and Hattori K. (1997) Strontium and neodymium isotope ratios in the Fraser River British Columbia: a riverine transect across the Cordilleran orogen. *Chemical Geology* **137,** 243-253.

Church M. and Slaymaker O. (1989) Disequilibrium of Holocene sediment yield in glaciated British Columbia. *Nature* **337,** 452-454.

Condie K.C. (1991) Another look at rare earth elements in shales. *Geochimica et Cosmochimica Acta* **55,** 2527-2531.

Drever J.I. (1994) The effect of land plants on weathering rates of silicate minerals. *Geochimica et Cosmochimica Acta* **58(10),** 2325-2332.

Drever J. I. and Hurcomb D. R. (1986) Neutralization of atmospheric acidity by chemical weathering in an alpine drainage basin in the North Cascades Mountains. *Geology* **14,** 221-224.

Drever J.I. and Zobrist J. (1992) Chemical weathering of silicate rocks as a function of elevation in the southern Swiss Alps. *Geochim. Cosmochim. Acta.* **56,** 3209-3216.

Dupré B., Gaillardet J., Rousseau D. and Allègre C.J. (1996) Major and trace elements of river-borne material: The Congo Basin. *Geochim. Cosmochim. Acta* **60,** 1301-1321.

Elderfield H., Upstill-Goddard R. and Sholkovitz E.R. (1990) The rare earth elements in rivers, estuaries, and coastal seas and their significance to the composition of ocean waters. *Geochimica et Cosmochimica Acta* **54**, 971-991.

Edmond J. M. and Huh Y. (1997) Chemical weathering yields from basement and orogenic terrains in hot and cold climates. In *Tectonic Uplift and Climate Change* (ed. W. F. Ruddiman), pp. 329–351. Plenum Press, New York.

Environment Canada (2001) *Surface Water and Sediment Data* [HYDAT CD-ROM]. Atmospheric Environment Program, Water Survey of Canada, Environment Canada, Ottawa.

Fetter C.W. (1994) *Applied Hydrogeology*. Prentice Hall, New Jersey.

Gaillardet J., Dupré B., Louvat P. and Allègre C. J. (1999) Global silicate weathering and CO_2 consumption rates deduced from the chemistry of large rivers. *Chem. Geol.* **159,** 3-30.

Gaillardet J., Millot R. and Dupré B. (2003) Chemical denudation rates of the western Canadian orogenic belt: the Stikine terrane. *Chemical Geology* **201,** 257-279.

Garrels R. M. and Mackenzie F. T. (1971) *Evolution of Sedimentary Rocks*. W.W. Norton & Company, New York

Garrels R.M. and Perry E.A.Jr. (1974) Cycling of carbon, sulfur, and oxygen through geologic time. In: *The Sea: Ideas and Observations on Progress in the Study of the Seas* (ed. E.D. Goldberg), pp. 303-336, John Wiley and Sons.

Garzanti E., Vezzoli G., Ando S., France-Lanord C., Singh S. and Foster G. (2004) Sand petrology and focused erosion in collision orogens: the Brahmaputra case. *Earth and Planetary Science Letters* **220,** 157-174.

Goldich S.S. (1938) A study in rock weathering. *Journal of Geology* **46,** 17-58.

Goldstein S.J. and Jacobsen S.B. (1988) Rare earth elements in river waters. *Earth and Planetary Science Letters* **89,** 35-47.

Hall G.E.M., Vaive J.E. and McConnell J.W. (1995) Development and application of a sensitive and rapid analytical method to determine the rare earth elements in surface waters. *Chemical Geology* **120,** 91-109.

Hoffman P.F. and Grotzinger J.P. (1993) Orographic precipitation, erosional unloading, and tectonic style. *Geology* **21,** 195-198.

Holland H.D., Lazar B. and McCaffrey (1986) Evolution of the atmosphere and oceans. *Nature* **320,** 27-33.

Langmuir D. (1997) *Aqueous Environmental Geochemistry*. Prentice-Hall.

McLennan, S.M. (1989) REE in sedimentary rocks: Influence of provenance and sedimentary processes. *Reviews in Mineralogy* **21,** 170-199.

Meybeck M. (1987) Global chemical weathering of surficial rocks estimated from river dissolved loads. *Am. J. Sci.* **287,** 401-428.

Milliman J.D. (1980) Sedimentation in the Fraser River and its estuary, southwestern British Columbia (Canada). *Estuarine Coastal Mar. Sci.* **10,** 609-633.

Milliman J.D. and Meade R.H. (1983) World delivery of river sediment to the oceans. *J. Geol.* **91,** 1–21

Milliman J.D. and Syvitski P.M. (1992) Geomorphic/Tectonic control of sediment discharge to the ocean: the importance of small mountainous rivers. *J. Geol.* **100,** 525–544.

Millot R., Gaillardet J., Dupré B. and Allègre J.C. (2003) Northern latitude chemical weathering rates: clues from the Mackenzie River Basin, Canada. *Geochimica et Cosmochimica Acta* **67,** 1305-1329.

Nesbitt H.W. (1979) Mobility and fractionation of REE during weathering of a granodiorite. *Nature* **279,** 206-210.

Raymo M. E. and Ruddiman W. F. (1992) Tectonic forcing of late Cenozoic climate. *Nature* **359,** 117–122.

Ruddiman, W.F. (ed) 1997. *Tectonic uplift and climate change.* New York: Plenum.

Sholkovitz E.R., Elderfield H., Szymczak R. and Casey K. (1999) Island weathering: river sources of rare earth elements to the Western Pacific Ocean. *Marine Chemistry* **68,** 39-57.

Sharp M., Creaser R.A. and Skidmore M. (2002) Strontium isotope composition of runoff from a glaciated carbonate terrain. *Geochimica et Cosmochimica Acta* **66(4),** 595-614.

Stumm W. and Morgan J.J. (1996) *Aquatic Chemistry: Chemical Equilibria and Rates in Natural Waters* 3rd Ed. Wiley, New York.

Summerfield M.A. and Hulton N.J. (1994) Natural controls of fluvial denudation rates in major world drainage basins. *J. Geophys. Res.* **99,** (B7) 13871-13883.

Taylor S.R. and McLennan S.M. (1985) *The Continental Crust: Its Compostition and Evolution.* Blackwell.

Telmer K. and Veizer J. (1999) Carbon fluxes, pCO_2 and substrate weathering in a large northern river basin, Canada: carbon isotope perspectives. *Chem. Geol.* **159,** 61-86.

Tranter M., Huybrechts P., Munhoven G., Sharp M. J., Brown G. H., Jones I. W., Hodson A. J., Hodgkins R. and Wadham J. L. (2002) Direct effect of ice sheets on terrestrial bicarbonate, sulphate and base cation fluxes during the last glacial cycle: minimal impact on atmospheric CO_2 concentrations. *Chem. Geol.* **190,** 33-44.

Walker J. C. G., Hays P. B. and Kasting J. F. (1981) A negative feedback mechanism for the long-term stabilization of Earth's surface temperature. *J. Geophys. Res.* **86,** (c10) 9776-9782.

Wheeler J. O., McFeely P. (1991) Tectonic Assemblage Map of the Canadian Cordillera and Adjacent parts of the United States of America. Geological Survey of Canada, Map 1712a.

4 Dissolved, adsorbed, organic bound and particulate mercury transport by the Fraser, Skeena and Nass Rivers (British Columbia, Canada): the role of rock weathering.

4.1 OVERVIEW

Water and suspended particulate samples were collected and analysed for mercury (Hg) concentrations from the three largest river systems draining the western Canadian Cordillera into the Pacific Ocean (Fraser, Skeena and Nass). In order to determine the distribution of Hg between labile and refractory phases, the suspended particulate was subjected to a sequential extraction, and each fraction analysed separately by cold vapour atomic fluorescence spectroscopy (CV-AFS). These are (in order of extraction): (i) Hg adsorbed to mineral surfaces – 1 N ammonium acetate, (ii) Hg bound to organic molecules – 1 N potassium hydroxide, and (iii) Hg contained within refractory oxide, sulphide, and some other minerals – concentrated aqua regia. The residual from this procedure was not analysed, but is considered to be minor. The total annual export of Hg to coastal waters by these rivers is 11×10^3 kg·yr^{-1}, of which 6% (650 kg·yr^{-1}) is in labile phases (dissolved < adsorbed < organic bound).

Chemical weathering of continental rocks transfers Hg from the geological reservoir (bedrock) to the surface geochemical reservoirs (pedosphere, biosphere, atmosphere, hydrosphere). Using measured chemical weathering rates of silicate, carbonate and sulphide minerals in the studied watersheds, the amount of Hg released from bedrock is calculated by mass balance. Using global average values of Hg in the rock types that occur in the basins, the mass balance calculation indicates that 2.5 to 100% of the riverine Hg flux can be attributed to chemical weathering for the region. The strong correlation between chemical weathering rates and fluxes of Hg in the rivers suggests weathering is the dominant control (near to 100%) on Hg release and transport. The mass balance results show that the rate of sulphide oxidation and the concentration of

Hg in sulphide minerals has the greatest influence on the amount of Hg liberated by chemical weathering.

There is a seasonal variability in the concentrations of Hg and relative distributions between the adsorbed, organic bound and mineral bound phases. During the high stage of the hydrograph (June), the labile Hg dominantly exists in the adsorbed phase, with little or no detectable organic bound Hg. The opposite distribution is observed during the low stage of the hydrograph (October). On average, mineral bound Hg concentrations are much higher in June than October, by as much as an order of magnitude in the main stems of the Fraser, Skeena and Nass. The seasonal variations indicate a change in composition and source of the suspended particulate matter from relatively unweathered rock flour in June (alpine source) to substantially more weathered material in October (valley source) which contains a greater percentage of organic material formed during soil development over the Holocene. The seasonal variation in Hg distribution between the adsorbed and organic bound phases indicates that Hg has a greater affinity to organic ligands than to direct adsorption to inorganic particulate surfaces. The change in mineral bound Hg concentration between the alpine and low-land derived particulate suggests that the development of soil may be associated with direct loss of Hg to the atmosphere.

4.2 INTRODUCTION

Current and historical release of mercury (Hg) into the environment by human activities has been documented by many researchers (e.g. Nriagu, 1993; Sunderland and Chmura, 2000; Hylander and Meili, 2003; Pironne et al., 1996). The toxicity of Hg is well known, and in specific acute cases has had disastrous impact on society, one of the worst known cases being widespread mercury poisoning in humans as a result of methyl-mercury emissions from a chlor-alkali plant into Minamata Bay, Japan (D'Itri and D'Itri, 1977). Factors that make Hg more insidious than other heavy metals include its high volatility. This results in a sufficiently long residence time in the atmosphere (~ 1 year, Fitzgerald, 1989) which allows Hg to be transported great distances, even to remote pristine regions. Furthermore, organo-Hg compounds like methyl-Hg are highly toxic, accumulate in the fatty tissues of organisms and are bio-magnified in the food web so that species at high trophic levels (including humans) can have a high risk of Hg toxicity (e.g. Nendza et al., 1997; Chan et al., 2003).

In an attempt to understand the fate of anthropogenic Hg, researchers have developed models and mass budgets that describe the global biogeochemical cycle of Hg, with a particular focus on atmospheric transport and deposition (e.g. Dastoor and Larocque, 2004; Mason et al., 1994; Seigneur et al., 1994). However, recent work has shown that the magnitude of natural Hg emissions to the atmosphere may be grossly underestimated (Lindberg et al., 1998; Rasmussen et al., 1998). Meanwhile others have shown common pollution indicators such as Hg in fish (Kraepiel et al., 2003) and Hg profiles in sediments (Telmer et al., 2004) are likely controlled by, or at least significantly influenced by, natural processes and therefore cannot be used as direct

proxies of Hg emissions by humans. Thus, the natural cycle of Hg remains poorly understood. This is a problem that must be resolved in order to effectively predict the fate of anthropogenic Hg.

A primary objective of this study is to provide new Hg flux data in rivers draining pristine areas of the Canadian Cordillera in order to provide insight into the natural Hg cycle. This work is part of a comprehensive geochemical reconnaissance of the region, and by exploiting multiple geochemical tracers to interpret the dissolved and particulate burden of these rivers, it is possible to apportion the riverine Hg to natural basinal sources (chemical weathering) and to external sources (atmospheric deposition).

4.2.1 The Geological Mercury Cycle

The exogenic cycle, literally "on the exterior" of the planet, can be defined as global cycling of elements at or near the earth's surface through the cycle of weathering, erosion, transportation, deposition, burial, diagenesis and uplift. The exogenic cycle impacts the earth's surface environment by the exchange of elements between the lithospheric reservoir (bedrock) and reservoirs that make up the earth's surface environment (pedosphere, biosphere, atmosphere, hydrosphere), as well as by the movement and redistribution of elements between the surface reservoirs. As with all other elements, the amount and distribution of Hg in the surface environment is affected by this natural cycle (see figure 4.1).

The breakdown of bedrock by chemical weathering facilitates a transfer of mercury (and other elements) from the lithosphere to the surface environment. Once released from rock forming minerals into more labile forms, mercury becomes involved in the biogeochemical system of Earth's surface. The fate within the exogenic cycle

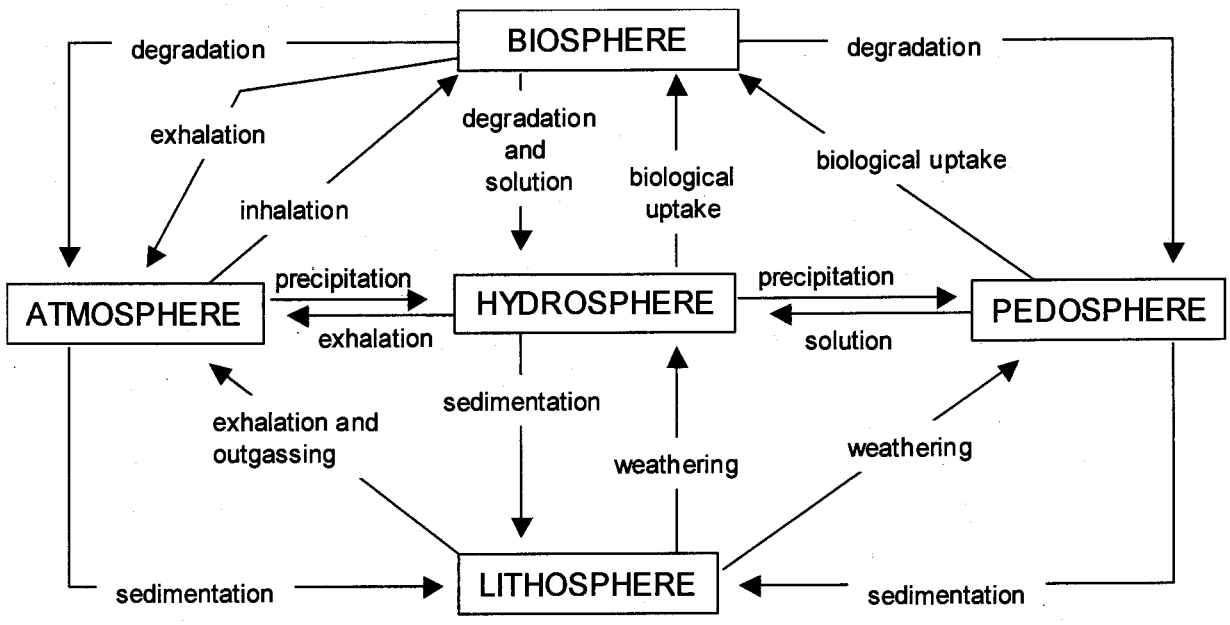

Figure 4.1 The geochemical cycle of mercury (modified from Jonasson and Boyle, 1972) showing the pathways between the lithosphere and the surface reservoirs (atmosphere, hydrosphere, pedosphere and biosphere), as well as the exchange pathways between the different surface reservoirs.

depends on many factors that include tectonics, global climate, ocean and atmosphere chemistry. Ultimately, return to the lithosphere is achieved through the formation of sedimentary rocks, and the subduction of ocean crust and its sedimentary blanket returns (Garrels and Mackenzie, 1971; Berner and Berner 1987).

Chemical and physical erosion of the continents is a major source of dissolved and particulate material into the oceans. Rivers are the main agent of transport of eroded material from the continents to the oceans. According to Garrels and Mackenzie (1971), approximately 90% of the material transport from the continents to the oceans occurs via the dissolved and particulate burden of rivers. This means that river fluxes directly reflect weathering and erosion within a watershed. Whether or not this assumption holds true for mercury remains unknown.

Current mass balance models of the global Hg cycle assume steady state between the release of Hg by weathering processes and the subsequent return of Hg to the lithosphere by sedimentation (e.g. Mason et al., 1994). This may be true on geologically significant timescales (millions of years), however, on the timescales relevant to human civilization (thousands of years and less), there is little evidence for or against this steady state assumption. The geological record shows that while the global cycles of elements such as carbon, sulphur, and oxygen, which are controlled by the weathering / sedimentation cycle are generally balanced (in steady state) on timescales greater than 10^6 years, it also shows that these cycles can deviate from steady state on shorter timescales (e.g. Kump 1989; see also chapter 2 for more discussion of this topic). Considering this, plus the fact that the Hg cycle has been significantly impacted by human activities there is little conclusive evidence that geological cycling of Hg should

be in steady state on millennial and shorter timescales. Here, a mass balance approach is used to determine the rate of release of Hg from bedrock into the surface environment by weathering of continental crust within the Canadian Cordillera.

4.2.2 Hg Release by Chemical Weathering of Bedrock

4.2.2.1 Weathering Reactions

Chemical weathering is the process of chemical breakdown of rock forming minerals at the earth's surface. Chemical weathering reactions are described as congruent, where complete dissolution of a mineral occurs; or incongruent, where insoluble secondary minerals are formed as a weathering byproduct. Weathering of calcite by carbonic acid is an example of congruent weathering:

$$CO_{2(aq)} + H_2O_{(l)} + CaCO_3(calcite) \rightarrow 2HCO^-_{3(aq)} + Ca^{2+}_{(aq)} \quad (1)$$

The albite weathering reaction is an example of incongruent weathering, where the clay mineral kaolinite is the weathering byproduct (secondary mineral):

$$2CO_{2(aq)} + 3H_2O_{(l)} + 2NaAlSi_3O_6(albite) \rightarrow 2HCO^-_{3(aq)} + 2Na^+_{(aq)} + 4SiO_{2(aq)} + Al_2Si_2O_5(OH)_4(kaolinite) \quad (2)$$

Pyrite oxidation is another important example of incongruent weathering, with iron oxyhydroxide (FeOOH) forming as a secondary mineral:

$$FeS_2(pyrite) + 1\frac{1}{4}O_{2(g)} + \frac{5}{2}H_2O_{(l)} \rightarrow FeOOH_{(s)} + 2H_2SO_{4(aq)} \quad (3)$$

Weathering reactions like the ones described by equations 1 to 3 illustrate the behaviour of the major elements of minerals during chemical weathering, but do not describe the behaviour or fate of trace elements such as Hg.

It is possible to make predictions regarding the fate of Hg in the weathering environment based on a general understanding of weathering processes and bedrock

composition. Chemical weathering effectively exposes all of the component ions of a mineral (trace and major alike) to a set of conditions that will facilitate either dissolution, or incorporation into secondary minerals. Thus, like the major elements, trace elements such as Hg must either go into solution, into secondary minerals, or volatilize. Whether Hg will be transferred into secondary minerals or into the dissolved phase by chemical weathering depends on the compatibility of Hg in the secondary phases that are forming, and may depend on other factors such as the dissolved composition and ambient pH. Furthermore, because Hg has low solubility in water, Hg that is liberated into solution by chemical weathering, and not incorporated into a secondary phase, will tend to adsorb onto mineral surfaces, or be complexed by organic ligands.

4.2.2.2 Labile and Refractory Phases of Hg

Mercury can exist in many different mineral and chemical phases. These phases will be classified as either *labile* or *refractory*. Labile Hg includes Hg that is in true aqueous solution, plus ionic and organic bound Hg that is associated with colloids or adsorbed to particulate surfaces. Refractory Hg is bound in mineral or organic phases that are not in equilibrium with the surrounding aqueous solution. The designation of labile and refractory phases is important because while labile Hg may be associated with solid phases through adsorption, it is still in direct chemical communication with the surrounding aqueous solution, and can easily become mobile and therefore potentially bio-available. Refractory Hg, on the other hand, becomes mobile through dissolution of the phase in which it resides. This does not mean that it will never become labile Hg, but the rates of mineral dissolution generally have half life periods of days to millions of years, which is orders of magnitude slower than half life periods of adsorption-desorption

and ion exchange reactions which are on the order of fractions of seconds to hours/days (e.g. Langmuir, 1997).

4.2.3 Sequential Extraction

In this study, four discrete phases of Hg are analysed in the dissolved and suspended particulate loads of the Cordilleran rivers: (i) dissolved Hg (Hg^{dis}), (ii) Hg adsorbed to mineral surfaces (Hg^{ads}), (iii) Hg complexed by organic compounds (Hg^{org}), and (iv) Hg bound in refractory minerals (Hg^{min}). The sum of Hg^{dis}, Hg^{ads}, and Hg^{org} being labile Hg, and Hg^{min} being refractory Hg. Hg^{dis} was analysed directly from filtered water samples. Mercury associated with the adsorbed, organic bound and mineral bound phases was separated by a sequential extraction technique. The practical details of the procedure are given in the Methods section of this paper. The sequential extraction steps are described qualitatively here.

1. Adsorbed Hg is extracted first, by treating the sample with ammonium acetate solution buffered to pH 5.5. The Hg^{2+} adsorbed to mineral surfaces is displaced by the ammonium ions (NH_4^+), by cation exchange. The ammonium acetate solution is only mildly acidic, thus dissolution of mineral phases is unlikely. This technique is similar to commonly used methods to determine cation exchange capacity in soil material (Fetter, 1994; Langmuir, 1997).

2. Organic bound Hg is then extracted by treating the sample with potassium hydroxide solution (KOH). Others have shown that alkaline solutions are effective at dissolving humic substances by desorbing them from mineral surfaces (Schnitzer and Skinner, 1968). This is qualitatively apparent in many samples, where the clear, colourless KOH solution turns to a tea-like clear brown solution after it is mixed with the particulate

samples. This coloration results from desorption of large organic molecules off of the particulate surfaces. The KOH extraction works as an anion exchange, where negatively charged large organic molecules, that may adsorb to and coat suspended mineral grains, are displaced from the mineral surfaces by the hydroxide ion (OH^-) provided by the KOH solution. When the supernatant laden with dissolved organic matter is removed from the residual particulate, mercury associated with these organic molecules is liberated into solution by digesting the KOH extract with bromine mono-chloride (BrCl).

3. Mineral bound Hg is determined by digesting the residual material in a concentrated aqua-regia / potassium dichromate solution, a method commonly used to determine total Hg (partial total) in soils and sediments. The Hg associated with the mineral bound fraction includes Hg bound within oxides and oxy-hydroxide minerals which form during sulphide oxidation. These types of minerals are known to scavenge heavy metals during weathering of sulphide bearing rocks (e.g. Scott, 1985; Cairns et al., 2001), and can have extremely high Hg concentrations (typical Hg concentrations in Fe and Mn oxides range from 0.1 to 1000 $\mu g \cdot g^{-1}$, Jonasson and Boyle, 1972). The term partial total has been adopted by the analytical community as the aqua-regia digests typically liberate 90% or greater amounts of trace elements in solids with the remaining 10% being analytically "invisible". However, it is important to consider that there is some Hg left in the silicate residual of an aqua-regia digest that is not accounted for in our analysis.

4.3 STUDY AREA

Water and sediment samples were collected from the Fraser, Skeena and Nass main stems and selected tributaries in June and October 2002 (Figure 1.1, Chapter 1). A detailed description of the watersheds and basin geology is given in chapter 1.

4.4 METHODS

4.4.1 Sample Collection

During the peak (June) and trough (October) of the 2002 hydrograph, water and suspended particulate samples (including field duplicates and blanks) were collected from 12 rivers draining the Fraser, Skeena and Nass watersheds. The water samples were filtered in the field through pre-weighed Millipore 0.45 μm HVLP polyvinyl filter membranes within one hour of collection directly into 125 mL HDPE bottles pre-injected with 0.6 mL concentrated bromine monochloride (BrCl). Pre-injection was performed daily or just before sample collection to avoid "inhalation" and oxidation of atmospheric Hg (a potential contamination source). Suspended particulate samples were collected by saving the sediment laden filter membranes. On return to the lab, the sediment laden filters were dried in a desiccator at room temperature in the dark. The total suspended sediment concentration (TSS) was estimated by weighing the mass (dry weight) of sediment captured per litre of water filtered. All drying, weighing and subsequent handling of the sediment samples was conducted under clean (class 100) conditions.

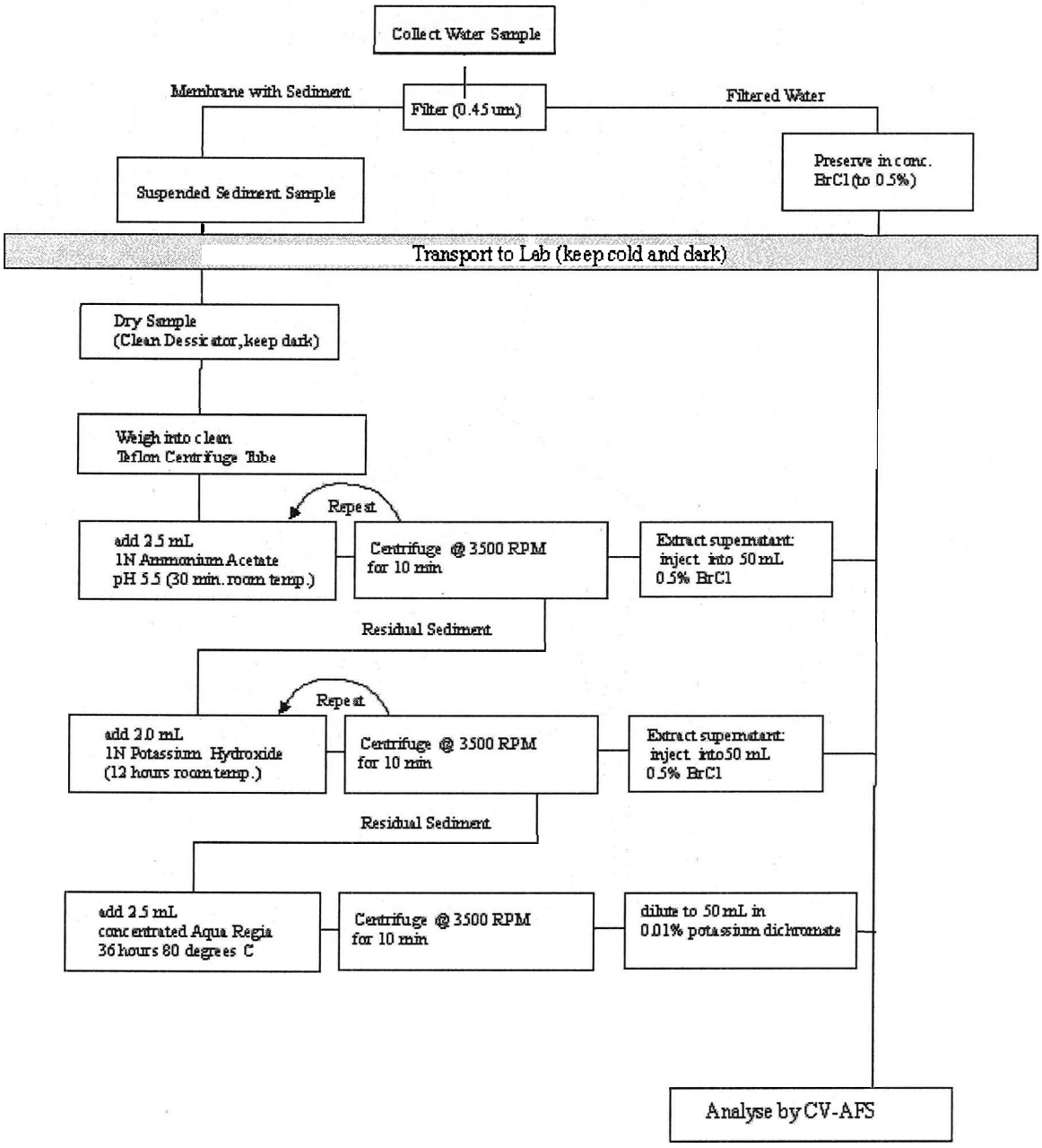

Figure 4.2 Flowchart of the sample collection and analytical methods used to determine dissolved Hg, adsorbed Hg, organic bound Hg and mineral bound Hg from the Cordilleran river water and suspended particulate samples.

4.4.2 Sequential Digestion

Figure 4.2 is a flowchart of the analytical procedures used in this study. The filters were dried by placing the vials containing the filter membranes (caps off) on their sides in a class 100 laminar flow hood, and then by storing in a desiccator for many days to ensure dryness. The sediment for analysis was collected from the filters by manually scraping it off with a clean plastic spatula onto weighing paper, and then weighing (10 to 50 mg) into acid washed Teflon centrifuge tubes.

The sediment samples, standards, and blanks and standard reference materials were then treated to the sequential digestion as follows:

Step 1. Adsorbed fraction. Treat sample with 2.5 mL 1 N ammonium acetate buffered to pH 5.5. Mix at room temperature for 30 minutes. Centrifuge. Pipette supernatant into 50mL of 0.5% BrCl solution. Repeat step 1.

Step 2. Organic bound fraction. Treat sample (residual from step 1) with 2 mL of 1N potassium hydroxide solution. Mix at room temperature for at least 12 hours (overnight). Centrifuge. Pipette supernatant into 50mL of 0.5% BrCl solution. Repeat step 2.

Step 3. Mineral bound (refractory) fraction. Treat the sample (residual from step 2) with 3.0 mL of concentrated Aqua Regia (3:1 HCl:HNO_3 + 0.01% Potassium Dichromate). Heat in a hot water bath (80 °C) for approximately 36 hours. Allow to cool. Transfer to 50mL centrifuge tubes. Dilute to 50mL with 2% HNO3 + 0.01% Potassium Dichromate. Centrifuge.

4.4.3 Instrumental Analysis

All mercury analyses were performed at the University of Victoria, School of Earth and Ocean Science using a PSA Millenium Merlin cold vapour atomic fluorescence

spectrometer (CVAFS) with a gold trap concentrator. 2% $SnCl_2$ in 10% HCl was used as the reductant. All calibration standards and procedure blanks were prepared and treated the same as the samples.

The dissolved material obtained from each step of the sequential leach described were quantitatively diluted to a volume that could be easily handled for analysis (about 50 mL per sample). Dissolved Hg, and the solutions obtained by *Step 1* and *Step 2* were concentrated on-line by passing the mercury vapour through the gold trap. Once the concentration step was complete, the Hg was thermally desorbed from the trap, and carried to the detector in a stream of argon. This concentration step was required so that a quantifiable signal could be observed by the detector. The solutions obtained from the aqua regia extraction (*Step 3*) were analysed directly by CV-AFS, because concentrations were high enough that the gold-trap step was not required.

4.4.4 Quality Control

4.4.4.1 Sample Handling and Preparation Protocol

Care was taken not to introduce any contaminants to the samples during collection in the field and during processing in the lab. The samples were transported and stored in polyethylene vials that were sealed in parafilm. Because Hg is highly particle reactive, and thus can be introduced to samples by ambient dust, the samples were handled in Class 100 laminar flow hoods to ensure a dust free environment. The bottle cleaning methods and preservation of dissolved Hg follow the protocol recommended by Hall (1998).

Calibration standards and procedure blanks, including field blanks, were subjected to the same digestion and analytical procedures as the samples. Hg was

undetectable in all blank samples. Only ultra pure reagents were used: Anachemia Environmental Grade HCl, Sigma Semiconductor Grade Potassium Hydroxide, ultra-pure Ammonium Acetate (prepared from Seastar *Baseline*™ reagents), 18MΩ water, and Fisher Environmental Grade nitric acid (HNO_3).

4.4.4.2 Accuracy and Precision

There is no standard reference material available that is certified for adsorbed or organic bound Hg. Also, there is no suspended river particulate standard reference material certified for Hg. Thus, calibration standards were prepared using a NIST traceable $HgCl_2$ solution. To test precision, selected samples were split and processed separately. The reproducibility for adsorbed Hg and organic bound Hg in sample splits was better than ± 8%, which is comparable to instrumental precision (± 5%), and greatly exceeds the reproducibility in duplicate samples collected in the field (± 30%). The reproducibility of the mineral bound Hg measurements was determined to be ±5% (equivalent to instrumental precision), based on results for field duplicate samples.

4.4.4.3 Method Limits of Detection

Method limits of detection are often reported as the lowest detectable concentration of analyte per unit mass or per unit volume of sample. This method of reporting is not appropriate for a CV-AFS instrument that utilizes a gold amalgamation concentrator. In this case the instrumental detection limit is governed by the total mass of Hg analysed and the method detection limit is limited only by the reagent purity. The working limit of detection of the CV-AFS method was determined to be 5 pg Hg. In the case of the dissolved Hg samples, the Hg from 60 mL of water was concentrated on the gold trap. This gave a detection limit of 0.08 $ng \cdot L^{-1}$ (80 ppq, 0.4 pmol).

4.5 RESULTS

The analytical results for the Cordilleran rivers are summarized in Tables 4.1 and 4.2. Table 4.1 lists the concentrations of the three particulate phases ($ng \cdot g^{-1}$ dry weight). Table 4.2 lists the concentrations of Hg in the dissolved and particulate phases, normalized to river water volume ($ng \cdot L^{-1}$).

In general, the distribution of Hg is heavily dominated by the refractory mineral bound phase. Figure 4.3 shows the seasonal variation in relative distribution of Hg between the three labile phases, as described in the following paragraphs.

4.5.1 Dissolved Hg

The concentrations of dissolved Hg range from < 0.08 to 1.7 $ng \cdot L^{-1}$, with no clear seasonal variability (Table 4.2). These concentrations are significantly lower than dissolved Hg measured in the Mackenzie river system, which range from 0.57 to 26.67 $ng \cdot L^{-1}$ (Leitch et al., 2004). These high Hg concentrations in the Mackenzie river system are attributed to weathering of sulphide rich, coal and petroleum bearing bedrock (Leitch et al., 2004). The dissolved concentrations measured during this study agree well with values measured in rivers draining the eastern United States (Lawson and Mason, 2001), and in major rivers draining the Siberian Plateau into the Arctic Ocean (Coquery et al., 1985).

Table 4.1 Mercury concentrations ($ng \cdot g^{-1}$ dry weight) in the adsorbed, organic bound and mineral bound phases of suspended particulate in the Cordilleran rivers.

			Hg^{ads}		Hg^{org}		Hg^{min}	
	Sample		$ng \cdot g^{-1}$ dry weight					
Station	*June*	*October*	*June*	*October*	*June*	*October*	*June*	*October*
1	101	201	88.0	7.1	9.3	58.0	9.5	105
2	102	202	23.0	20.5	8.0	32.6	541	42
4	104	203	17.4	na	17.3	na	262	na
5	105	--	12.3	na	7.3	na	513	na
7	107	205	8.7	9.3	12.5	67.2	36.7	90
8	109	206	9.4	4.5	10.4	119	506	209
8	110	207	21.7	na	16.7	na	505	na
9	111	208	83.8	8.5	273	20.0	605	180
10	112	209	28.9	na	14.5	na	1346	na
12	114	210	23.8	na	0.0	na	1048	na
13	115	211	19.8	4.3	7.0	49.1	1104	115
13	116	212	nd	13.1	8.9	157	1278	121
14	117	--	nd	na	5.2	na	1975	na
15	118	213	11.7	3.0	8.7	28.2	1112	364
16	119	215	53.3	na	6.2	na	1273	na
17	120	216	25.9	3.4	7.4	41.7	46.1	176
18	121	214	37.3	na	23.2	na	734	na
20	123	218	5.0	na	5.6	na	4.8	na
21	124	219	34.2	7.5	15.2	167	8.1	278
23	126	221	58.3	26.9	4.4	198	121	111
24	127	222	59.3	6.3	70.3	32.4	1722	89

Table 4.2. Hg concentrations per litre of water ($ng \cdot L^{-1}$) in the dissolved, adsorbed, organic bound and mineral bound phases of the Cordilleran rivers. Values in brackets were below the calculated method limit of detection. "na" indicates sample not analysed; "nd" indicates analyte below limit of detection.

			Hg^{dis}		Hg^{ads}		Hg^{org}		Hg^{min}	
Station	Sample		← $ng \cdot L^{-1}$ →							
	June	Oct	June	October	June	October	June	October	June	October
1	101	201	0.35	0.3	4.4	0.05	0.5	0.4	0.5	0.7
2	102	202	nd	0.3	2.8	0.67	1.0	1.1	66.5	1.4
4	104	203	nd	nd	2.2	na	2.2	na	33.5	na
5	105	--	nd	na	1.1	na	0.5	na	60.4	na
7	107	205	0.29	0.5	0.8	0.05	1.1	0.4	3.3	0.5
8	109	206	0.7	1.2	1.0	0.30	1.1	7.8	52.6	13.7
8	110	207	0.98	nd	3.3	na	2.5	na	76.4	na
9	111	208	na	0.7	0.5	0.02	1.7	0.0	3.7	0.4
10	112	209	0.97	na	3.9	na	2.0	na	82.2	na
12	114	210	na	na	4.2	na	na	na	185	na
13	115	211	1.12	1.3	2.9	0.17	1.0	1.9	164	4.5
13	116	212	1.31	1.3	nd	0.52	1.2	6.2	176	4.8
14	117	--	1.68	na	nd	na	0.6	na	211	na
15	118	213	0.89	1.6	1.4	1.78	1.0	16.7	130	210
16	119	215	0.59	na	4.4	na	0.5	na	106	na
17	120	216	0.83	na	1.6	0.01	0.5	0.2	2.8	0.7
18	121	214	nd	nd	1.2	na	0.8	na	24.4	na
20	123	218	nd	nd	0.1	na	0.1	na	0.1	na
21	124	219	0.13	nd	0.5	0.02	0.2	0.4	0.7	0.6
23	126	221	nd	0.4	0.7	0.04	0.1	0.3	1.6	0.2
24	127	222	0.8	na	1.5	0.38	1.8	1.9	44.2	5.3

(a) Fraser River

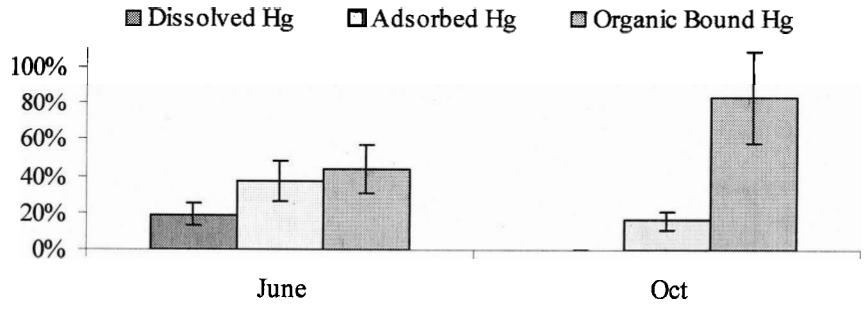

(b) Skeena River

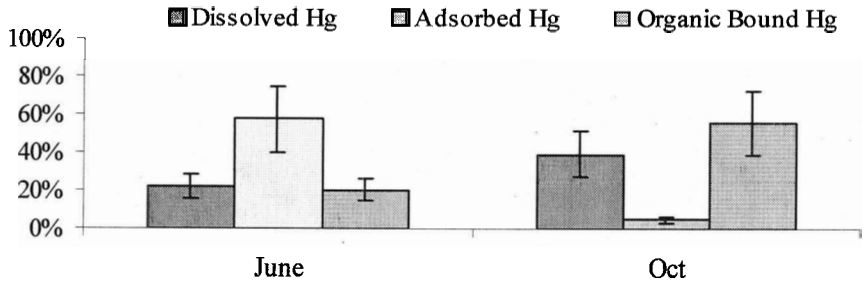

(c) Nass River

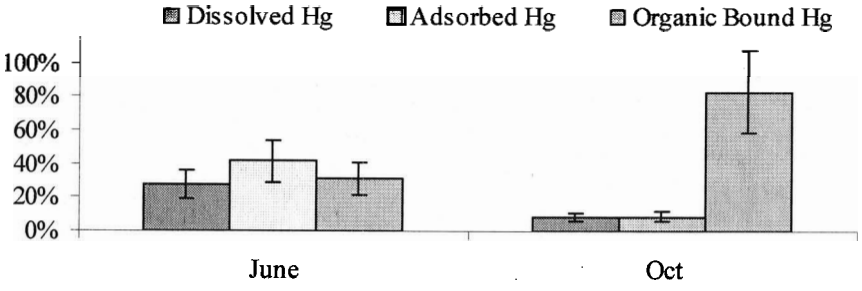

(d) Squamish River

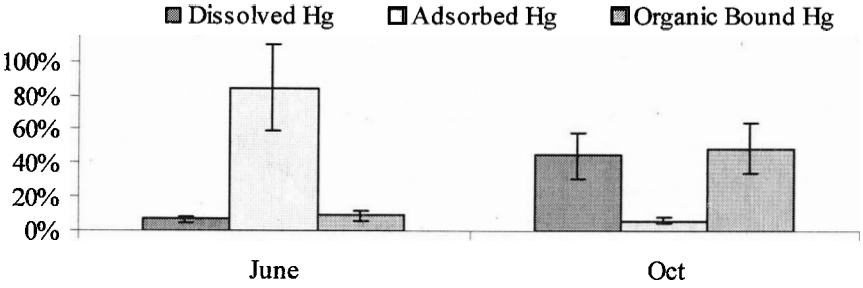

Figure 4.3 Seasonal variability in relative labile Hg distribution (presented as percent of total labile Hg in $ng \cdot L^{-1}$) observed in the Cordilleran watersheds. The relative amount of adsorbed Hg decreases from June to October, while the relative amount of organic bound Hg increases.

4.5.2 Adsorbed Hg

The dry weight concentrations of adsorbed Hg shows a broad range, from 3.0 to 88 $ng \cdot g^{-1}$. This likely reflects variable particulate composition, and therefore variable capacity to adsorb Hg. Complementary work on adsorbed rare earth elements in the same suspended particulate samples is discussed in Chapter 3, and shows distinct variability between the June and October samples, where the particulate in the October samples have dramatically increased adsorptive capacity (~ 50×) for rare earth elements compared to the June samples. This is however, not the case for Hg. In fact, many stations have lower concentrations of adsorbed Hg in October than June, showing that adsorption of Hg onto mineral surfaces is controlled by different factors than for rare earth elements.

4.5.3 Organic Bound Hg

Much of the difference in adsorption of Hg versus rare earth elements can be explained by the organic bound fractions. Whereas organic bound rare earth elements were essentially undetectable in these samples, the dry weight concentrations of organic bound range from 4.4 to 273 $ng \cdot g^{-1}$. Many stations show a significant increase in organic bound Hg concentrations in October over June such that in October the labile Hg is dominantly associated with the organic fraction of the particulate (see Figure 4.3), and so, like the rare earth elements (chapter 3), the concentration of labile Hg per dry weight of particulate increases in the October samples.

The increased relative and absolute concentration of Hg^{org} can be explained by increased organic content of the suspended matter in October compared to the spring snow-melt period (high water stage of the hydrograph, June). In October, the suspended particulate is dominated by erosion of the alluvial soils that line the valleys of the

Cordilleran watersheds, while in June, the suspended particulate is dominated by erosion of freshly weathered bedrock from the alpine regions – rock flour – as illustrated by the results of the rare earth element study (chapter 3). The rock flour has not undergone significant alteration from the source bedrock. Sulphide and carbonate minerals which weather much more rapidly than silicates will have very likely been weathered out of the rock flour, leaving behind secondary oxide minerals which are a likely candidate to host the mineral bound Hg. This is supported by studies of weathering processes in glaciated alpine catchments that show significant coupled sulphide-carbonate weathering, but minimal to undetectable silicate weathering (Anderson et al., 2000; Sharp et al., 2002). Because there is little vegetation in the alpine regions, and physical erosion is high, there is little to no opportunity for organic debris to accumulate. Thus little organic bound Hg is observed.

In October, the alluvial soil material that dominates the particulate load of the rivers has been shown to contain a higher proportion of secondary minerals compared to the June samples (chapter 3). The main differences between the composition of the June and October particulate are likely: (i) a significant component of clay minerals due to increased silicate weathering in the valley regions, and (ii) increased organic content due to the growth and decay of vegetation in the lower altitude regions of the watersheds. Hg is known to have a strong affinity to organic ligands (e.g. Benoit et al., 2001).

The fact that the relative proportion of Hg^{ads} decreases while the relative proportion of Hg^{org} increases from June to October (Figure 4.4) indicates that organic ligands out-compete adsorption sites, and labile Hg will be preferentially associated with the organic bound phase. This may be important in terms of the fate of Hg released by

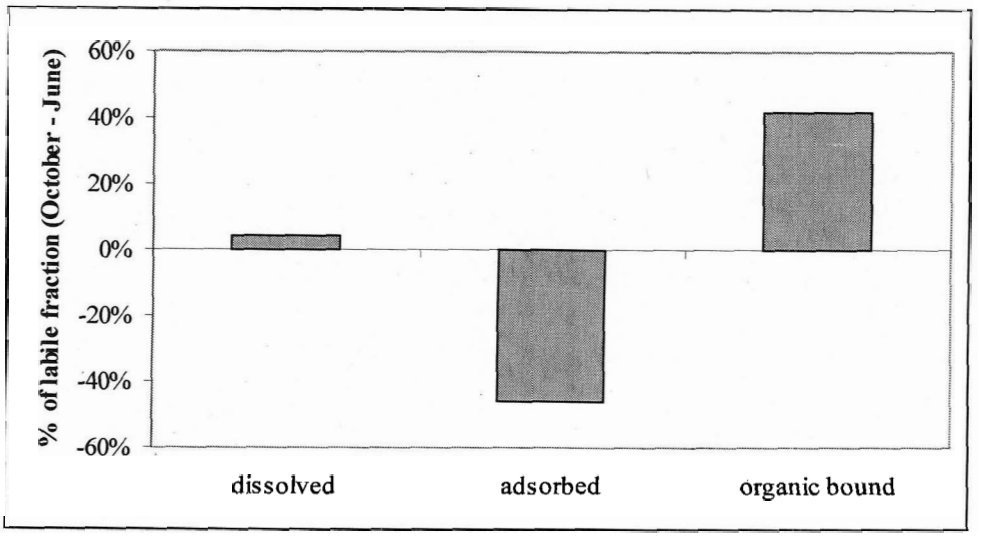

Figure 4.4 This figure shows the change in labile Hg proportions from June to October for the average of the Fraser, Skeena, Nass and Squamish rivers. Thus the average organic bound component of the labile Hg is 40% greater in October than in June, likewise, the average adsorbed component of the labile Hg is about 45% lower in October than in June. The dissolved component shows little change.

weathering because Hg associated with the adsorbed versus the organic bound phase likely have different bio-availability (e.g. Benoit et al., 2001).

The results presented here suggest that the distribution of Hg within river particulate depends on the maturity of the soil material being eroded, which is analogous to the age of the landscape being eroded. Young landscapes produce particulate with higher Hg^{ads} / Hg^{org} ratios. This suggests that rivers draining recently uplifted and rapidly eroding mountainous regions will have a greater proportion of Hg^{ads} compared to rivers draining mature landscapes with significant soil development. How this impacts bio-availability is uncertain.

4.5.4 Mineral Bound Hg

Hg within the Cordilleran rivers is dominantly transported within the mineral bound phase. The dry weight concentrations of Hg^{min} are highly variable, ranging from 4.8 to 1975 $ng \cdot g^{-1}$, with a median value of 262 $ng \cdot g^{-1}$. Similarly, total Hg concentrations measured on suspended particulate within the Mackenzie river system by Leitch et al. (2004) mostly range from 6 to 89 $ng \cdot g^{-1}$, but with some as high as 29000 $ng \cdot g^{-1}$. Large industrial sources of Hg are lacking in all of these river systems, therefore, natural weathering is the most likely explanation for the high concentrations of mineral bound Hg. It is possible that the very high samples contain detrital sulphides.

Comparison of Hg^{min} dry weight concentrations at specific stations shows that for many, the concentration decreases by as much as a factor of 10 from June to October (Table 4.1). In a few cases the concentrations stay about the same, or increase slightly. The seasonal variability of Hg^{min} is discussed below (section 4.8).

4.6 MERCURY DELIVERY TO BRITISH COLUMBIA'S COASTAL WATERS

Annual fluxes of Hg on a per catchment ($kg \cdot yr^{-1}$) and per area ($kg \cdot km^{-2} \cdot yr^{-1}$) basis are listed for the Fraser, Skeena, Nass and Squamish watersheds and sampled tributaries in Table 4.3. Figure 4.5 shows the annual Hg fluxes per km^2 for the Fraser, Skeena, Nass and Squamish rivers. These fluxes (Hg_{annual}) were extrapolated from measured Hg concentrations in these rivers as:

$$Hg_{annual} = \left([Hg]_{June} \times 0.7 + [Hg]_{October} \times 0.3\right) \times D \qquad (4)$$

$[Hg]$ represents the measured concentrations (mass per litre) of each of the respective fractions of Hg (dissolved, adsorbed, organic bound and mineral bound) for each of the June and October campaigns. D is the average annual water discharge based on historical hydrographic data collected by Environment Canada (2001). The June and October concentrations are weighted by multiplying by 0.7 and 0.3 respectively to represent the Cordilleran hydrograph. 70% of the water discharged by the Cordilleran rivers occurs during the summer months (Environment Canada, 2001a; also see Chapter 1 - Figure 1.3). It is assumed that the concentrations measured in June are representative of the typical summer (May to September) composition of these waters, and likewise that the concentrations measured in October are representative of the typical composition of these rivers during the remainder of the year. These estimates are based on labile REE concentrations measured in samples collected closest to the mouths of these rivers

The total annual delivery of Hg to British Columbia's coastal waters by the Fraser, Skeena, Nass and Squamish rivers is 11000 ± 550 $kg \cdot yr^{-1}$ of which approximately 6% (650 ± 200 $kg \cdot yr^{-1}$) is in the labile phases, and the remaining 94% (10000 ± 550 $kg \cdot yr^{-1}$) is in the mineral bound phase. This shows that a significant amount of the Hg

Table 4.3 Mercury delivery to British Columbia's coastal waters by the Cordilleran rivers.

	Hg^{dis}	Hg^{ads}	Hg^{org}	Hg^{min}	Hg_{river}	Hg^{dis}	Hg^{ads}	Hg^{org}	Hg^{min}	Hg_{river}
			$kg \cdot yr^{-1}$					$g \cdot km^{-2} yr^{-1}$		
Fraser	50	91	110	2646	2903	0.2	0.4	0.5	12	13
Skeena	38	67	42	3715	3895	0.9	1.6	1.0	88	92
Nass	27	36	140	3761	4111	1.5	2.0	7.6	203	222
Squamish	3	23	3	4	35	1.1	10.0	1.4	1.7	15
Total	118	218	295	10125	10944	0.4	0.8	1.1	36	39
Fraser Tributaries										
Thompson	3	13	3	28	53	0.1	0.2	0.1	0.5	1.0
N.Thompson	1	4	3	9	19	0.1	0.2	0.2	0.4	1.0
Chilcotin	1	2	3	8	14	0.1	0.1	0.1	0.4	0.7
Blackwater	0	0	1	3	5	0.0	0.0	0.1	0.2	0.4
Lillooet	0	9	4	184	199	0.2	4.0	1.8	85	92
Cayoosh	0	1	1	11	12	0.0	0.8	0.8	13	14
Skeena Tributaries										
Bulkley	2	5	2	9	18	0.3	0.6	0.2	1.3	2.5
Zymoetz	0	10	0	430	439	0.0	3.3	0.0	144	147

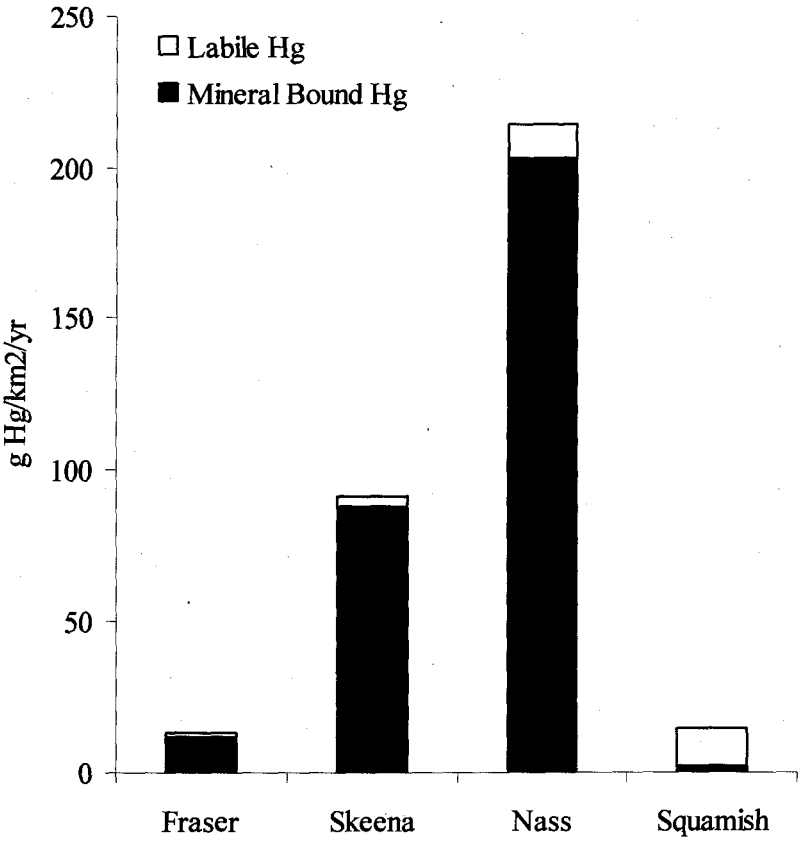

Figure 4.5 Annual mercury fluxes per km^2 for the Fraser, Skeena, Nass and Squamish watersheds. This figure shows how variable the area normalized fluxes are across the Cordillera, indicating that atmospheric deposition is not the dominant source of Hg in the rivers. Note that the area normalized fluxes from the Squamish and Fraser rivers are similar in magnitude, but that in the Squamish River, Hg is almost entirely within the labile phases.

associated with the suspended particulate of these rivers exists in phases that are potentially available for biological uptake or other transformations. The mass of Hg transported by the rivers, and the distribution of Hg between labile and refractory phases does not, however, identify or differentiate between natural and anthropogenic sources. It does however, help to understand potential fates of Hg in the environment.

4.6.1 Labile Mercury Flux

Labile mercury has been defined for this study as all Hg associated with the dissolved and suspended particulate load that is not bound within crystalline (refractory) mineral phases. While not in the dissolved phase at the time of sampling, Hg^{ads} and Hg^{org} may easily become dissolved due to changes in redox, ionic strength (ion exchange), or pH changes. The mixing of river water with seawater will cause such changes and therefore could facilitate desorption of labile Hg from suspended particulate within the estuaries of these rivers, possibly impacting bio-availability. Since almost all of the labile Hg is in the particulate load, using dissolved Hg as an estimate of bio-availability (commonly done) is likely a gross underestimation.

To put perspective on the significance of the amount of labile Hg delivered to the ocean by these rivers (630 $kg \cdot yr^{-1}$) it is useful to consider the amount of fish that could be contaminated by this Hg if it all found its way into marine biomass. 630 $kg \cdot yr^{-1}$ is enough Hg to bring 1.3×10^9 kg of fish to the advisory limit of 0.5 $\mu g \cdot g^{-1}$ as set by the Canadian Food Inspection Agency (Canadian Food Inspection Agency, 2002). In 2002, the reported total annual commercial catch for British Columbia was an order of magnitude lower (0.29×10^9 kg) (Fisheries and Oceans Canada, Statistical Services). Thus the magnitude of labile Hg delivered to British Columbia's coastal waters is certainly great enough to be of

ecological concern. This illustrates that riverine transport of Hg to coastal waters should not be overlooked with respect to resource management.

4.6.2 Mineral Bound Mercury Flux

Ninety four percent of the total Hg transported by the Cordilleran rivers is in the mineral bound fraction. Most of this is deposited in the estuaries and marine sedimentary basins. It is possible that some of this Hg is re-mobilized during sedimentation and enters the water column either as dissolved Hg^{2+} or gaseous Hg^0, post deposition, as a result of diagenetic reactions within the sediment column (Telmer et al., 2004). Recent measurements of Hg in sediment cores collected near the mouth of the Fraser River show total Hg dry weight concentrations of ~60 $ng \cdot g^{-1}$ (Johannesen et al., in review). This is lower than either of the June or October measurements of Hg^{min} at station 24, which is close to the head of the Fraser Estuary (1722 and 89 $ng \cdot g^{-1}$ in June and October respectively). However, Milliman (1980) has shown that ~ 80% of the sediment delivery to the Fraser estuary occurs during the Spring freshet, as represented by the June samples. Thus the annual integrated concentration of suspended particulate (as represented by the near surface samples) would have a Hg concentration of ~ 1400 $ng \cdot g^{-1}$, which is about 20 times more concentrated than the sediment collected from the estuary. Two possible explanations for the discrepancy between the measured Hg^{min} in the river, and the measured concentration of Hg in the estuary sediments are:

(i) The suspended particulate sampled and analysed is not representative of the bulk particulate load of the Fraser River, and therefore the material that is deposited on the estuary. This would imply that the actual concentration of Hg in the bulk particulate load of the Fraser

River is much lower (by about 20 times) than the concentrations measured.

(ii) There is loss of Hg from the particulate during or shortly after deposition on the estuary which may occur through diagenetic alteration of the minerals deposited. On deposition, there is usually a rapid depletion of oxygen very close to the sediment/water interface due to the decay of organic matter. The resulting redox change could allow dissolution of Hg bearing oxide and oxy-hydroxide minerals thus facilitating dissolution and dissipation of Hg back into the water column (e.g. Telmer et al., 2004).

The particulate (and water) samples were all collected near the surface of each river, from a depth of about 30 cm. Due to the tendency for suspended particulate to settle out of suspension under the influence of gravity, the total amount as well as the size and density of material in suspension increases with depth in the water column (e.g. Boggs, 1987). Other work has shown that Hg concentrations in soil particulate are highest in the finest size fractions of the particulate (e.g. Plouffe, 1997). Thus it is likely that the coarser material transported at depth or as bedload within the river has a lower concentration of Hg than the material sampled near the surface. It would be necessary to collect and analyse depth integrated particulate samples from the rivers in order to robustly know if the concentration of Hg in the estuarine sediments are well represented by the samples collected in this study. However, the amount of sediment transported by the Fraser River as estimated by Milliman (1980), at 12 to 30 million tons annually is similar to the estimate produced using samples from this study (3 million tons annually). The

difference between the two estimates does not account for the 20 times dilution required to explain the measured Hg concentrations in the Fraser estuary sediments. The disparity suggests there is a loss of Hg from the river borne particulate post sedimentation on the estuary. Supporting observations have been made in a lacustrine environment (Telmer et al.2004) where higher Hg concentrations were measured in particulate samples collected within the water column (collected on sediment traps) than in the resulting sediments. Telmer et al. (2004) also show Hg concentration gradients within pore waters that support upward diffusion of Hg out of the sediment column.

4.6.3 Small Coastal Catchments

The Squamish catchment (2330 km^2) is very small in comparison to Fraser, Skeena and Nass (277700 km^2 cumulatively), however it is included in this study as an example of a small coastal catchment draining directly into the Pacific Ocean. Along the coast of British Columbia, there are numerous small rivers (by area) that drain the coastal mountains directly into the Pacific Ocean. The total cumulative catchment area of these rivers is similar to the area drained by the Fraser, Skeena and Nass systems, and the coastal rivers are characterized by high runoff and high particulate flux (Milliman and Syvitski, 1992) thus their total particulate fluxes, and by association their Hg fluxes, are likely of a similar (or possibly greater) magnitude as the larger systems.

The results presented here show that Hg distribution in the Squamish River is dominated by labile Hg in both the June (92% labile Hg) and October (53% labile Hg) samples. Thus the labile Hg inputs to British Columbia's coastal waters from these small coastal catchments may be extremely important in comparison to the Fraser, Skeena and

Nass systems. The logistics of sampling these numerous and remote rivers is beyond the scope of the current study.

4.7 MERCURY SOURCE APPORTIONMENT IN THE CORDILLERAN RIVERS

Quantification of natural sources of Hg are required to evaluate the amount of pollution derived Hg in the environment. To do so in this study we determine Hg from bedrock weathering (Hg_w), then consider the residual (residual Hg, Hg_{res}). That is, $Hg_w = Hg_{river} - Hg_{res}$.

4.7.1 Weathering Mass Balance

In chapter 2 of this thesis, chemical weathering rates in the Fraser, Skeena and Nass watersheds were determined for silicate, carbonate and sulphide minerals using dissolved major element concentrations, $\delta^{13}C$ in dissolved inorganic carbon, and $\delta^{34}S$ in dissolved sulphate from samples collected at the same time as the mercury samples. All naturally occurring minerals contain some amount of Hg. Thus Hg_w is equal to the mass of bedrock that has been chemically weathered, times the amount of Hg in that bedrock. As with all elements, Hg is not evenly distributed among rocks and minerals. Therefore, it is necessary to estimate Hg_w using mineral specific weathering rates and published values for Hg concentrations in common rock forming minerals (e.g. Jonasson and Boyle, 1972), and the ratio of Hg in each rock type to a major element. For example, calcium (Ca) in rivers can be apportioned to carbonate and silicate weathering. Thus, the amount of Hg released by weathering a specific rock type (r) in a given watershed is equal to the ratio of Hg to Ca in r times the mass of Ca released by weathering r (Ca_r)

Table 4.4 Typical Hg concentrations in generic rock forming minerals.

	Hg Concentration ($\mu g \cdot g^{-1}$)		
	low[1]	median	high[1]
pyrite	0.1	5[2]	100
carbonate	0.01	0.056[3]	0.2
silicate	0.007	0.056[3]	0.2

[1] Jonasson and Boyle (1972)
[2] estimated median sulphide Hg concentration.
[3] from Wedepohl's (1995) estimate of Hg concentration in upper continental crust.

$$Hg_r = \left(\frac{Hg}{Ca}\right)_r \times Ca_r \quad (5)$$

Here, the weathering rates of silicate, carbonate and sulphide minerals (chapter 2) and typical concentrations of Hg in rock forming minerals (Table 4.4) are used to derive a set of mass balance equations to determine Hg_w for the Cordilleran watersheds, where Hg_w is the sum of Hg derived by silicate, carbonate and sulphide weathering (Hg_{sil}, Hg_{carb}, Hg_{sulp} respectively).

Hg derived by chemical weathering

$$Hg_w = Hg_{sil} + Hg_{carb} + Hg_{sulp} \quad (6)$$

Hg derived by silicate weathering

$$Hg_{sil} = \left(\frac{Hg}{Ca+Mg}\right)_{sil} \times (Ca+Mg)_{sil} \quad (7)$$

Hg derived by carbonate weathering

$$Hg_{carb} = \left(\frac{Hg}{Ca+Mg}\right)_{carb} \times (Ca+Mg)_{carb} \quad (8)$$

Hg derived by sulphide weathering

$$Hg_{sulp} = \left(\frac{Hg}{S}\right)_{sulp} \times S_{sulp} \quad (9)$$

The ratios of Hg to Ca +Mg in silicate and carbonate rocks are used here because Ca and Mg derived by weathering each rock type were determined simultaneously (chapter 2). Sulphide minerals do not contain Ca or Mg, however, the amount of sulphur (S) in the rivers derived by sulphide oxidation was determined using $\delta^{34}S$ in dissolved sulphate. Pyrite is by far the most abundant sulphide mineral, so for the mass balance equations, it

Table 4.5. Mass balance calculation results for Hg_{sil}, Hg_{carb}, Hg_{sulp} and Hg_w. These results are separated into "low", "median" and "high" values, which correspond to the bedrock Hg concentrations listed in table 4. The values of Hg_{res} refer to the residual Hg, $Hg_{res} = Hg_{river} - Hg_w$(median). Negative values indicate the calculated Hg_w is greater than the measured Hg_{river}.

	Mass Balance Results													
	Low				Median				High					
	Hg_{sil}	Hg_{carb}	Hg_{sulp}	$Hg_{w(low)}$	Hg_{sil}	Hg_{carb}	Hg_{sulp}	$Hg_{w(median)}$	Hg_{sil}	Hg_{carb}	Hg_{sulp}	$Hg_{w(high)}$	Hg_{res}	
	kg·yr^{-1}												kg·yr^{-1}	g·yr^{-1}km^{-2}
Fraser	7.1	155.7	24.0	186.9	197.8	218.0	1201.9	1617.8	706.4	778.7	24038.0	25523.2	1285	5.9
Skeena	1.7	31.1	8.0	40.8	48.6	43.6	399.7	491.9	173.7	155.5	7993.6	8322.9	3403	81
Nass	1.4	31.0	11.8	44.2	38.4	43.4	589.6	671.4	137.2	155.1	11791.7	12083.9	3440	186
Squamish	0.2	1.0	0.5	1.7	6.7	1.3	24.9	32.9	23.9	4.8	497.2	525.9	2	0.9
Total	10.4	218.8	44.3	273.6	291.6	306.4	2216.0	2814.0	1041.3	1094.2	44320.5	46456.0	8130	29
Fraser Tributaries														
Thompson	2.3	29.6	7.2	39.0	63.1	41.4	357.8	462.3	225.4	147.8	7155.7	7528.9	-409	-7
N. Thompson	0.7	14.6	2.5	17.8	18.5	20.5	124.4	163.4	66.1	73.1	2488.6	2627.7	-144	-7
Chilcotin	0.4	3.5	1.3	5.1	10.9	4.9	63.0	78.7	38.9	17.5	1259.2	1315.5	-64	-3
Blackwater	0.3	2.2	0.0	2.6	8.5	3.1	2.3	14.0	30.5	11.2	46.9	88.6	-9	-1
Lillooet	0.2	2.2	1.5	3.9	5.5	3.1	76.7	85.3	19.8	10.9	1533.9	1564.6	114	53
Cayoosh	0.0	0.7	0.3	1.1	0.8	1.0	15.4	17.2	2.8	3.6	308.4	314.8	-5	-5
Skeena Tributaries														
Bulkley	0.2	3.7	1.5	5.4	5.1	5.2	75.5	85.8	18.4	18.4	1510.4	1547.2	-68	-9
Zymoetz	0.2	4.3	0.4	4.9	6.1	6.0	21.4	33.5	21.8	21.3	428.1	471.2	406	132

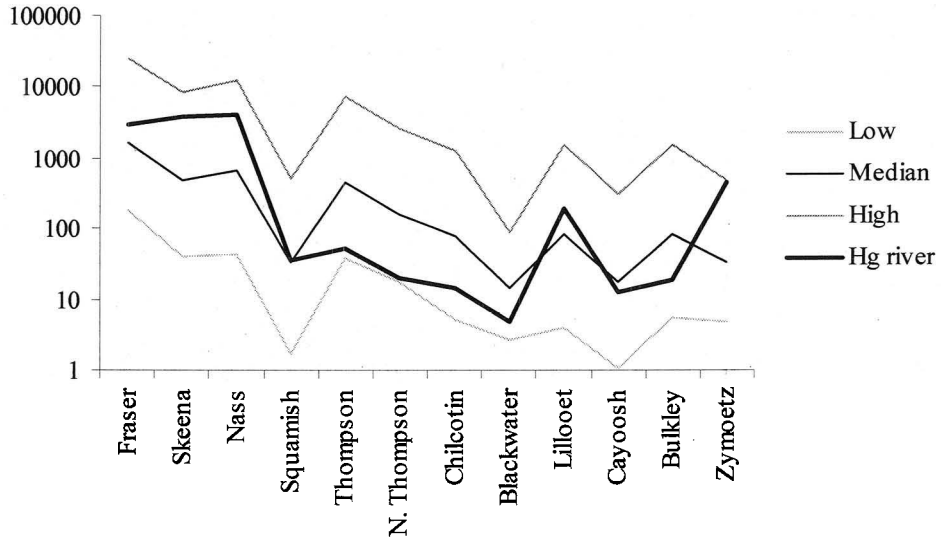

Figure 4.6 Calculated results for Hg_w (low, median and high), and the measured values of Hg_{river} for each of the watersheds (all values in kg $Hg \cdot yr^{-1}$). For all of the watersheds, the measured values of Hg_{river} are within the boundaries set by $Hg_{w(low)}$ and $Hg_{w(high)}$.

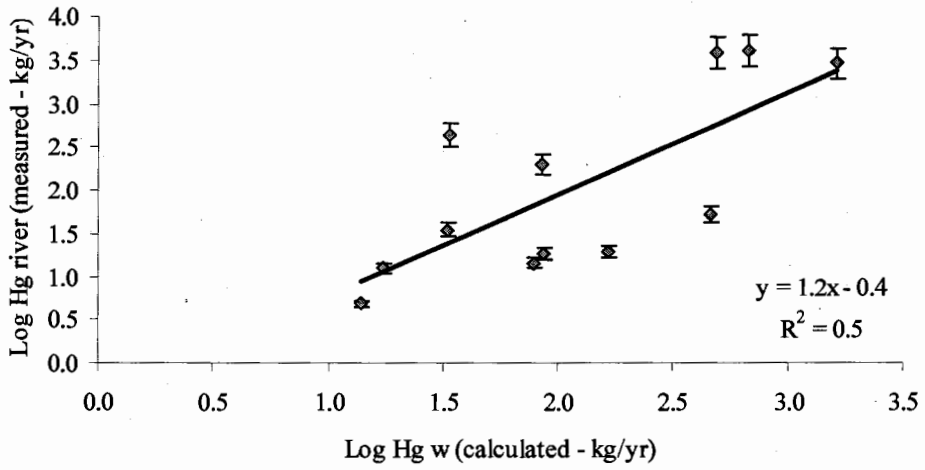

Figure 4.7 Measured Hgriver plotted as a function of calculated Hgw(median). This figure shows a clear correlation between the two. The scatter in the data can be explained by regional variations in bedrock Hg concentrations, which is not accounted for by the mass balance calculations. Both axes are plotted as log units in order to accommodate the large range in values.

is assumed that sulphide weathering in the Canadian Cordillera is dominated by pyrite oxidation. Thus, Hg/S ratios typical of pyrite are used.

4.7.2 Weathering Mass Balance Results

Three sets of results for Hg_w are presented (Table 4.5, Figure 4.6), calculated using the low, median and high bedrock Hg concentrations listed in Table 4.4. The low and high values represent minimum and maximum limits for Hg_w. The median values are presented as conservative estimates of Hg_w. The total median Hg_w values accounts for 25% of Hg_{river} for the entire region. The low Hg_w accounts for 2.5%; and, the high Hg_w accounts for more than 100%. Figure 4.7 plots the measured values of Hg_{river} versus the median values of Hg_w. There is a clear correlation between the measured and the calculated values, as indicated by the trendline. There is significant scatter in the data, however, the fact that there is a correlation shows that Hg_w is a significant component of Hg_{river}, and suggests that the median values of Hg in the rocks that were used may in fact be low – since they explain only 25% of Hg_{river} yet there is a good correlation. A perfect fit is not expected as the diverse lithologies that make up the Cordilleran orogen defy such a simple 3 component model.

4.7.3 Mercury in Sulphide Minerals

Table 4.5 and Figure 4.8 show that the mass balance results are highly sensitive to the concentration of Hg selected for pyrite. 5 $\mu g \cdot g^{-1}$ was chosen as a reasonable conservative estimate for Hg in pyrite. However, Jonasson and Boyle (1972) report the typical range of Hg concentration in pyrite to be from 0.1 to 100 $\mu g \cdot g^{-1}$ (variability of 4 orders of magnitude). They also show that pyrite (and other sulphide minerals) can

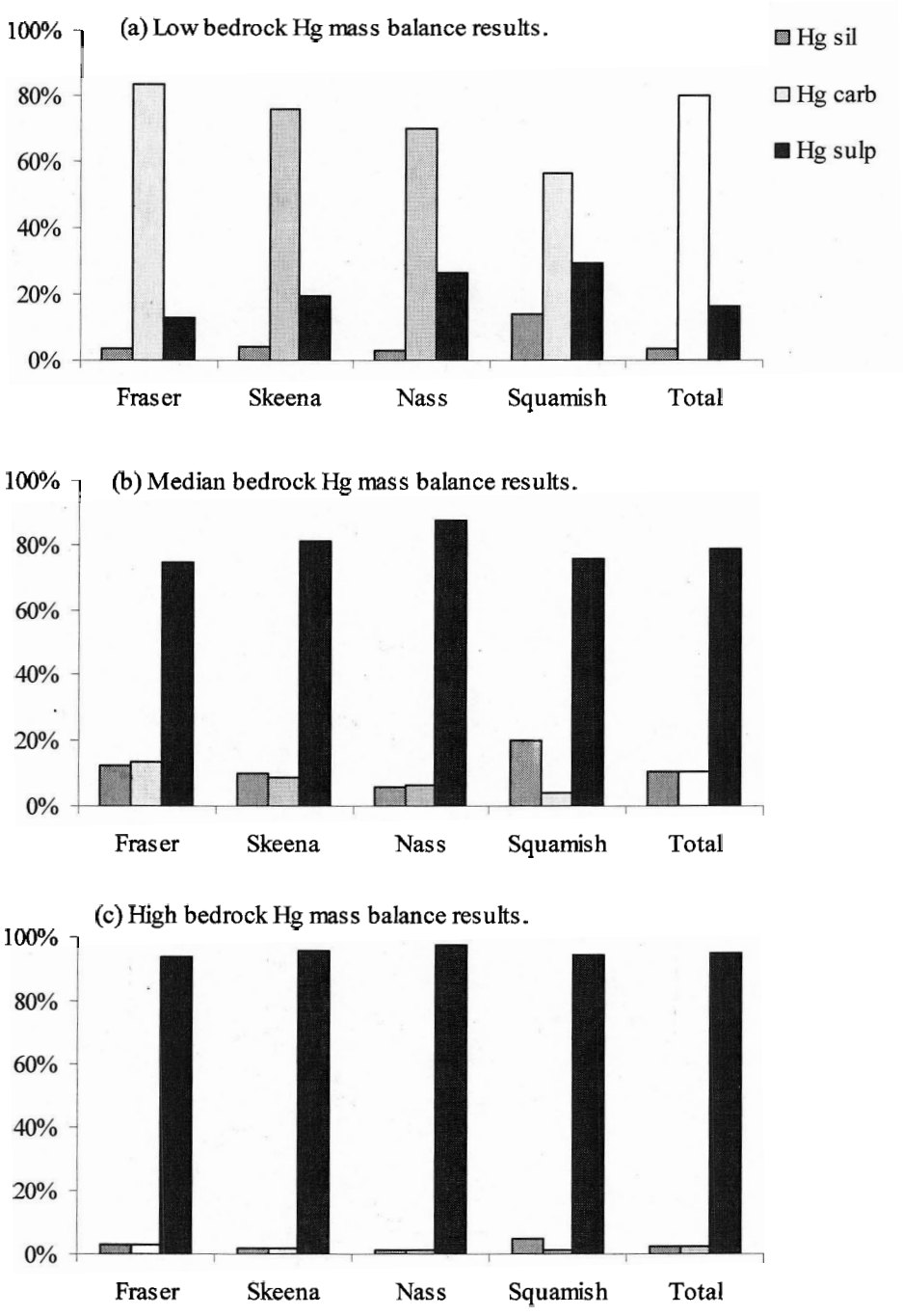

Figure 4.8 Relative contributions of silicate, carbonate and sulphide weathering to Hg_w for the mass balance calculations with low, median and high Hg concentrations in bedrock. Note that except for the low Hg results (4a) sulphide weathering dominates Hg_w.

contain much higher concentrations of Hg, up to percent levels (1% Hg being 2 orders of magnitude more concentrated than the maximum normal value of 100 $\mu g \cdot g^{-1}$). Thus the value of 5 $\mu g \cdot g^{-1}$ Hg in pyrite may in fact be too low to accurately represent the average of Cordilleran sulphides. This means that the current estimates of Hg_w may in fact be a minimum estimate of weathering derived Hg in the Cordilleran rivers, which is supported by the correlation observed in Figure 4.7.

A complication arises from the fact that it is likely for bedrock (and particularly sulphide minerals) to have highly variable Hg concentrations, considering the complex amalgamation of lithologies that make up the Cordilleran orogen. Certainly this would explain much of the scatter in the data plotted in Figure 4.7. The mass balance could be refined by obtaining accurate Hg concentrations for the bedrock in each of the Cordilleran watersheds. However, adequate characterisation of Hg concentrations in bedrock across the Fraser, Skeena and Nass watersheds would require a significant field sampling and analytical campaign. This is beyond the scope of the current study.

4.7.4 Atmospheric Deposition of Hg?

It is reasonable to assume that the Hg in the Cordilleran rivers not accounted for by Hg_w is from atmospheric deposition or from pollution within the basin. Because the anthropogenic contribution to atmospheric Hg currently far exceeds natural sources (e.g. Nriagu and Pacyna, 1988; Hylander and Meili 2003; Fitzgerald 1989) then Hg_{res} can be considered dominantly pollution Hg.

There are no major point sources of atmospheric Hg within the studied watersheds, and the closest up-wind major industrial centre is Japan. Thus the deposition of Hg from the atmosphere should be close to global background levels, and reasonably

uniform throughout the region depending on the deposition mechanism. The values of Hg_{res} as normalised to basin area (kg Hg·km^{-2}yr^{-1}) should be the same for each watershed. This is not observed in the calculated results (Table 4.5). As with the values of Hg_w, the values of Hg_{res} are subject to the variability of bedrock Hg concentrations.

It is interesting that the measured area normalized Hg export from each watershed (Table 4.3) is also highly variable. This shows that atmospheric deposition onto the watersheds is not likely to be the dominant input of Hg as observed in the rivers. This may be interpreted as an indication that atmospheric input of Hg into the watersheds is not currently coupled to the output by rivers (e.g. Lawson and Mason 2001; Mason et al., 1994). However, the rare earth element distributions within the Cordilleran rivers give strong evidence that soil formation and erosion within these watersheds is currently in steady state (chapter 3). Further evidence is given by the decrease in Hg concentration of the suspended particulate from June to October (Table 4.1). The October particulate represents alluvial soil material that has had longer exposure to atmospheric deposition, and therefore should have higher Hg concentration than the freshly exposed June particulate. The fact that the October samples have lower Hg concentrations therefore is a further indication that atmospheric deposition is not a dominant source of Hg in these watersheds.

4.8 SEASONAL VARIATIONS IN PARTICULATE MERCURY CONCENTRATIONS

The large decrease in the concentration of mineral bound Hg in the suspended particulate observed in many of the samples cannot be explained by chemical weathering processes alone. As has been described in chapter 3, there is a shift in suspended

particulate source in the Cordilleran rivers between the June and October sampling campaigns which can be explained by seasonal hydrographic changes. In June, when the hydrograph is dominated by the spring snowmelt, the suspended particulate in the rivers is likewise dominated by freshly eroded material being shed off the alpine regions of the Cordillera; while in October, the hydrograph is dominated by groundwater base flow, and suspended particulate is derived from the lowland alluvial soils.

At many of the sample locations the dry weight concentration of mineral bound Hg decreases by as much as an order of magnitude from June to October. Assuming the alluvial soils are derived from the same bedrock starting material as the freshly eroded alpine material (as indicated by rare earth element results, chapter 3), then the total Hg content of both materials should be similar. In fact, based on the conclusions of Lawson and Mason (2001) and Mason et al. (1994) (that terrestrial soils are an important sink for atmospheric Hg) the older soil material that dominates the October suspended load should have a higher concentration of Hg than the freshly eroded material, due to the longer exposure time to atmospheric deposition, however, this is not the case.

The decrease in Hg content of the October suspended material may be explained by loss of volatile Hg^0 to the atmosphere during soil evolution. A number of studies show that emission of Hg from soils, water surfaces, and from plants via transpiration, account for a significant flux of Hg to the atmosphere, and can even exceed Hg deposition rates (Kozuchowski and Johnson, 1978; Lindberg et al., 1998; Lindberg et al., 2002; Bash et al., 2004). Some recent studies have shown that transpiration by plants is an efficient mechanism for emission of Hg to the atmosphere (Lindberg et al., 1998; Lindberg et al., 2002), a process that was suggested as early as the 1970's (Kothny 1973, Kozuchowski

and Johnson 1978). A common interpretation is that Hg evasion from plants, soils and water is really re-evasion of recently deposited Hg from the atmosphere. However, Lindberg et al. (2002) show that uprooted but living (and transpiring) macrophytes in the everglades show negligible emission of Hg compared to plants with roots connected to the underlying sediment, suggesting the source of the transpired Hg is the sediment (soil).

Thus the source of this evaded Hg could be from weathering of bedrock. This implies that chemical weathering coupled with plant activity (two important soil forming processes) may provide a mechanism to transfer Hg from the lithosphere to the atmosphere. This implies during soil formation, bedrock Hg can be removed from the catchment either by erosion of soil material, or by volatilization to the atmosphere. It is likely the availability of bedrock Hg for transfer to the atmosphere will decrease with increasing landscape age. Thus young landscapes with high erosion rates providing fresh mineral surfaces could provide a significant source of Hg to the atmosphere. The fate of this Hg and how and where it is re-deposited needs further investigation.

4.9 CONCLUSIONS

The concentration and mass transport of mercury by the Fraser, Skeena, Nass and Squamish river systems have been reported based on historical hydrographic data, and samples collected in June and October 2002. The results show that a total of $11 \times 10^3 \pm 550$ kg $Hg \cdot yr^{-1}$ is delivered by these rivers to British Columbia's coastal waters, with approximately 6% of this total in labile phases: (in order of increasing importance) dissolved, adsorbed to mineral surfaces directly, or combined with organic ligands. The particulate associated labile phases of Hg may enter the dissolved phase

during transport or sedimentation, and should be considered as a potential source of Hg available to biota.

Conservative mass balance calculations show that 2.5 to 100% of the Hg flux can be accounted for by chemical weathering of bedrock within the Cordilleran watersheds. However, the strong correlation between measured chemical weathering rates and measured Hg flux rates support a contribution of Hg to the rivers by weathering of close to 100%. The mass balance results also show that pyrite oxidation is the dominant weathering source of Hg in the rivers. These results are presented here as an estimate of the magnitude of Hg release to the surface environment by chemical weathering, and cannot be better constrained without better data regarding bedrock concentrations of Hg.

Importantly, weathering of bedrock does facilitate a transfer of Hg from the lithosphere to the surface environment (hydrosphere, atmosphere, biosphere). The magnitude of this flux remains unknown, but could be significant particularly in regions where sulphide oxidation is occurring. With a comprehensive dataset of global chemical weathering rates, and of Hg concentrations in minerals, it would be possible to use the mass balance equations presented here to calculate a global rate of Hg release by chemical weathering.

4.10 REFERENCES

Anderson S. P., Drever, J. I., Frost C. D. and Holden P. (2000) Chemical weathering in the foreland of a retreating glacier. *Geochim. Cosmochim. Acta* **64,** 1173-1189.

Bash J.O., Miller D.R., Meyer T.H. and Bresnahan P.A. (2004) Northeast United States and Southeast Canada natural mercury emissions estimated with a surface emission model. *Atmospheric Environment* **Article in press.**

Benoit J.M., Mason R.P., Gilmour C.C. and Aiken G.R. (2001) Constants for mercury binding by dissolved organic matter isolates from the Florida Everglades. *Geochim. Cosmochim. Acta* **65,** 4445-4451.

Berner E. K. and Berner R. A. (1987) *The global water cycle: Geochemistry and environment*. Prentice-Hall, New Jersey.

Boggs S.Jr. (1987) Principles of Sedimentology and Stratigraphy. Merril, Ohio.

Cairns C.J., McQueen K.G. and Leah P.A. (2001) Mineralogical controls on element dispersion in regolith over two mieralised shear zones near the Peak, Cobar, New South Wales. *Journal of Geochemical Exploration* **72,** 1-21.

Canadian Food Inspection Agency (2002) *Fact Sheet – Mercury and Fish Consumption.* Canadian Food Inspection Agency (CFIA). Also available on the world wide web at: http://www.inspection.gc.ca/english/corpaffr/foodfacts/mercurye.pdf

Chan H.M., Scheuhammer A.M., Ferran A., Loupelle C., Holloway J. and Weech S. (2003) Impacts of mercury on freshwater fish-eating wildlife and humans. *Human and Ecological Risk Assessment* **9,** 867-883.

Coquery M., Cossa D. and Martin J.M. (1995) The distribution of dissolved and particulate mercury in three Siberian estuaries and adjacent arctic coastal waters. *Water Air and Soil Pollution* **80,** 653-664.

Dastoor A.P. and Larocque Y. (2004) Global circulation of atmospheric mercury: a modelling study. *Atmospheric Environment* **38,** 147-161.

D'Itri P.A. and D'Itri F.M. (1977) Mercury contamination; a human tragedy. In: *Environmental Science and Technology* (eds. R.L. Metcalf, J.N. Pitts (Jr.), W. Stumm). John Wiley and Sons, New York.

Fetter C.W. (1994) *Applied Hydrogeology*. Prentice Hall, New Jersey.

Fisheries and Oceans Canada, Statistical Services available on the world wide web at: http://www.dfo-mpo.gc.ca/communic/statistics/main_e.htm

Fitzgerald W.F. (1989) Atmospheric and oceanic cycling of mercury. In: *Chemical Oceanography*. Academic Press, New York.

Garrels R. M. and Mackenzie F. T. (1971) *Evolution of Sedimentary Rocks*. W.W. Norton & Company, New York

Hall, G.E.M. (1998) Cost-effective protocols for the collection, filtration and preservation of surface waters for detection of metals and metalloids at ppb (g/L) and ppt (ng/L) levels. In: *Aquatic Effects Technology Evaluation Program (Task Force on Water Quality Issues)*, CANMET, Ottawa, p. 123.

Hylander L.D. and Meili M. (2003) 500 years of mercury production: global annual inventory by region until 2000 and associated emissions. *The Science of the Total Environment* **304,** 13-27.

Johannessen S., Macdonald R. and Eek M. (in review) Mercury in Strait of Georgia sediments: A story of contamination and mixing. Submitted to *Environmental Science and Technology* (2004).

Jonasson I.R. and Boyle R.W. (1972) Geochemistry of mercury and origins of natural contamination of the environment. *Transactions of the Canadian Institute of Mining and Metallurgy and of the Mining Society of Nova Scotia* **75,** 8-15.

Kothny E.L. (1973) The three-phase equilibrium of mercury in nature. *Trace Elements in the Environment*, ACS**#123,** American Chemical Society.

Kozuchowski I. Johnson D.L. (1978) Gaseous emissions of mercury from an aquatic vascular plant. *Nature* **224,** 468-469.

Kraepiel A.M.L., Keller K., Chin H.B., Malcom E.G. and Morel F.M.M. (2003) Sources and variations of mercury in tuna. *Environmental Science and Technology* **37,** 5551-5558.

Kump L.R. (1989) Chemical stability of the atmosphere and ocean. *Palaeogeogr. Palaeoclimatol. Palaeoecol.* **75,** 123-136.

Langmuir D. (1997) *Aqueous Environmental Geochemistry*. Prentice Hall, New Jersey.

Lawson N.M. and Mason R.P. (2001) Concentration of mercury, methylmercury, cadmium, lead, arsenic, and selenium in the rain and stream water of two contrasting watersheds in western Maryland. *Water Research* **35,** 4039-4052.

Leitch D., Wang F., Stern G., Lemes M. and Dick T. (2004) Impacts of climate variation on mercury dynamics in the Mackenzie River and Beaufort Sea. In: *Proceedings of the 7th International Conference on Mercury as a Global Pollutant Ljubljana 2004* (Eds. M. Horvat, N. Ogrinc, J. Kotnik).

Lindberg S.E., Hanson P.J., Meyers T.P. and Kim K.H. (1998) Air/surface exchange of mercury vapor over forests – the need for a reassessment of continental biogenic emissions. *Atmospheric Environment* **32(5),** 895-908.

Lindberg S.E., Dong W. and Meyers T. (2002) Transpiration of gaseous elemental mercury through vegetation in a subtropical wetland in Florida. *Atmospheric Environment* **36,** 5207-5219.

Mason R.P., Fitzgerald W.F. and Morel F.M.M. (1994) The biogeochemical cycling of elemental mercury: Anthropogenic influences. *Geochim. Cosmochim. Acta* **58,** 31191-3198.

Milliman J.D. and Syvitski J.P.M. (1992) Geomorphic/tectonic control of sediment discharge to the ocean: The importance of small mountainous rivers. *Journal of Geology* **100,** 525-544.

Nendza M., Herbst T., Kussatz C. and Geis A. (1997) Potential for secondary poisoning and biomagnification in marine organisms. *Chemosphere* **35,** 1875-1885.

Nriagu J. (1993) Legacy of mercury pollution. *Nature* **363,** 589.

Nriagu J. and Pacyna J.M. (1988) Quantitative assessment of worldwide contamination of air, water and soils by trace metals. *Nature* **333,** 134-139.

Pirrone N., Keeler G.J. and Nriagu J. (1996) Regional differences in worldwide emissions of mercury to the atmosphere. *Atmospheric Environment* **30,** 3379.

Plouffe A. (1997) Physical partitioning of mercury in till: and example from central British Columbia, Canada. *Journal of Geochemical Exploration* **59(3),** 219-232.

Rasmussen P.E., Friske P.W.B., Azzaria L.M. and Garrett R.G. (1998) Mercury in the Canadian environment: Current research challenges. *Geoscience Canada* **25,** 1-13.

Schnitzer M. and Skinner S.I.M (1968) Alkali versus acid extraction of soil organic matter. *Soil Science* **105,** 392-396.

Scott K.M. (1986) Elemental partitioning into Mn- and Fe-oxides derived from dolomitic shale-hosted Pb—Zn deposites, northwest Queensland, Australia. *Chemical Geology* **57,** 395-414.

Seigneur C., Vijayaraghavan K., Lohman K., Karamchandani P. and Scott C. (2004) Global source attribution for mercury deposition in the United States. *Environmental Science and Technology* **38,** 555-569.

Sharp M., Creaser R.A. and Skidmore M. (2002) Strontium isotope composition of runoff from a glaciated carbonate terrain. *Geochimica et Cosmochimica Acta* **66(4),** 595-614.

Sunderland E.M. and Chmura G.L. (2000) An inventory of historical mercury emissions in Maritime Canada: implications for present and future contamination. *The Science of the Total Environment* **256,** 39-57.

Telmer K.H., Desjardins M.J. and Fergusun P. (2004) Mercury in Lake Sediments and Porewaters: Multiple Evidence for Remobilization. In: *Mercury Cycling in a Wetland-Dominated Ecosystem: A Multidisciplinary Study*. Chapter 5.

Wedepohl K.H. (1995) The composition of the continental crust. *Geochimica et Cosmochimica Acta* **59,** 217-239.

5 Conclusions

5.1 SUMMARY OF CONTRIBUTIONS

This thesis provides a new geochemical data set for the Fraser, Skeena and Nass watersheds of British Columbia, Canada, including dissolved concentrations of major elements, trace elements, rare earth elements and mercury; $\delta^{13}C$ in dissolved inorganic carbon; $\delta^{34}S$ and $\delta^{18}O$ in dissolved sulphate; and suspended particulate concentrations of rare earth elements and mercury. Interpretation of this data set provides insight into the watershed scale chemical and physical erosion processes that are important within the Canadian Cordillera, and insight into how weathering in accretionary orogens may be important globally. Important contributions of this work are:

(1) The dominant weathering processes in the Canadian Cordillera are: (i) carbonate dissolution by carbonic acid > (ii) silicate dissolution by carbonic acid ≈ (iii) carbonate dissolution by sulphuric acid derived from the oxidation of sulphides (coupled *sulphide-carbonate weathering*). DIC fluxes due to (ii) and (iii) are equivalent (~60×10^3 mol $C \cdot km^{-2} \cdot yr^{-1}$).

(2) Because coupled sulphide carbonate weathering is occurring in the Canadian Cordillera at a rate equivalent to silicate weathering by carbonic acid, and because of the long marine residence time of sulphate, it is possible for coupled sulphide carbonate weathering to provide a source of CO_2 to the atmosphere on 10^7 year timescales. Low sulphide-carbonate weathering rates in central Canada indicate that orogenic uplift, and not response to Pleistocene glaciation is the dominant control on sulphide-carbonate weathering. *Sulphide-carbonate weathering* may provide a negative feedback to tectonic uplift induced cooling.

(3) REE patterns in the dissolved and adsorbed phases (*labile REE*) of the rivers vary widely across the Cordilleran watersheds, and predictably reflect basin lithology. Main stem samples reflect mixtures of the tributaries, suggesting *labile REE* patterns are conservative in the rivers. This supports using *labile REE* as a weathering and hydrographic tracer.

(4) Consistent proportionality of the relative distribution of REE between the dissolved and adsorbed phases shows that the adsorbed REE patterns can serve as a proxy for the dissolved REE patterns and vice versa. This is important because the adsorbed REE are easier to collect and to analyse than the dissolved REE. A new method for the analysis of adsorbed REE is presented (ammonium acetate extraction followed by ICP-MS analysis).

(5) $Kd_{REE}^{ads/dis}$ values in June (high water stage, average $\approx 1 \times 10^3$) are approximately 50 times lower than $Kd_{REE}^{ads/dis}$ values in October (low water stage, average $\approx 50 \times 10^3$), indicating a change in composition and source of the suspended particulate matter from recently eroded rock flour (alpine source) in June, to older alluvial soils (valley source with a higher percentage of clay minerals) in October. This seasonal shift indicates silicate weathering is dominantly occurring in the valley regions of the watersheds, while the alpine regions have high physical erosion rates and little to no silicate weathering. Also, because ~80% of the sediment transport in these rivers occurs during the late spring to early summer, this shows that the suspended particulate budget is dominated by current uplift and erosion, not remobilization of Pleistocene glacial till. This suggests uplift and erosion in the Canadian Cordillera is approaching steady state.

(6) Annual Hg export to coastal waters by these rivers is 11 x 10^3 kg·yr^{-1}, of which 6% (650 kg·yr^{-1}) is in labile phases (dissolved < adsorbed < organic bound). Mass balance

indicates that 2.5 to 100% of this flux can be attributed to chemical weathering. However, the strong correlation between chemical weathering rates and Hg fluxes suggests that weathering is the dominant control (near to 100%) on Hg release and transport. The results also show that sulphide oxidation and Hg concentration in sulphide minerals has the greatest influence on the amount of Hg liberated by chemical weathering.

(7) As with the REE, seasonal variation in Hg concentrations and distribution exist. In June, labile Hg dominantly exists in the adsorbed phase, but dominantly in the organic bound phase in October, which indicates Hg has greater affinity to organic ligands than direct adsorption to inorganic particulate surfaces. Also, mineral bound Hg concentrations are much higher in June than October. This change in Hg concentration between the alpine and low-land derived particulate suggests that the development of soil may be cause loss of Hg to the atmosphere.

5.2 RECOMMENDATIONS FOR FUTURE WORK

(1) A detailed study of chemical and physical weathering in the Chilcotin and Blackwater watersheds (large tributaries to the Fraser River) would be useful – these adjacent systems have nearly identical bedrock geology (Eocene back-arc basalts), but have very different river chemistry and sediment fluxes. A detailed comparison weathering in these two watersheds would give insight into the factors other than lithology that control chemical weathering at temperate latitudes.

(2) Production of a standard reference material suitable for suspended river sediment. Ideally this material would include analyses of labile and refractory constituents. Such a SRM does not currently exist. This work has shown the potential for the use of labile chemistry as a geochemical tracer. The use of a common reference material for such

work would allow comparison of parallel research by other workers. As it is, without a means of "intercalibration", comparison of datasets is prone to uncertainty which is difficult to constrain.

(3) Through the course of this study, a large geochemical dataset has been collected and archived for the Canadian Cordillera. It would have been an excessively long project to study in detail every element that was analysed. This data should continue to be "mined" as necessary and used in future studies.

(4) S*ulphide-carbonate weathering* has been shown to be a key factor with respect to the (i) solute fluxes in the Cordilleran rivers, (ii) weathering induced CO_2 budgets for the region, and, (iii) Hg release by chemical weathering. *Sulphide-carbonate weathering* is difficult to quantify in rivers without using a combination of major element and stable isotope techniques (as used in chapter 2). It is possible that *sulphide-carbonate weathering* is more important than has previously been assumed in regions other than the Canadian Cordillera. Existing data-sets should be re-evaluated so that the global importance of *sulphide-carbonate weathering* can be quantified.

Appendix A. Field Station Locations and ID.

Table A.1

Station	Sample		Field ID		River / Location	Latitude	Longitude
	June	Oct	June	Oct		degrees N	degrees W
1	101	201	JSP-02-1	JSP-02-201	Squamish / Cheekeye	49.850	123.233
2	102	202	JSP-02-2	JSP-02-202	Lillooet / Pemberton	50.500	122.967
4	104	203	JSP-02-4	JSP-02-204	Cayoosh / Lillooet	50.650	121.967
5	105	--	JSP-02-5	--	Fraser / Gang Ranch	51.517	122.283
7	107	205	JSP-02-7	JSP-02-207	Chilcotin / Farwell	51.817	122.550
7	108	--	JSP-02-8	--	Chilcotin / Farwell (dup)	51.817	122.550
8	109	206	JSP-02-9	JSP-02-209	Fraser / Sheep Cr (W)	51.967	122.267
8	110	207	JSP-02-10	JSP-02-210	Fraser / Sheep Cr (E)	51.983	122.267
9	111	208	JSP-02-11	JSP-02-211	Blackwater / Blackwater crossing	53.283	123.133
10	112	209	JSP-02-12	JSP-02-212	Skeena / Hazelton	55.375	127.688
11	113	--	JSP-02-13	--	Skeena / Usk	54.983	128.350
12	114	210	JSP-02-14	JSP-02-215	Zymoetz / Terrace	54.533	128.467
13	115	211	JSP-02-16	JSP-02-216	Skeena / Terrace	54.517	128.550
13	116	212	JSP-02-17	JSP-02-217	Skeena / Terrace	54.500	128.550
14	117	--	JSP-02-18	--	Nass / Greenville	55.050	129.467
15	118	213	JSP-02-19	JSP-02-218	Nass / Canyon City	55.183	129.233
16	119	215	JSP-02-20	JSP-02-220	Nass / Meziadin	56.050	129.167
17	120	216	JSP-02-21	JSP-02-221	Bulkley / Telkwa	54.683	127.050
18	121	214	JSP-02-22	JSP-02-219	Fraser / McBride	53.300	120.133
19	122	217	JSP-02-23	JSP-02-223	Fraser / Tete Jaune	52.967	119.417
20	123	218	JSP-02-24	JSP-02-224	N. Thompson Headwaters	52.467	119.150
21	124	219	JSP-02-25	JSP-02-225	N. Thompson / McLure	51.067	120.200
23	126	221	JSP-02-27	JSP-02-227	Thompson / Spences Br	50.383	121.383
24	127	222	JSP-02-29	JSP-02-228	Fraser / Alexandra	49.700	121.400
24	128	--	JSP-02-30	--	Fraser / Alexandra	49.700	121.400

Appendix B. Analytical Results For the Cordilleran River Water and Suspended Particulate

Table B.0.1 Definitions for abbreviations:

nd	not detected
na	not analysed
ICP-MS	Direct analysis by inductively coupled plasma mass spectrometer
CHL-ICP-MS	Chelation concentration followed by analysis by ICP-MS
IC	ion chromatograph
CF-IRMS	continuous flow isotope ratio mass spectrometer
DT	Digital Titrator
Quanta-G	Quanta-G multi-meter probe

Table B.2 Physical parameters and dissolved inorganic carbon in the Cordilleran river samples (June Campaign)

	parameter	Temp	pH	DO	SpC	ORP	HCO_3^-	H_2CO_3	CO_3^{2-}	ΣDIC	pCO_2
	analytical method	QuantaG	QuantaG	QuantaG	QuantaG	QuantaG	DT	calc	calc	calc	calc
Station	Sample	°C	-log[H^+]	$mg \cdot L^{-1}$	$mS \cdot s^{-1}$	mV	$\mu mol \cdot L^{-1}$	$\mu mol \cdot L^{-1}$	$\mu mol \cdot L^{-1}$	$\mu mol \cdot L^{-1}$	mbar
1	101	7.02	5.94	12.53	0.012	335	79.9	205.4	0.0	285.4	6.06
2	102	9.29	6.77	11.84	0.035	286	234.8	89.3	0.1	324.1	2.63
4	104	7.21	7.45	13.17	0.059	233	517.5	41.1	0.7	559.3	1.21
5	105	13.6	8.31	11.2	0.094	220	1009.1	11.1	9.6	1029.8	0.33
7	107	13.74	7.86	11.5	0.060	411	586.5	18.1	2.0	606.6	0.53
7	108	14.11	7.93	12.2	0.060	386	587.5	15.5	2.3	605.3	0.46
8	109	13.19	8.2	11.55	0.090	328	1051.1	14.8	7.8	1073.7	0.44
8	110	13.3	8.25	11.7	0.091	326	1069.0	13.5	8.9	1091.4	0.40
9	111	17.77	8.41	10.33	0.104	294	1298.8	11.3	15.6	1325.8	0.33
10	112	7.08	7.69	18.13	0.048	320	445.6	20.4	1.0	467.0	0.60
11	113	7.71	8.24	18.99	0.047	303	471.6	6.1	3.8	481.5	0.18
12	114	5.93	8.64	15.62	0.037	299	417.6	2.1	8.5	428.3	0.06
13	115	8.1	8.3	15.3	0.048	293	451.6	5.1	4.2	460.9	0.15
13	116	7.5	8.44	13.22	0.044	301	447.6	3.6	5.8	457.0	0.11
14	117	7.7	7.6	13.3	0.055	290	516.5	29.0	1.0	546.5	0.86
15	118	7.55	7.79	15.1	0.059	259	539.5	19.6	1.6	560.7	0.58
16	119	6.3	7.66	19.1	0.064	332	579.5	28.4	1.2	609.1	0.84
17	120	8.28	7.86	14.6	0.039	325	407.6	12.6	1.4	421.6	0.37
18	121	9.15	8.46	14.66	0.091	307	881.2	6.8	11.9	899.9	0.20
19	122	10.1	8.95	14.12	0.100	270	1047.1	2.6	43.6	1093.3	0.08
20	123	8.45	8.31	12.84	0.052	291	473.6	5.2	4.5	483.3	0.15
21	124	10.46	7.85	13.7	0.050	280	468.6	14.8	1.6	485.0	0.44
23	126	12.51	8.29	11.81	0.061	286	611.5	7.0	5.6	624.1	0.21
24	127	12.5	8.49	12.59	0.079	279	979.1	7.1	14.2	1000.4	0.21
24	128	12.5	8.49	12.59	0.079	279	979.1	7.1	14.2	1000.4	0.21
max		17.77	8.95	19.1	0.104	411	1298.8	205.4	43.6	1325.8	6.06
min		5.93	5.94	10.33	0.012	220	79.9	2.1	0.0	285.4	0.06
median		9.15	8.24	13.17	0.059	294	539.5	12.6	4.2	560.7	0.37
mean		10.042	8.0072	13.6676	0.062	301.32	646.1	23.9	6.8	676.8	0.71
stdev		3.113721	0.626901	2.349222	0.023	40.76224	303.0	41.8	9.0	290.5	1.23

Table B.3 Physical parameters and dissolved inorganic carbon in the Cordilleran river samples (October Campaign)

parameter		Temp	pH	DO	SpC	ORP	HCO_3^-	H_2CO_3	CO_3^{2-}	ΣDIC	pCO_2
analytical method		QuantaG	QuantaG	QuantaG	QuantaG	QuantaG	DT	calc	calc	calc	calc
Station	Sample	°C	-log[H^+]	mg·L^{-1}	mS·s^{-1}	mV	µmol·L^{-1}	µmol·L^{-1}	µmol·L^{-1}	µmol·L^{-1}	mbar
1	201	8.4	6.4	11.8	0.025	224	167.0	148.9	0.0	315.9	4.4
2	202	6.9	7.0	11.6	0.067	263	991.5	232.4	0.4	1224.4	6.9
4	203	9.3	7.7	10.88	0.115	271	1039.6	48.6	2.3	1090.6	1.4
7	205	8.6	7.9	11.15	0.069	256	709.1	21.9	2.4	733.4	0.6
8	206	8.6	7.8	9.85	0.111	260	1214.7	40.2	3.8	1258.7	1.2
8	207	8.6	7.8	9.4	0.111	258	1252.1	44.4	3.7	1300.2	1.3
9	208	7.6	8.5	11.1	0.146	257	2064.5	15.7	28.5	2108.7	0.5
10	209	5.0	7.8	9.9	0.075	268	717.6	25.5	2.1	745.1	0.8
12	210	6.9	7.4	10.9	0.052	284	582.6	51.9	0.7	635.2	1.5
13	211	7.8	7.4	9.05	0.056	282	582.6	51.9	0.7	635.2	1.5
13	212	7.8	7.4	9.05	0.056	282	582.6	51.9	0.7	635.2	1.5
15	213	6.9	7.7	10.0	0.075	280	473.0	21.1	1.1	495.3	0.6
16	215	5.4	7.5	9.0	0.084	477	766.1	49.5	1.2	816.8	1.5
17	216	8.3	7.6	8.98	0.043	268	442.3	23.8	0.9	466.9	0.7
18	214	6.3	7.7	6.67	0.099	259	905.1	45.4	1.9	952.3	1.3
19	217	6.8	7.7	6.3	0.117	267	1204.4	55.1	2.8	1262.2	1.6
20	218	5.3	7.6	5.71	0.073	257	673.5	35.3	1.3	710.2	1.0
21	219	10.9	7.8	5.93	0.069	268	696.2	26.5	1.9	724.6	0.8
23	221	13.4	8.0	4.5	0.077	260	791.1	17.7	3.7	812.5	0.5
24	222	10.2	8.0	4.75	0.102	272	1126.5	26.4	5.0	1157.9	0.8
max		13.4	8.5	11.80	0.146	477.0	2064.5	232.4	28.5	2108.7	6.9
min		5.0	6.4	4.50	0.025	224.0	167.0	15.7	0.0	315.9	0.5
median		7.8	7.7	9.23	0.075	267.5	741.8	42.3	1.9	778.8	1.2
mean		7.9	7.6	8.83	0.081	275.7	849.1	51.7	3.3	904.1	1.5
stdev		2.0	0.4	2.34	0.030	49.2	405.4	51.1	6.1	405.7	1.5

Table B.4 Dissolved cations and anions for the Cordilleran rivers (June Campaign).

	parameter	Na^+	K^+	Mg^{2+}	Ca^{2+}	F^-	Cl^-	SO_4^{2-}	NO_3^-
	analytical method	IC	IC	IC	IC	IC	IC	IC	IC
Station	Sample	$\mu mol \cdot L^{-1}$	$\mu mol \cdot L^{-1}$	$\mu mol \cdot L^{-1}$	$\mu mol \cdot L^{-1}$	$\mu mol \cdot L^{-1}$	$\mu mol \cdot L^{-1}$	$\mu mol \cdot L^{-1}$	$\mu mol \cdot L^{-1}$
1	101	22.2	11.9	12.6	35.4	1.0	8.5	10.8	3.2
2	102	51.8	25.6	28.7	120.5	2.4	14.2	54.9	4.5
4	104	47.1	24.8	50.3	257.2	3.6	16.3	67.0	4.5
5	105	69.8	17.8	126.4	429.1	2.2	13.2	54.7	6.0
7	107	87.2	24.4	84.0	227.9	2.6	7.5	71.2	0.0
7	108	88.8	25.7	83.1	226.4	2.6	8.6	69.9	0.0
8	109	61.8	15.0	119.8	429.6	2.3	11.0	52.1	6.0
8	110	61.0	15.3	119.6	421.6	2.1	11.7	55.9	5.7
9	111	213.3	63.5		317.1	5.1	10.0	12.7	0.0
10	112	43.4	9.2	55.7	210.6	1.6	4.1	55.0	3.3
11	113	43.5	10.5	52.5	201.3	1.9	4.5	48.9	3.3
12	114	33.3	10.6	33.3	167.2	1.5	4.5	18.1	2.8
13	115	44.7	11.9	54.6	212.8	1.9	4.8	47.5	3.1
13	116	47.6	11.9	45.7	199.8	4.3	14.7	34.6	3.7
14	117	43.1	13.9	74.1	237.7	1.8	5.4	67.4	4.6
15	118	44.3	10.0	76.7	249.7	1.7	5.3	75.5	5.3
16	119	44.4	8.6	84.9	275.1	1.7	3.7	89.4	5.1
17	120	44.4	11.5	41.0	178.2	1.6	6.0	27.4	2.1
18	121	25.8	14.7	144.8	412.7	1.9	6.1	123.1	5.4
19	122	28.7	8.2	205.8	435.9	2.0	9.8	119.8	5.1
20	123	16.4	26.5	46.1	247.5	1.6	3.7	66.4	10.2
21	124	37.8	20.0	53.1	228.6	2.5	5.8	45.5	7.1
23	126	69.9	24.4	71.4	262.9	2.7	14.4	53.1	5.6
24	127	59.0	19.0	96.2	366.8	2.4	11.1	56.3	4.8
24	128	61.0	19.7	97.9	379.3	2.2	11.9	55.2	7.8
max		213.3	63.5	205.8	435.9	5.1	16.3	123.1	10.2
min		16.4	8.2	12.6	35.4	1.0	3.7	10.8	0.0
median		44.7	15.0	72.8	247.5	2.1	8.5	55.0	4.6
mean		55.6	18.2	77.4	269.2	2.3	8.7	57.3	4.4
stdev		37.5	11.2	43.1	105.2	0.9	4.0	27.2	2.4

Table B.5 Dissolved cations and anions for the Cordilleran rivers (October Campaign).

parameter		Na^+	K^+	Mg^{2+}	Ca^{2+}	F^-	Cl^-	SO_4^{2-}	NO_3^-
analytical method		IC	IC	IC	IC	IC	IC	IC	IC
Station	Sample	$\mu mol \cdot L^{-1}$	$\mu mol \cdot L^{-1}$	$\mu mol \cdot L^{-1}$	$\mu mol \cdot L^{-1}$	$\mu mol \cdot L^{-1}$	$\mu mol \cdot L^{-1}$	$\mu mol \cdot L^{-1}$	$\mu mol \cdot L^{-1}$
1	201	56.4	14.3	nd	74.6	0.8	31.8	31.2	2.2
2	202	134.1	27.7	42.6	198.5	2.4	56.2	126.4	nd
4	203	67.7	22.2	101.0	468.5	4.2	19.6	225.7	2.1
7	205	100.7	19.2	99.3	214.8	1.7	7.6	64.8	0.0
8	206	82.9	8.8	152.6	423.9	1.2	62.0	93.4	3.7
8	207	84.1	10.7	151.1	421.9	1.2	17.6	92.9	3.7
9	208	236.3	53.6	376.7	373.8	5.3	9.6	18.7	nd
12	210	38.5	7.3	31.6	215.3	1.0	4.1	38.8	1.9
13	211	44.1	6.9	42.4	220.5	1.0	5.1	46.4	2.4
13	212	44.6	7.0	41.7	221.6	1.2	6.1	56.4	2.4
16	215	31.1	10.1	150.1	371.0	1.3	6.6	171.2	5.4
17	216	53.1	5.8	109.7	291.1	1.3	4.1	140.0	5.5
18	214	38.5	7.4	26.8	169.3	0.9	5.6	38.7	nd
19	217	32.8	5.1	225.7	407.2	1.6	60.8	165.9	4.6
20	218	20.9	25.8	58.2	291.9	1.2	2.6	107.4	6.5
21	219	44.8	18.4	61.1	259.6	2.1	6.7	67.4	4.5
23	221	89.3	20.4	80.7	276.6	2.2	22.3	84.9	3.9
24	222	83.2	12.9	129.2	383.6	1.4	17.3	81.0	3.8
max		236.3	53.6	376.7	468.5	5.3	62.0	225.7	6.5
min		20.9	5.1	26.8	74.6	0.8	2.6	18.7	0.0
median		54.8	11.8	99.3	283.9	1.3	8.6	83.0	3.7
mean		71.3	15.8	110.6	293.5	1.8	19.2	91.7	3.5
stdev		50.5	11.8	87.7	106.9	1.2	20.2	55.8	1.7

Table B.6 Stable light isotopes (dissolved) for the Cordilleran river samples (June campaign).

	paramter	δD_{H2O}	$\delta^{18}O_{H2O}$	$\delta^{13}C_{DIC}$	$\delta^{34}S_{SO4}$	$\delta^{18}O_{SO4}$
	analytical method	cf-irms	cf-irms	cf-irms	cf-irms	cf-irms
Station	Sample	‰$_{VSMOW}$	‰$_{VSMOW}$	‰$_{VPDB}$	‰$_{CDT}$	‰$_{VSMOW}$
1	101	-124.5	-16.6	-9.8	na	na
2	102	-138.5	-19.0	-7.1	na	na
4	104	-141.3	-18.7	-5.9	na	na
5	105	-146.2	-18.7	-7.6	na	na
7	107	-146.8	-18.6	-5.9	na	na
7	108	-146.8	-18.5	-5.9	na	na
8	109	-147.4	-18.5	-7.5	na	na
8	110	-146.6	-19.0	-7.7	na	na
9	111	-140.7	-17.6	-9.0	na	na
10	112	-152.8	-20.3	-6.8	na	na
11	113	-152.2	-22.3	-7.1	na	na
12	114	-143.6	-22.4	-7.1	na	na
13	115	-150.0	-19.8	-6.7	na	na
13	116	-147.0	-19.4	-7.8	na	na
14	117	-145.7	-19.6	-7.3	na	na
15	118	-148.0	-19.9	-6.2	na	na
16	119	-149.9	-19.4	-6.2	na	na
17	120	-142.2	-18.5	-8.0	na	na
18	121	-156.3	-20.2	-6.1	na	na
19	122	-157.7	-20.8	-5.5	na	na
20	123	-153.9	-20.2	-5.2	na	na
21	124	-146.9	-19.5	-6.0	na	na
23	126	-139.0	-21.3	-6.5	na	na
24	127	-145.0	-18.9	-7.4	na	na
24	128	-143.9	-19.1	-7.3	na	na
max		-124.5	-16.6	-5.2		
min		-157.7	-22.4	-9.8		
median		-146.8	-19.4	-7.1		
mean		-146.1	-19.5	-7.0		
stdev		6.7	1.3	1.1		

Table B.7 Stable light isotopes (dissolved) for the Cordilleran river samples (October campaign).

	paramter	δD_{H2O}	$\delta^{18}O_{H2O}$	$\delta^{13}C_{DIC}$	$\delta^{34}S_{SO4}$	$\delta^{18}O_{SO4}$
	analytical method	cf-irms	cf-irms	cf-irms	cf-irms	cf-irms
Station	Sample	‰$_{VSMOW}$	‰$_{VSMOW}$	‰$_{VPDB}$	‰$_{CDT}$	‰$_{VSMOW}$
1	201	-114.0	-15.6	-5.9	3.2	na
2	202	-123.1	-17.0	-4.1	1.6	-4.2
4	203	-132.7	-17.9	-3.7	-8.9	-2.5
7	205	-137.5	-18.0	-4.3	-2.2	-2.9
8	206	-133.8	-17.5	-6.6	7.5	-2.0
8	207	-135.0	-17.2	-6.4	7.8	-6.7
9	208	-137.6	-16.7	-8.0	8.0	na
10	209	-136.1	-18.0	-4.8	-5.0	-10.3
12	210	-124.2	-16.3	-5.1	1.6	-3.6
13	211	-121.6	-16.2	-4.9	-2.8	-7.7
13	212	-122.1	-16.8	-5.3	-2.7	-4.4
15	213	-120.3	-16.0	-6.0	-4.0	-3.5
16	215	-135.6	-18.0	-4.8	-4.7	-8.8
17	216	-135.2	-17.6	-5.2	-0.3	na
18	214	-143.2	-18.8	-4.7	9.2	-5.6
19	217	-150.6	-19.7	-4.5	13.5	-7.1
20	218	-138.6	-18.4	-4.4	14.1	1.2
21	219	-141.9	-18.6	-4.6	9.5	2.7
23	221	-138.0	-18.0	-5.9	4.0	-4.6
24	222	-134.8	-17.5	-6.8	5.4	-5.1
max		-114.0	-15.6	-3.7	14.1	2.7
min		-150.6	-19.7	-8.0	-8.9	-10.3
median		-135.1	-17.5	-5.0	2.4	-4.4
mean		-132.8	-17.5	-5.3	2.7	-4.4
stdev		9.1	1.0	1.1	6.5	3.3

Table B.8 Dissolved trace elements (1) Cordilleran river samples, June campaign. Results in ppb.

		Li	B	Mg	Al	Si	P	Ca	Sc	Ti	V	Cr	Mn	Fe	Co
Station	Sample	icp-ms	icp-ms	icp-ms	icp-ms	icp-ms	icp-ms	icp-ms	icp-ms	icp-ms	icp-ms	icp-ms	icp-ms	icp-ms	icp-ms
1	101	0.81	1.53	165	71.0	882	nd	1297	0.21	4.84	0.21	0.04	3.49	49.6	0.05
2	102	2.91	3.65	726	90.7	1913	nd	4660	0.44	8.07	0.35	0.09	16.47	90.9	0.13
4	104	1.17	3.29	1246	58.7	1739	nd	8963	0.42	3.11	0.21	0.09	9.53	92.2	0.14
5	105	1.43	6.08	3366	35.2	1671	nd	15688	0.39	nd	0.25	0.08	2.75	72.3	0.08
7	107	0.83	13.50	2338	81.0	2170	nd	8026	0.48	5.15	0.62	0.20	5.52	89.1	0.08
7	108	0.91	12.72	2259	94.6	2361	nd	10832	0.52	8.03	0.51	0.09	5.51	108.0	0.09
8	109	1.46	4.68	3305	59.1	1619	nd	20113	0.38	4.44	0.28	0.11	8.18	117.8	0.14
8	110	1.56	4.29	3205	84.0	1653	nd	19786	0.34	5.00	0.34	0.08	9.76	135.2	0.18
9	111	2.32	6.61	6980	20.8	7252	nd	14589	1.41	3.98	0.87	0.12	6.95	130.9	0.05
10	112	0.75	3.45	1488	122.2	1621	nd	12036	0.36	3.66	0.25	0.09	15.59	150.5	0.20
11	113	0.73	3.32	1403	131.5	1765	nd	11954	0.39	3.00	0.28	0.11	18.21	143.2	0.19
12	114	0.39	1.47	816	74.3	1501	nd	10853	0.32	2.60	0.31	nd	18.55	64.8	0.05
13	115	1.05	3.46	1502	251.2	1970	nd	12789	0.45	7.23	0.44	0.11	23.52	223.5	0.25
13	116	0.59	1.61	1244	31.4	1590	nd	9819	0.36	1.54	0.23	0.10	14.69	50.0	0.08
14	117	1.62	1.24	1660	175.3	1266	nd	9754	0.26	6.21	0.38	0.31	27.99	237.0	0.47
15	118	1.33	1.56	2332	67.2	1368	nd	11706	0.30	2.56	0.18	0.13	12.63	117.1	0.18
16	119	1.43	1.76	2580	70.3	1455	nd	12639	0.31	1.86	0.17	nd	12.04	125.3	0.19
17	120	0.37	0.59	1195	59.9	1732	nd	7388	0.41	2.66	0.28	nd	14.35	90.6	0.07
18	121	4.02	nd	3696	52.6	1222	nd	16206	0.19	4.29	0.08	nd	11.07	88.1	0.21
19	122	2.68	1.65	4509	58.1	738	nd	15233	0.20	1.89	0.03	nd	1.11	55.5	0.06
20	123	2.12	nd	1044	32.0	1064	nd	8108	0.19	2.55	0.04	nd	3.72	51.8	0.12
21	124	1.57	0.44	1270	47.1	1407	nd	7999	0.33	3.69	0.12	nd	3.00	59.3	0.08
23	126	1.51	0.77	1635	36.4	1770	nd	9461	0.33	3.39	0.19	0.10	2.91	50.2	nd
24	127	1.45	1.56	2385	69.6	1519	nd	13890	0.34	5.21	0.29	0.12	5.11	87.2	0.10
24	128	1.46	1.45	1914	20.3	1414	nd	11841	0.20	1.42	0.19	nd	2.87	26.8	0.05
max		4.02	13.50	6980	251.2	7252		20113	1.41	8.07	0.87	0.31	27.99	237.0	0.47
min		0.37	0.44	165	20.3	738		1297	0.19	1.42	0.03	0.04	1.11	26.8	0.05
median		1.43	1.76	1660	67.2	1619		11706	0.34	3.68	0.25	0.10	9.53	90.6	0.11
mean		1.46	3.51	2170	75.8	1786		11425	0.38	4.02	0.28	0.12	10.22	100.3	0.14
stdev		0.84	3.46	1440	51.0	1195		4263	0.23	1.92	0.18	0.06	7.11	51.4	0.09

Table B.9 Dissolved trace elements (2) Cordilleran river samples, June campaign. Results in ppb.

		Ni	Cu	Zn	Ga	Ge	As	Se	Rb	Sr	Y	Zr	Mo	Ag	Sb
Station	Sample	icp-ms	icp-ms	icp-ms	icp-ms	icp-ms	icp-ms	icp-ms	icp-ms	icp-ms	icp-ms	icp-ms	icp-ms	icp-ms	icp-ms
1	101	nd	0.74	nd	0.016	nd	0.07	nd	0.50	7.7	0.048	0.008	0.178	nd	nd
2	102	0.21	1.37	0.2	0.029	nd	0.16	nd	0.92	28.0	0.113	0.020	0.995	nd	0.0
4	104	0.55	0.67	nd	0.019	nd	1.69	nd	0.39	54.3	0.094	0.038	1.053	nd	0.1
5	105	0.66	1.24	nd	0.003	nd	0.26	nd	0.54	82.3	0.081	0.086	0.671	nd	0.0
7	107	0.42	1.12	nd	0.028	nd	0.31	nd	0.66	49.8	0.058	0.074	0.988	nd	0.1
7	108	0.29	0.94	nd	0.039	nd	0.38	nd	0.63	50.3	0.076	0.085	0.994	nd	0.1
8	109	0.66	1.21	nd	0.013	nd	0.22	nd	0.51	82.1	0.132	0.114	0.596	nd	0.0
8	110	0.72	1.37	nd	0.012	nd	0.25	nd	0.57	79.9	0.143	0.197	0.608	nd	0.0
9	111	0.98	0.79	nd	nd	nd	0.58	nd	1.76	62.4	0.106	0.237	0.785	nd	0.0
10	112	0.58	1.87	nd	0.011	nd	0.21	nd	0.25	60.8	0.181	0.076	0.436	nd	0.1
11	113	0.34	1.46	nd	0.019	nd	0.23	nd	0.26	56.6	0.199	0.074	0.529	nd	0.0
12	114	nd	0.98	nd	0.021	nd	0.19	nd	0.34	32.4	0.179	0.036	0.457	nd	0.0
13	115	0.34	1.73	nd	0.062	nd	0.33	nd	0.40	59.7	0.278	0.104	0.510	nd	0.0
13	116	0.27	1.12	nd	0.017	nd	0.18	nd	0.34	53.9	0.162	0.045	0.470	nd	0.0
14	117	1.63	1.81	0.7	0.060	nd	0.29	nd	0.39	81.5	0.298	0.028	0.564	nd	0.1
15	118	0.91	0.79	nd	0.052	nd	0.27	nd	0.22	93.0	0.094	0.025	0.566	nd	0.1
16	119	0.79	0.80	nd	0.021	nd	0.17	nd	0.10	88.1	0.125	0.019	0.625	nd	0.1
17	120	0.32	1.18	nd	0.032	nd	0.21	nd	0.28	33.4	0.208	0.059	0.279	nd	0.0
18	121	1.31	0.73	nd	0.004	nd	0.10	nd	1.20	115.4	0.146	0.076	0.070	nd	nd
19	122	1.10	0.40	nd	0.012	nd	0.04	nd	0.16	108.1	0.156	0.013	0.047	nd	nd
20	123	0.76	0.47	nd	nd	nd	nd	nd	2.36	55.4	0.098	nd	0.130	nd	nd
21	124	0.65	0.48	nd	0.009	nd	0.06	nd	1.15	52.7	0.103	0.042	0.717	nd	0.0
23	126	0.49	0.71	nd	0.012	nd	0.08	nd	1.14	65.9	0.100	0.056	0.622	nd	nd
24	127	0.72	1.13	nd	0.016	nd	0.20	nd	0.65	70.6	0.110	0.059	0.561	nd	0.0
24	128	0.53	0.98	nd	0.005	nd	0.17	nd	0.58	70.5	0.075	0.032	0.499	nd	0.0
max		1.63	1.87	0.7	0.062		1.69		2.36	115.4	0.30	0.237	1.053		0.1
min		0.21	0.40	0.2	0.003		0.04		0.10	7.7	0.05	0.008	0.047		0.0
median		0.65	0.98	0.5	0.017		0.21		0.51	60.8	0.11	0.058	0.564		0.0
mean		0.66	1.04	0.5	0.022		0.28		0.65	63.8	0.13	0.067	0.558		0.0
stdev		0.35	0.41	0.3	0.017		0.32		0.53	24.7	0.06	0.055	0.278		0.0

Table B.10 Dissolved trace elements (3) Cordilleran river samples, June campaign. Results in ppb.

		Cd	Sn	Cs	Ba	La	Ce	Pr	Nd	Sm	Eu	Gd	Dy	Ho	Er
Station	Sample	icp-ms	icp-ms	icp-ms	icp-ms	icp-ms	icp-ms	icp-ms	icp-ms	icp-ms	icp-ms	icp-ms	icp-ms	icp-ms	icp-ms
1	101	nd	nd	nd	3.37	0.045	0.077	0.014	0.057	0.011	nd	nd	0.012	0.009	0.014
2	102	nd	nd	0.020	10.42	0.070	0.129	0.017	0.108	0.030	nd	0.042	0.023	0.007	0.018
4	104	nd	nd	nd	9.12	0.041	0.068	0.013	0.072	0.020	nd	0.036	0.024	0.004	0.014
5	105	nd	nd	nd	12.39	0.055	0.076	0.015	0.065	0.013	nd	nd	0.016	0.008	0.011
7	107	nd	nd	nd	6.83	0.037	0.088	0.011	0.064	0.019	nd	nd	0.018	0.004	0.013
7	108	nd	nd	nd	6.61	0.044	0.093	0.014	0.065	0.012	nd	0.029	0.018	0.005	0.009
8	109	nd	nd	nd	11.79	0.102	0.202	0.027	0.121	0.031	0.007	0.064	0.028	0.008	0.016
8	110	nd	nd	0.010	12.74	0.134	0.248	0.037	0.160	0.029	0.007	0.068	0.039	0.010	0.019
9	111	nd	nd	nd	7.69	0.045	0.056	0.013	0.051	0.016	nd	0.035	0.020	0.008	0.015
10	112	nd	nd	0.013	11.92	0.092	0.176	0.028	0.149	0.051	0.015	0.095	0.037	0.017	0.029
11	113	nd	nd	0.020	13.95	0.086	0.166	0.031	0.160	0.045	0.012	0.079	0.052	0.015	0.027
12	114	nd	nd	0.011	16.61	0.068	0.120	0.021	0.108	0.030	0.008	0.058	0.039	0.014	0.030
13	115	nd	nd	0.033	16.51	0.143	0.273	0.043	0.185	0.072	0.020	0.127	0.067	0.018	0.030
13	116	nd	nd	nd	16.03	0.057	0.076	0.015	0.058	0.023	0.014	0.051	0.027	0.009	0.023
14	117	nd	nd	0.028	26.47	0.153	0.330	0.043	0.219	0.070	0.059	0.161	0.074	0.021	0.043
15	118	nd	nd	0.009	19.98	0.037	0.084	0.015	0.058	0.016	0.019	0.025	0.022	0.007	0.017
16	119	nd	nd	0.013	24.65	0.053	0.094	0.021	0.080	0.017	0.024	0.059	0.027	0.009	0.014
17	120	nd	nd	nd	14.54	0.086	0.123	0.029	0.128	0.032	0.015	0.056	0.039	0.010	0.026
18	121	nd	nd	nd	6.26	0.199	0.266	0.042	0.160	0.030	0.013	0.061	0.034	0.009	0.020
19	122	nd	nd	nd	7.94	0.259	0.260	0.060	0.263	0.048	0.016	0.071	0.032	0.010	0.014
20	123	nd	nd	0.029	3.81	0.124	0.146	0.028	0.106	0.029	0.012	0.064	0.015	0.007	0.016
21	124	nd	nd	0.014	5.25	0.107	0.122	0.022	0.109	0.026	0.026	0.043	0.024	0.010	0.020
23	126	nd	nd	nd	7.16	0.083	0.125	0.021	0.070	0.009	0.010	0.038	0.019	0.007	0.009
24	127	nd	nd	nd	10.71	0.085	0.123	0.018	0.065	0.023	0.010	0.036	0.023	0.008	0.022
24	128	nd	nd	nd	9.57	0.037	0.066	0.012	0.034	0.008	0.005	0.028	0.014	0.005	0.007
max				0.033	26.47	0.259	0.330	0.060	0.263	0.072	0.059	0.161	0.074	0.021	0.043
min				0.009	3.37	0.037	0.056	0.011	0.034	0.008	0.005	0.025	0.012	0.004	0.007
median				0.014	10.71	0.083	0.123	0.021	0.106	0.026	0.014	0.057	0.024	0.009	0.017
mean				0.018	11.69	0.090	0.143	0.024	0.109	0.028	0.016	0.060	0.030	0.010	0.019
stdev				0.009	5.96	0.055	0.077	0.012	0.058	0.017	0.012	0.033	0.016	0.004	0.008

Table B.11 Dissolved trace elements (4) Cordilleran river samples, June campaign. Results in ppb.

		Tm	Yb	Lu	Hf	Ta	W	Au	Hg	Tl	Pb	Th	U
Station	Sample	icp-ms	icp-ms	icp-ms	icp-ms	icp-ms	icp-ms	icp-ms	icp-ms	icp-ms	icp-ms	icp-ms	icp-ms
1	101	0.002	0.011	nd	nd	nd	nd	nd	nd	0.002	nd	0.007	0.033
2	102	0.002	0.019	nd	nd	nd	nd	nd	nd	0.003	0.121	nd	0.039
4	104	0.001	0.020	0.010	nd	nd	nd	nd	nd	0.004	0.022	nd	0.113
5	105	0.001	0.010	nd	nd	nd	nd	nd	nd	0.004	0.010	0.019	0.200
7	107	0.001	0.005	0.008	nd	nd	nd	nd	nd	0.021	0.066	nd	0.092
7	108	0.001	0.014	nd	nd	nd	nd	nd	nd	0.002	0.024	0.008	0.098
8	109	0.003	0.016	nd	0.002	nd	nd	nd	nd	0.003	0.082	0.034	0.172
8	110	0.003	0.016	nd	nd	nd	nd	nd	nd	0.003	0.132	0.036	0.170
9	111	0.002	0.012	nd	0.007	nd	nd	nd	nd	0.001	nd	0.006	0.109
10	112	0.003	0.024	nd	0.002	nd	nd	nd	nd	nd	0.183	0.005	0.025
11	113	0.003	0.027	nd	nd	nd	nd	nd	nd	nd	0.084	0.007	0.036
12	114	0.003	0.031	nd	nd	nd	nd	nd	nd	nd	0.029	nd	0.035
13	115	0.004	0.027	nd	0.016	nd	nd	nd	nd	0.001	0.203	0.024	0.037
13	116	0.001	0.018	0.030	nd	nd	nd	nd	nd	0.004	0.023	0.002	0.035
14	117	0.005	0.030	nd	0.004	nd	nd	nd	nd	0.001	0.265	0.013	0.048
15	118	0.002	nd	nd	nd	nd	nd	nd	nd	nd	0.056	0.003	0.020
16	119	0.001	nd	nd	nd	nd	nd	0.0	nd	nd	0.054	0.002	0.019
17	120	0.003	0.017	0.016	nd	nd	nd	nd	nd	nd	0.025	0.004	0.022
18	121	0.001	nd	0.034	0.003	nd	nd	nd	nd	0.001	0.108	0.026	0.401
19	122	0.002	nd	nd	nd	nd	nd	nd	nd	nd	0.039	0.029	0.351
20	123	nd	nd	nd	nd	nd	nd	nd	nd	0.001	0.015	0.025	0.113
21	124	0.003	nd	0.034	0.004	nd	nd	nd	nd	0.002	0.036	0.030	0.229
23	126	0.002	nd	nd	nd	nd	nd	nd	nd	0.004	0.030	0.021	0.267
24	127	0.002	nd	nd	0.009	nd	nd	nd	nd	0.010	0.057	0.034	0.245
24	128	nd	nd	nd	nd	nd	nd	nd	nd	0.003	nd	0.020	0.252
max		0.005	0.031	0.034	0.016					0.021	0.265	0.036	0.401
min		0.001	0.005	0.008	0.002					0.001	0.010	0.002	0.019
median		0.002	0.018	0.023	0.004					0.003	0.055	0.019	0.098
mean		0.002	0.019	0.022	0.006					0.004	0.076	0.017	0.126
stdev		0.001	0.007	0.012	0.005					0.005	0.068	0.012	0.111

Appendix C. Hydrometric Data

Table C.1 Environment Canada Gauging Stations.

Station ID	Gauging Station Name (River and Location)	Lat	Long	Gross Drainage	n	status
Fraser and Tributaries		deg. N	deg. W	km^2		
08MF005	Fraser at Hope	49.38	121.45	217000	92	a
08MD013	Fraser at Big Bar Cr.	51.19	122.13	146000	38	d
08MC018	Fraser at Marguerite	52.53	122.44	114000	54	a
08KA005	Fraser at McBride	53.29	120.11	6890	51	a
08KA007	Fraser at Red Pass	52.98	119.00	1700	49	a
08LF051	Thompson near Spences Bridge	50.36	121.39	54900	53	a
08LB064	North Thompson at McLure	51.04	120.24	19600	46	a
08MB005	Chilcotin Below Big Creek	51.85	122.65	19300	34	a
08KG001	West-Road (Blackwater) near Cinema	53.31	122.89	12400	52	a
08MG005	Lilloet at Pemberton Meadows	50.34	122.8	2160	85	a
08ME002	Cayoosh Cr. Near Lillooet	50.67	121.96	878	58	a
Skeena and Tributaries						
08EF001	Skeena at Usk	54.63	128.43	42200	72	a
08EB003	Skeena River at Glen Vowell	55.30	127.67	25900	28	d
08EE004	Bulkley at Quick	54.62	126.90	7360	74	a
08EF005	Zymoetz Above OK Creek	54.48	128.33	2980	41	a
Nass						
08DB001	Nass above Shumal Creek	55.26	129.09	18500	69	a
Squamish						
08GA022	Squamish Near Brackendale	49.79	123.20	2330	53	a

a = active
d = discontinued
n = number of years of data collection

Table C.2 Mean monthly discharge 2002 ($m^3 \cdot s^{-1}$)

Station ID	Jan	Feb	Mar	Apr	May	Jun	Jul	Aug	Sep	Oct	Nov	Dec	mean
08MF005	922	719	576	1800	5490	9300	6740	2960	2330	2160	1300	863	2930
08MC018	350	298	264	1140	2820	4500	3060	1530	1390	1410	824	468	1500
08KA005	33.5	26.5	22.3	43.2	136	732	549	260	213	135	71.1	50	189
08KA007	6.87	5.49	4.77	5.58	25	197	131	50.8	41.6	25.1	12	8.14	42.8
08LF051	268	232	205	357	1290	2650	2020	830	504	348	248	228	765
08LB064	112	86.4	65.6	212	882	1620	1020	370	277	188	112	90.5	420
08MB005	24.9	21.3	18.4	29.4	65	238	264	193	128	58	31.2	21.1	91
08KG001	11.2	12.3	11	35.2	120	76.1	28.7	15.5	15.8	16.5	14.8	13.2	30.9
08MG005	45	24.9	20.3	63.5	130	321	302	202	128	49.6	43.5	34.2	114
08ME002	1.32	1.25	1.24	1.23	10.4	56.1	30.4	2.61	3.19	1.7	1.31	1.25	9.33
08EF001	179	148	136	310	1970	4060	1920	968	1190	859	517	316	1050
08EE004	33.9	26.8	21.7	61.3	394	617	313	148	139	103	81	74.5	168
08EF005	25.2	15.1	10.5	35.5	229	450	228	123	169	105	107	36.2	128
08DB001	131	105	103	197	1290	2590	1640	1310	1250	722	379	208	827
08GA022	156	60.3	41.3	150	279	545	493	326	235	80.9	180	117	222

Table C.3 Historical mean monthly discharge ($m^3 \cdot s^{-1}$)

Station ID	Jan	Feb	Mar	Apr	May	Jun	Jul	Aug	Sep	Oct	Nov	Dec	mean
08MF005	923	866	858	1800	4900	7000	5560	3560	2370	1930	1590	1110	2710
08MD013	551	520	519	1220	2980	3940	3070	2090	1520	1310	1030	722	1520
08MC018	437	419	464	1230	2820	3460	2730	1800	1280	1130	876	536	1400
08KA005	33.8	30.6	31.9	59.8	242	570	542	373	209	128	76	46.7	196
08KA007	7.24	5.97	5.31	7.72	56.4	153	133	80.1	46.1	28.1	15.5	9.67	45.7
08LF051	238	220	224	390	1400	2320	1770	991	626	471	405	301	780
08LB064	89	82.5	93.9	234	883	1340	937	548	349	260	196	117	427
08MB005	28.3	27	28.2	42.3	96.7	208	260	230	132	77.5	49.9	33.1	101
08KG001	11.8	11.8	14.3	56.8	109	68.5	46.9	27.1	20.7	19.4	18	13.2	32.6
08MG005	32.6	30.5	33.1	58.7	154	276	310	260	154	94.6	57.7	39.2	124
08ME002	4.3	3.9	4.1	6.8	26.3	52.8	40.6	16.3	8.3	6.5	5.9	4.9	14.9
08EF001	194	169	159	420	1890	2840	1750	957	756	836	532	282	911
08EB003	108	97.2	86.9	191	1090	1960	1280	682	542	591	287	142	588
08EE004	38.9	31.2	28.2	79.8	305	368	233	146	103	111	102	61	134
08EF005	26.4	22.3	22.4	52.1	197	295	199	126	103	115	66.3	35.6	105
08DB001	147	135	130	346	1270	2070	1670	1180	874	828	440	209	776
08GA022	92.1	91.7	90.2	139	309	470	492	405	270	220	163	111	237

Appendix D. Rare Earth Element Concentration System Program Details for AIM1250 Autosampler and Dionex GP50 Gradient Pump

Table D.1 Relay definitions for AIM1250.

	closed	**opened**
Relay A	Turn GP50 on	Turn GP50 off
Relay B	Start GP50 Program	Reset GP50 program
Relay C	turn peristaltic pump on	turn peristaltic pump off
Relay D	not used	not used

Table D.2 Event actions that must be defined for the AIM1250 program

Event	Action Definition
Into Sample Rack 1	close Relay C Delay = 0 s, Duration = U4 s
Into Sample Rack 4	close relay C Delay = 0 s, Duration = 10 s
Into Wash	close Relay C Delay = 0 s, Duration = U3 s

Table D.3 User defined parameters for the AIM1250 program ("define at run-time parameters").

ID	Description	Equation	Max Value
U1	# of samples	LINE1	1000
U2	Start at position #?	LINE2	21
U3	Pre-Run Wash Time (s)	LINE3	1000
U4	Sip Time (s)	LINE4	1000
U5	Column Load Time (s)	LINE5	1000
U6	Column Wash Time (s)	LINE6	1000
U7	Drain Time (s)	LINE5 + LINE6	1000
U8	Elution Time (s)	LINE8	1000
U9			
U10	Final Wash Time (s)	LINE10	1000
U11	Drain Time (s)	LINE5 + LINE6 + LINE7	1000

Table D.4 Timings entered at run-time by user. These are the timings used during the concentration of the Cordilleran water samples, actual timings required will vary depending on sample loop size (here a 22 mL loop was used), peristaltic pump speed, tubing diameter, and general condition of tubing.

Parameter	Time (s)
Pre Run Wash Time	30
Sip Time	259
Column Load Time	600
Ca/Mg Wash Time	120
Elution Time	120

Table D.5 Concord software method "sequence of events" program for AIM 1250 autosampler / fraction collector used in the automated concentration system.

Num	Step	Tray
1	Close Relay A	Left
2	Wash	Left
3	Open Relay B	Left
4	Sample Rack 1	Left
5	Close Relay B	Left
6	Sample Rack 4	Left
7	Sample Rack 3	Left
8	Sample Rack 1	Left
9	Sample Rack 4	Left
10	Sample Rack 3	Left
11	Sample Rack 1	Left
12	Sample Rack 4	Left
13	Sample Rack 3	Left
14	Sample Rack 1	Left
15	Sample Rack 4	Left
16	Sample Rack 3	Left
17	Sample Rack 2	Left
18	Repeat, go to step 2	Left

Table D.6 Eluents used for the concentration program.

Eluent Bottle	Eluent
A	1 N Ammonium Acetate
B	2 N Nitric Acid
C	Deionized Water

Table D.7 Gradient pump (GP50) program.

	Eluent				V5	Flow	V6	
Time	%A	%B	%C	%D	V	ml/min	Col	
Init	100				L	2.5	B	Initialisation Conditions
0.00	100				L	2.5	B	Begin Load Sample Loop
4.32	100				L	2.5	B	End Load Sample Loop
4.33	100				L	1.5	A	Begin Load CC-1 Column
14.32	100				L	1.5	B	End Load CC-1 Column
14.33	100				L	2.5	B	Begin Load Sample Loop
18.64	100				L	2.5	B	End Load Sample Loop
18.65	100				L	1.5	A	Begin Load CC-1 Column
28.64	100				L	1.5	B	End Load CC-1 Column
28.65	100				L	2.5	B	Begin Load Sample Loop
32.96	100				L	2.5	B	End Load Sample Loop
32.97	100				L	1.5	A	Begin Load CC-1 Column
42.96	100				L	1.5	B	End Load CC-1 Column
42.97	100				L	2.5	B	Begin Load Sample Loop
47.28	100				L	2.5	B	End Load Sample Loop
47.29	100				L	1.5	A	Begin Load CC-1 Column
57.28	100				L	1.5	B	End Load CC-1 Column
57.29	100				L	2.5	B	Begin Ammonium Acetate Rinse
61.28	100				L	2.5	B	End Ammonium Acetate Rinse
61.29			100		L	4.0	B	Begin Water Rinse
62.28			100		L	4.0	B	End Water Rinse
62.29		40	60		I	4.0	B	Begin Elution
64.58		40	60		L	4.0	B	End Elution
64.59		100			L	4.0	B	Begin Nitric Acid Rinse (column cleanup)
65.58		100			L	4.0	B	End Nitric Acid Rinse
65.59			100		L	4.0	B	Begin Water Rinse
66.58			100		L	4.0	B	End Water Rinse
66.59		100			L	2.5	B	Reset Initial Conditions